CIVIL ENGINEERING STUDIES
STRUCTURAL RESEARCH SERIES NO. 332

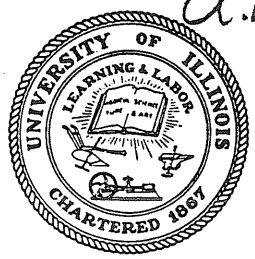

FINITE ELEMENT ANALYSIS OF SKEWED SHALLOW SHELLS

by
D. A. W. PECKNOLD
and
W. C. SCHNOBRICH

Issued as a Technical
Report of a Research
Program Sponsored

by

THE OFFICE OF NAVAL RESEARCH
DEPARTMENT OF THE NAVY
Contract N 00014-67-A-0305-0010

UNIVERSITY OF ILLINOIS
URBANA, ILLINOIS
JANUARY, 1968

FINITE ELEMENT ANALYSIS OF SKEWED SHALLOW SHELLS

by

D. A. W. Pecknold

and

W. C. Schnobrich

Issued as a Technical
Report of a Research
Program Sponsored

by

The Office of Naval Research
Department of the Navy
Contract N 00014-67-A-0305-0010

University of Illinois
Urbana, Illinois

January, 1968

ACKNOWLEDGMENTS

This report was prepared as a doctoral dissertation by Mr. D. A. W. Pecknold, under the direction of Dr. W. C. Schnobrich.

The investigation was conducted as a part of a research study supported by the Office of Naval Research under contract number N 00014-67-A-0305-0010.

The cooperation of the staff of the Department of Computer Science at the University of Illinois in the use of the IBM 7094 computer is gratefully acknowledged.

TABLE OF CONTENTS

TABLE OF CONTENTS, Continued

TABLE OF CONTENTS, Continued

TABLE OF CONTENTS, Continued

LIST OF TABLES

LIST OF FIGURES

LIST OF FIGURES, Continued

LIST OF FIGURES, Continued

LIST OF FIGURES, Continued

1. INTRODUCTION

1.1 General

Shallow doubly curved translational shells are efficient and aesthetically attractive structures and as such are being used with increasing frequency in roof construction. Due to the realization that the membrane or "momentless" theory is not always applicable, especially in the case of hyperbolic paraboloids bounded by characteristics, the bending theory of this type of shell has received a great deal of attention in recent years (28, 46, 39, 4, 9, 17).*

The so-called "shallow shell theory" of Margeurre (28) and Vlasov (46) is often used since it is reasonably accurate for the range of shell dimensions commonly used in practice, (46) and since it is considerably simplified in comparison with more "exact" shell theories. The fundamental approximation on which the shallow shell theory is based is that quadratic terms involving the slopes of the shell middle surface are negligible compared to unity. While there is some uncertainty regarding the magnitude of the errors introduced by the approximations, a common rule-of-thumb is that if the maximum rise/span ratio of the shell is less than one-fifth the theory produces results sufficiently accurate for practical purposes (46).

---

* Numbers in parentheses refer to references listed in the List of References.

The shallow shell theory is normally formulated in terms of either a stress function and normal displacement (ϕ-w formulation) or in terms of middle-surface displacements (u-v-w formulation). The ϕ-w formulation results in a pair of coupled fourth-order partial differential equations, and the u-v-w formulation results in a set of three coupled partial differential equations, two of second order and one of fourth order.

Thus, despite the simplifying assumptions which are made, the problem is still a difficult one mathematically with the result that comparatively few analytical solutions have been obtained. Most of these are of the Lèvy type (4, 9) in which the quantities of interest are expanded in infinite series which allow the reduction of the partial differential equations to ordinary differential equations, but which impose simple support boundary conditions on two opposite edges. A recent study (21) has quantitatively demonstrated the sensitivity of shells to boundary conditions thus emphasizing the importance of developing methods of analysis which are not restricted to special boundary conditions, particularly those specified by the simple support case.

Evidently the most promising approach to the problem is a numerical one, especially in light of complicating factors such as non-rectangular planform, eccentric edge beams, tie rods, column supports, and non-uniform shell thickness, some or all of which often exist in practice.

Among numerical procedures a distinction is often made between procedures which are regarded as mathematical approximations, such as finite differences and variational methods, and those which are regarded as physical approximations, such as various discrete element systems.

Das Gupta (13), Soare (43), Mirza (31), Russell and Gerstle (41) and others have presented finite difference solutions of the shallow shell equations particularly as related to various hyperbolic paraboloids bounded by characteristics. Some care is required in the application of finite differences to these shells, however, so that a "consistent" (35, 20) set of equations is obtained.* Abu-Sitta has applied finite difference methods to elliptical paraboloids (1) and has, in addition, carried out experimental work (2).

In the application of variational methods to the analysis of shallow shells (10), the problem of selection of approximating functions restricts the versatility of the method since a definite choice of such functions applies only to specific boundary conditions. In addition, the

---

* For both the ϕ-w and u-v-w formulations, in the case of hyperbolic paraboloids bounded by characteristics, interlacing grids should be used. For shallow shells bounded by lines of principal curvature, only the u-v-w formulation requires interlacing grids. This necessity is due to the appearance of odd-order mixed derivatives in the governing equations and the fact that small errors in the inplane displacements when multiplied by large stiffnesses may result in very large errors in the stresses.

treatment of non-classical boundary conditions presents serious difficulties. Among discrete element procedures which have been applied to shell problems are methods using the lumped parameter model (42, 32), the framework or lattice model (37) and the finite element technique. While it is justified to classify the first two methods as physical idealizations,* in some applications** the finite element method is really a matrix formulation of the Rayleigh-Ritz variational method. Finite element approaches to plane stress (11) and plate bending (47, 30) have met with notable success, however, much work is still being carried out in refining the method in these areas of application.

A natural extension of the scope of the finite element method is to shell problems. Most of the early attempts to so extend the method employed assemblages of flat elements to approximate the curved surface of the shell. Such an idealization may not be entirely satisfactory, however, since errors are introduced which are distinct from those involved in assuming the form of displacements in the

---

* The lumped parameter model may be regarded as a physical interpretation of finite difference approximations since the governing equations of the model are equivalent to the consistent difference equations of the problem. However, the model facilitates the formulation of boundary conditions without using fictitious grid points.

** The applications referred to are those in which the shape of the structure is not idealized. When, for example, flat elements are used to approximate a curved surface, a physical idealization is also involved.

structure (or element). Thus no direct relationship with the Rayleigh-Ritz procedure is apparent. Curved elements have been used for axisymmetric shells (44) and, for the cases that have been reported, more accurate results have been obtained than with flat elements.

1.2 Object and Scope

The objective of this study is to extend the finite element method to the bending analysis of skewed shallow shells subjected to a wide variety of boundary conditions. The effects of eccentric edge beams and tie rods on the behavior of such shells are of particular interest. Normally, torsional rigidity (13) and the inplane bending stiffness of edge beams (41) are neglected as well as their eccentricity, if any, with respect to the shell middle surface. Inclusion of these factors presents no difficulty in the present analysis.

Since the crucial step in the finite element method is the selection of appropriate displacement functions, it is deemed worthwhile to examine the effect of different assumptions. Thus, two different displacement shapes which have been used in plate bending analyses are adapted for use in shallow shell analysis.

A variety of numerical examples are presented. In order to establish the validity of the method, comparisons are made with analytical solutions for simply supported

shells of three main types: elliptical and hyperbolic paraboloids bounded by lines of principal curvature, and hyperbolic paraboloids bounded by characteristics. The results of several skewed plate problems are also presented, since one of the assumed displacement fields satisfies certain convergence criteria in this case.

Limited comparisons are made with other numerical results to further substantiate the reliability of the analysis.

Several problems of more practical interest are then analyzed in order to investigate the effects of edge beams, tie rods and skewedness. Here attention is restricted to hyperbolic paraboloids bounded by characteristics.

In order to isolate the effects of different boundary conditions, fixed dimensions are chosen for each of the three main shells analyzed and these dimensions are retained throughout. Thus, no attempt is made to provide data in amounts or range sufficient for design, but merely to indicate the effects mentioned above.

1.3 Notation

The symbols used in this study are defined where they first appear. For convenience, frequently used symbols are summarized below.

2a, 2b	Dimensions of element in x and y directions respectively.

B	(20x20) matrix relating $\alpha_{(k)}$ to $u_{(k)}$; $u_{(k)} = B\alpha_{(k)}$
D	Bending stiffness of shell, $= Eh^3/12(1-\nu^2)$
D^m, D^b	(3x20) matrices expressing strains in terms of constants $\alpha_{(k)}$, $\varepsilon^m = D^m\alpha_{(k)}$, $\varepsilon^b = D^b\alpha_{(k)}$
e	Eccentricity of beam axis with respect to shell middle surface
$\hat{e}_x, \hat{e}_y, \hat{e}_{x'}, \hat{e}_{y'}$	Unit vectors in shell tangent plane
E	Young's Modulus
$\bar{E}^m$, $\bar{E}^b$	(3x3) membrane and bending stress-strain matrices in orthogonal coordinates
E^m, E^b	(3x3) membrane and bending stress-strain matrices in oblique coordinates
h	Thickness of shell
$K_{(k)}$	Stiffness matrix of k^{th} element
$K^m_{(k)}$, $K^b_{(k)}$	Membrane and bending stiffness matrices of k^{th} element $(K_{(k)} = K^m_{(k)} + K^b_{(k)})$
L_x, L_y	Span of shell in x and y directions
$L_{(k)}$	(20xN) localizing matrix expressing relationship between element and structure displacements, $u_{(k)} = L_{(k)}u$
$\vec{M}_x$, $\vec{M}_y$	Moment vectors acting on faces x = constant and y = constant
$M_{\bar{x}}$, $M_{\bar{y}}$, $M_{\bar{\bar{xy}}}$	Bending moment components in orthogonal coordinates
M_x, M_y, M_{xy}	Bending moment components in oblique coordinates
N	Membrane stiffness of shell, $= Eh/(1-\nu^2)$

$\vec{N}_x$, $\vec{N}_y$	Stress resultant vectors acting on faces x = constant and y = constant
$N_{\bar{x}}$, $N_{\bar{y}}$, $N_{\bar{xy}}$	Membrane forces in orthogonal coordinates
N_x, N_y, N_{xy}	Membrane forces in oblique coordinates
$\hat{n}$	Unit vector normal to shell middle surface
$P_{(k)}$	Generalized nodal loading vector for k^{th} element
P	(Nx1) column vector of structure nodal loads
$\vec{p}$	Vector of distributed external loading
$p_{\bar{u}}$, $p_{\bar{v}}$, $p_{\bar{w}}$	Components of $\vec{p}$ in orthogonal coordinates
p_u, p_v, p_w	Components of $\vec{p}$ in oblique coordinates
$\vec{q}$	Displacement vector of shell middle surface
$Q_{\bar{x}}$, $Q_{\bar{y}}$	Transverse shears in orthogonal coordinates
Q_x, Q_y	Transverse shears in oblique coordinates
$\bar{r}$, $\bar{s}$, $\bar{t}$	Curvatures of shell middle surface in orthogonal coordinates
r, s, t	Curvatures of shell middle surface in oblique coordinates
R	Radius of curvature of edge beam
T	(3x3) transformation matrix relating orthogonal and skew forces, $\bar{\sigma}^m = T\sigma^m$, $\bar{\sigma}^b = T\sigma^b$
$u_{(k)}$	Nodal displacements of k^{th} element
$\bar{U}^m$, $\bar{U}^b$	Membrane and bending strain energy in orthogonal coordinates
U^m, U^b	Membrane and bending strain energy in oblique coordinates, $U^m = \bar{U}^m$, $U^b = \bar{U}^b$

$\bar{U}$, U	Total strain energy in orthogonal and oblique coordinates, $\bar{U} = U$
u	(Nx1) column vector of structure displacements
$\bar{u}$, $\bar{v}$, $\bar{w}$	Components of displacement vector $\vec{q}$ in orthogonal coordinates
u, v, w	Orthogonal projections of $\vec{q}$ on $\hat{e}_x$, $\hat{e}_y$ and $\hat{n}$ respectively
V	Total potential energy
$\bar{x}$, $\bar{y}$, $\bar{z}$	Cartesian coordinates of point on middle surface
x, y	Surface coordinates interpreted as oblique axes in $\bar{x}$, $\bar{y}$ plane
x', y'	Conjugate axes in shell tangent plane
$\alpha_{(k)}$	(20x1) column vector of generalized coordinates
$\varepsilon_{\bar{x}}$, $\varepsilon_{\bar{y}}$, $\gamma_{\bar{x}\bar{y}}$	Membrane strains in orthogonal coordinates
ε_x, ε_y, γ_{xy}	Membrane strains in oblique coordinates
$\bar{\varepsilon}^m$, $\bar{\varepsilon}^b$	(3x1) column vectors of membrane and bending strains in orthogonal coordinates, $\bar{\varepsilon}^m = (\varepsilon_{\bar{x}}, \varepsilon_{\bar{y}}, \gamma_{\bar{x}\bar{y}})^T$, $\bar{\varepsilon}^b = (\kappa_{\bar{x}}, \kappa_{\bar{y}}, 2\kappa_{\bar{x}\bar{y}})^T$
ε^m, ε^b	(3x1) column vectors of membrane and bending strains in oblique coordinates $\varepsilon^m = (\varepsilon_x, \varepsilon_y, \gamma_{xy})^T$, $\varepsilon^b = (\kappa_x, \kappa_y, 2\kappa_{xy})^T$
ζ	Distance of an arbitrary point from the shell middle surface, measured along $\hat{n}$
$\vec{\theta}$	Rotation vector of shell middle surface
$\theta_{\bar{x}}$, $\theta_{\bar{y}}$, $\theta_{\bar{n}}$	Components of $\vec{\theta}$ in orthogonal coordinates
θ_x, θ_y, θ_n	Components of $\vec{\theta}$ in oblique coordinates

$\bar{\kappa}_x$, $\bar{\kappa}_y$, $2\bar{\kappa}_{xy}$	Bending strains in orthogonal coordinates
κ_x, κ_y, $2\kappa_{xy}$	Bending strains in oblique coordinates
λ	Dimensionless tie rod stiffness parameter
ν	Poisson's Ratio
ξ, η	Dimensionless element coordinates, $\xi = x/a$, $\eta = y/b$
$\vec{\sigma}_x$, $\vec{\sigma}_y$	Vector stresses acting on faces x = constant and y = constant
$\sigma_x, \sigma_y, \tau_{xy}, \tau_{xz}, \tau_{yz}$	Components of $\vec{\sigma}_x$ and $\vec{\sigma}_y$ in oblique coordinates
$\bar{\sigma}^m$, $\bar{\sigma}^b$	(3x1) column vectors of membrane and bending stresses in orthogonal coordinates $\bar{\sigma}^m = (\bar{N}_x, \bar{N}_y, \bar{N}_{xy})^T$, $\bar{\sigma}^b = (\bar{M}_x, \bar{M}_y, \bar{M}_{xy})^T$
σ^m, σ^b	(3x1) column vectors of membrane and bending stresses in oblique coordinates, $\sigma^m = (N_x, N_y, N_{xy})^T$, $\sigma^b = (M_x, M_y, M_{xy})^T$
χ	Skew angle (angle between x and y coordinate lines)
Ω	Potential of external loads

2. BASIC EQUATIONS

2.1 General

The objective of the present chapter is to develop an expression for the strain energy of a shell defined in reference to a system of oblique coordinates. This is motivated by a desire to describe the quantities of interest in as natural a manner as possible, consistent with the geometrical shape of the shell. Subsequently, use will be made of the strain energy expression in the application of the finite element method.

No attempt is made here to justify the assumptions of shallow shell theory or to re-derive the governing equations in Cartesian coordinates as various authors (28, 46, 36, 17) have already considered these matters in some depth. Remarks on the assumptions involved in shallow shell theory are confined to a reminder that the basic, although not sole, assumption is that quadratic terms involving the slopes of the shell middle surface are negligible compared to unity. If the shell middle surface is a second order surface, this assumption leads directly to the approximation that the curvatures of the surface are constant. An additional consequence is that the geometry of the surface is, in effect, approximated by that of its projection on the horizontal plane. Thus, if the parametric representation of the shell middle surface is given in the form

$$\bar{x} = \bar{x}$$
$$\bar{y} = \bar{y} \qquad (2.1)$$
$$\bar{z} = \bar{z}(\bar{x},\bar{y})$$

where $(\bar{x},\bar{y},\bar{z})$ are Cartesian coordinates, the approximation is made that the $(\bar{x},\bar{y})$ coordinate lines are orthogonal on the middle surface. It is in this sense that the term "orthogonal coordinates" will be used throughout the remainder of this study.

In the case of oblique coordinates (x,y) in the horizontal plane, the corresponding assumption is that the angle between the x and y axes in the horizontal plane is equal to the angle between the tangents to the x and y coordinate lines on the middle surface.

2.2 Shells Considered

The shell considered in the subsequent analysis is a thin shallow isotropic homogeneous elastic shell which is parallelogram shaped in planform. Its middle surface is given in terms of the parametric representation

$$\bar{x} = x + y \cos \chi$$
$$\bar{y} = y \sin \chi \qquad (2.2)$$
$$\bar{z} = k_1 x + k_2 y + \frac{rx^2}{2} + sxy + \frac{ty^2}{2}$$

where χ, k_1, k_2, r, s, and t are constants, and $(\bar{x},\bar{y},\bar{z})$ are the Cartesian coordinates of a point on the middle surface. The parameters (x,y) are surface coordinates which are interpreted as oblique axes in the horizontal plane, with included

angle χ, as shown in Fig. 1. The constants r, s and t which appear in Eq. (2.2) represent approximations to the curvatures and twist of the middle surface and will appear in the governing equations of the shell. The constants k_1 and k_2 are included for generality, although they do not appear subsequently, since the quantities of interest are described in a manner which is independent of the spatial orientation of the shell. For example, quantities are referred to unit vectors which are tangent and normal to the shell rather than to unit vectors which are directed along the Cartesian axes. The notations

$$\begin{aligned} r &\equiv \bar{z}_{,xx} \\ s &\equiv \bar{z}_{,xy} \\ t &\equiv \bar{z}_{,yy} \end{aligned} \tag{2.3}$$

and

$$\begin{aligned} \bar{r} &\equiv \bar{z}_{,\bar{x}\bar{x}} \\ \bar{s} &\equiv \bar{z}_{,\bar{x}\bar{y}} \\ \bar{t} &\equiv \bar{z}_{,\bar{y}\bar{y}} \end{aligned} \tag{2.4}$$

are used, where the commas denote partial differentiation with respect to the variable indicated by the subscript. (Bars will generally designate quantities referred to the $(\bar{x},\bar{y})$ axes while unbarred quantities are referred to the skew axes (x,y)). The third of Eqs. (2.2), when differentiated, agrees with Eqs. (2.3).

When the shallow shell approximations

$$\bar{z}_{,\bar{x}}^{\,2} \ll 1$$
$$\bar{z}_{,\bar{y}}^{\,2} \ll 1 \qquad (2.5)$$
$$\bar{z}_{,\bar{x}}\, \bar{z}_{,\bar{y}} \ll 1$$

are made, the quantities (r,s,t) and $(\bar{r},\bar{s},\bar{t})$ represent the curvatures and twist of the middle surface, referred to the (x,y) and $(\bar{x},\bar{y})$ axes respectively, as mentioned previously. Equations (2.3) and (2.4) determine the sign convention for curvatures and twist of the middle surface. A surface of positive curvatures ($\bar{r} > 0$, $\bar{t} > 0$, $\bar{s} = 0$) and a surface of positive twist ($\bar{r} = \bar{t} = 0$, $\bar{s} > 0$) are shown in Fig. 1.

The transformations relating the curvatures and twists in the two coordinate systems, obtained by use of the chain rule for partial differentiation, are

$$\bar{r} = r$$
$$\bar{s} = -r \cot \chi + s \csc \chi \qquad (2.6)$$
$$\bar{t} = r \cot^2 \chi - 2s \csc \chi \cot \chi + t \csc^2 \chi$$

2.3 Review of Governing Equations in Orthogonal Coordinates

The governing equations in orthogonal coordinates are listed here for convenience. Details of their derivation may be found, for example, in Flügge and Conrad (17), Vlasov (46), or Novozhilov (36).

The sign conventions adopted for forces, moments and displacements in the orthogonal coordinate system are shown in Fig. 2. Double-headed arrows represent moment

vectors according to the right hand rule. It should be noted that tangential and normal components of displacement are used rather than components along the $(\bar{x},\bar{y},\bar{z})$ axes. The in-plane, or membrane stress resultants $N_{\bar{x}}$, $N_{\bar{y}}$, $N_{\bar{x}\bar{y}}$ and the bending stress resultants $M_{\bar{x}}$, $M_{\bar{y}}$, $M_{\bar{x}\bar{y}}$, $Q_{\bar{x}}$, $Q_{\bar{y}}$ represent appropriate stresses integrated through the thickness of the shell. They are defined as forces or moments per unit length of the middle surface. The displacement vector, $\vec{q}$, of the middle surface is resolved into components $\bar{u}$ and $\bar{v}$ tangent to the $\bar{x}$ and $\bar{y}$ coordinate lines and $\bar{w}$, normal to the surface. Similarly the vector of distributed load, $\vec{p}$, is resolved into components $(p_{\bar{u}}, p_{\bar{v}}, p_{\bar{w}})$.

2.3.1. Strain-Displacement Relations

The strain displacement relations for the shell in orthogonal coordinates are listed here. The membrane strain-displacement relations are

$$\begin{aligned} \varepsilon_{\bar{x}} &= \bar{u},_{\bar{x}} - \bar{r}\bar{w} \\ \varepsilon_{\bar{y}} &= \bar{v},_{\bar{y}} - \bar{t}\bar{w} \\ \gamma_{\bar{x}\bar{y}} &= \bar{u},_{\bar{y}} + \bar{v},_{\bar{x}} - 2\bar{s}\bar{w} \end{aligned} \tag{2.7}$$

and the bending strain-displacement relations are

$$\begin{aligned} \kappa_{\bar{x}} &= - \bar{w},_{\bar{x}\bar{x}} \\ \kappa_{\bar{y}} &= - \bar{w},_{\bar{y}\bar{y}} \\ 2\kappa_{\bar{x}\bar{y}} &= - 2\bar{w},_{\bar{x}\bar{y}} \end{aligned} \tag{2.8}$$

2.3.2. Stress-Strain Relations

In orthogonal coordinates, the stress-strain relations are

$$\begin{aligned} \bar{N}_x &= N\,(\bar{\varepsilon}_x + \nu\bar{\varepsilon}_y) \\ \bar{N}_y &= N\,(\bar{\varepsilon}_y + \nu\bar{\varepsilon}_x) \\ \bar{N}_{xy} &= N\,(\tfrac{1-\nu}{2})\,\bar{\gamma}_{xy} \end{aligned} \tag{2.9}$$

$$\begin{aligned} \bar{M}_x &= D\,(\bar{\kappa}_x + \nu\bar{\kappa}_y) \\ \bar{M}_y &= D\,(\bar{\kappa}_y + \nu\bar{\kappa}_x) \\ \bar{M}_{xy} &= D\,(\tfrac{1-\nu}{2})(2\bar{\kappa}_{xy}) \end{aligned} \tag{2.10}$$

where $N = \dfrac{Eh}{1-\nu^2}$, $D = \dfrac{Eh^3}{12(1-\nu^2)}$

and E is Young's Modulus, ν is Poisson's Ratio and h is the thickness of the shell.

The usual approximations $\bar{N}_{xy} = \bar{N}_{yx}$ and $\bar{M}_{xy} = \bar{M}_{yx}$ are implied here. This is a result of the equality of the in-plane shear stresses, and of discarding terms of the order of $\bar{r}h$ and $\bar{t}h$ in comparison with unity, which is permissible for a thin shallow shell. Kirchhoff's assumption is also used in the derivation of Eqs. (2.7) to (2.10).

In matrix form the above equations become

$$\bar{\sigma}^m = \bar{E}^m\,\bar{\varepsilon}^m \tag{2.11}$$

$$\bar{\sigma}^b = \bar{E}^b\,\bar{\varepsilon}^b \tag{2.12}$$

where

$$\bar{\sigma}^m \equiv \begin{bmatrix} \bar{N}_x \\ \bar{N}_y \\ \bar{N}_{xy} \end{bmatrix} \tag{2.13}$$

$$\bar{\sigma}^b \equiv \begin{bmatrix} \bar{M}_x \\ \bar{M}_y \\ \bar{M}_{xy} \end{bmatrix} \tag{2.14}$$

$$\bar{\varepsilon}^m \equiv \begin{bmatrix} \bar{\varepsilon}_x \\ \bar{\varepsilon}_y \\ \bar{\gamma}_{xy} \end{bmatrix} \tag{2.15}$$

$$\bar{\varepsilon}^b \equiv \begin{bmatrix} \bar{\kappa}_x \\ \bar{\kappa}_y \\ 2\bar{\kappa}_{xy} \end{bmatrix} \tag{2.16}$$

$$\bar{E}^m = \frac{Eh}{1-\nu^2} \begin{bmatrix} 1 & \nu & 0 \\ \nu & 1 & 0 \\ 0 & 0 & \frac{1-\nu}{2} \end{bmatrix} \tag{2.17}$$

and

$$\bar{E}^b = \frac{Eh^3}{12(1-\nu^2)} \begin{bmatrix} 1 & \nu & 0 \\ \nu & 1 & 0 \\ 0 & 0 & \frac{1-\nu}{2} \end{bmatrix} \tag{2.18}$$

The superscript "m" refers to membrane quantities and the superscript "b" refers to bending quantities.

2.3.3. Strain Energy

The strain energy $\bar{U}$, of the shallow shell is composed of the membrane strain energy $\bar{U}^m$, and the bending

strain energy, $\bar{U}^b$. Strain energy due to shear deformation is assumed to be negligible. In terms of the notation introduced in Sec. 2.3.2.,

$$\bar{U}^m = \tfrac{1}{2} \int\int \bar{\sigma}^{m,T}\ \bar{\varepsilon}^m\ d\bar{x}\ d\bar{y} = \tfrac{1}{2} \int\int \bar{\varepsilon}^{m,T}\ \bar{E}^{m,T}\ \bar{\varepsilon}^m\ d\bar{x}\ d\bar{y} \qquad (2.19)$$

$$\bar{U}^b = \tfrac{1}{2} \int\int \bar{\sigma}^{b,T}\ \bar{\varepsilon}^b\ d\bar{x}\ d\bar{y} = \tfrac{1}{2} \int\int \bar{\varepsilon}^{b,T}\ \bar{E}^{b,T}\ \bar{\varepsilon}^b\ d\bar{x}\ d\bar{y} \qquad (2.20)$$

and $$\bar{U} = \bar{U}^m + \bar{U}^b \qquad (2.21)$$

where the superscript T denotes transposition of the designated vector or matrix, and the integration extends over the middle surface of the shell.

2.4 Definitions of Forces and Moments in Oblique Coordinates

When defining various quantities in an oblique coordinate system, it is convenient to introduce a conjugate set of axes (x',y') in the shell tangent plane, as shown in Fig. 3, such that the pairs of axes (x,y') and (x',y) are orthogonal.

Unit vectors in the tangent plane to the shell middle surface along axes x, y, x' and y' are denoted by $\hat{e}_x$, $\hat{e}_y$, $\hat{e}_{x'}$ and $\hat{e}_{y'}$, respectively (Fig. 3). The unit normal vector, $\hat{n}$, to the middle surface is given by

$$\begin{aligned} \hat{n} &= \hat{e}_{x'} \times \hat{e}_y \\ \text{or} \qquad \hat{n} &= \hat{e}_x \times \hat{e}_{y'} \end{aligned} \qquad (2.22)$$

where "$\times$" denotes the vector cross product; the right hand rule again being used.

The distance from the middle surface to an arbitrary point off the middle surface is denoted by ζ, measured positively along the positive normal $\hat{n}$. Therefore the position vector, $\vec{R}$, of an arbitrary point may be written in the form

$$\vec{R} = \vec{r}\,(x,y) + \zeta\hat{n}, \qquad (2.23)$$

where $\vec{r}$ is the position vector of a point on the middle surface. Thus (x,y,ζ) form a three-dimensional coordinate system, called "shell coordinates" (27). The (x,y,ζ) coordinates are orthogonal curvilinear coordinates if and only if the (x,y) surface coordinates are lines of principal curvature of the surface (27). As a result, in all other cases, the relative directions of the unit vectors $\hat{e}_x$, $\hat{e}_y$, $\hat{e}_{x'}$ and $\hat{e}_{y'}$ change throughout the thickness of the shell. This fact is neglected in shallow shell theory and is neglected in this extension to oblique coordinates, since the angle between the unit vectors $\hat{e}_x$ and $\hat{e}_y$ on the middle surface is approximated by the angle χ in the horizontal plane.

The vector stresses acting on the faces x = constant and y = constant are denoted by $\vec{\sigma}_x$ and $\vec{\sigma}_y$ respectively, as shown in Fig. 4.

These vector stresses depend on the coordinate ζ. The vectors of membrane stress resultants and bending moments, (per unit length of the middle surface) may now be defined as

$$\vec{N}_x = \int \vec{\sigma}_x \, d\zeta$$

$$\vec{N}_y = \int \vec{\sigma}_y \, d\zeta$$

$$\vec{M}_x = \int (\zeta \hat{n} \times \vec{\sigma}_x) \, d\zeta \qquad (2.24)$$

$$\vec{M}_y = \int (\zeta \hat{n} \times \vec{\sigma}_y) \, d\zeta$$

where $\vec{N}_x$ and $\vec{M}_x$ act on the face x = constant and $\vec{N}_y$ and $\vec{M}_y$ act on the face y = constant as shown in Fig. 5. The integrations extend over the thickness of the shell. The approximation referred to in Sec. 2.3.2, i.e., rh, th $<<$ 1, has been made here also; that is, the elements of cross sectional area on both the x = constant and y = constant faces are approximated by $1 \cdot d\zeta$.

In thin shell theory the equilibrium conditions of the shell are expressed in terms of these integrated quantities. Thus equilibrium is enforced in a macroscopic sense, rather than pointwise throughout the thickness of the shell.

The quantities $\vec{\sigma}_x$, $\vec{\sigma}_y$, $\vec{N}_x$, $\vec{N}_y$, $\vec{M}_x$ and $\vec{M}_y$ are physical quantities. They may be represented in a variety of forms by referring them to various sets of unit vectors. In the case of oblique axes, several alternative representations are possible. The choice of representation is made here on the basis of convenience. For example, let $\vec{\sigma}_x$ and $\vec{\sigma}_y$ be written in the form

$$\vec{\sigma}_x = \sigma_x \hat{e}_x + \tau_{xy} \hat{e}_y + \tau_{xz} \hat{n}$$
$$\vec{\sigma}_y = \tau_{xy} \hat{e}_x + \sigma_y \hat{e}_y + \tau_{yz} \hat{n} \qquad (2.25)$$

No notational difference has been retained for the shear stresses τ_{xy} and τ_{yx} since they are equal even in non-orthogonal shell coordinates (27). Eqs. (2.25) are to be regarded as definitions of σ_x, σ_y, τ_{xy}, τ_{xz} and τ_{yz}. They could be defined in other ways if so desired, as long as they are subsequently used in a manner consistent with their definitions.

The membrane stress resultant vectors are represented in the form

$$\vec{N}_x = N_x \hat{e}_x + N_{xy} \hat{e}_y + Q_x \hat{n}$$
$$\vec{N}_y = N_{yx} \hat{e}_x + N_y \hat{e}_y + Q_y \hat{n} \qquad (2.26)$$

It is advantageous to express the bending moment vectors in terms of linear combinations of the unit vectors $\hat{e}_{x'}$ and $\hat{e}_{y'}$. Therefore

$$\vec{M}_x = - M_{xy} \hat{e}_{x'} + M_x \hat{e}_{y'}$$
$$\vec{M}_y = - M_y \hat{e}_{x'} + M_{yx} \hat{e}_{y'} \qquad (2.27)$$

It is again emphasized that Eqs. (2.26) and (2.27) are the <u>definitions</u> of the scalar quantities N_x, N_y, N_{xy}, N_{yx}, Q_x, Q_y, M_x, M_y, M_{xy} and M_{yx}. The representations of the vectors $\vec{N}_x$, $\vec{N}_y$, $\vec{M}_x$ and $\vec{M}_y$ are illustrated in Fig. 6.

Eqs. (2.24), (2.25), (2.26) and (2.27) are used to obtain expressions for the various scalar stress resultants

in terms of the stress components integrated through the thickness of the shell. Substitution of Eqs. (2.25) into Eqs. (2.24), and integration with respect to ζ, considering the unit vectors to be independent of ζ, yields

$$\begin{aligned}
\vec{N}_x &= \hat{e}_x \left[\int \sigma_x \, d\zeta\right] + \hat{e}_y \left[\int \tau_{xy} \, d\zeta\right] + \hat{n} \left[\int \tau_{xz} \, d\zeta\right] \\
\vec{N}_y &= \hat{e}_x \left[\int \tau_{xy} \, d\zeta\right] + \hat{e}_y \left[\int \sigma_y \, d\zeta\right] + \hat{n} \left[\int \tau_{yz} \, d\zeta\right] \\
\vec{M}_x &= \hat{e}_{x'} \left[-\int \tau_{xy} \, \zeta \, d\zeta\right] + \hat{e}_{y'} \left[\int \sigma_x \, \zeta \, d\zeta\right] \\
\vec{M}_y &= \hat{e}_{x'} \left[-\int \sigma_y \, \zeta \, d\zeta\right] + \hat{e}_{y'} \left[\int \tau_{xy} \, \zeta \, d\zeta\right]
\end{aligned} \tag{2.28}$$

Comparison of Eqs. (2.28) with Eqs. (2.26) and (2.27) yields

$$\begin{aligned}
N_x &= \int \sigma_x \, d\zeta \\
N_y &= \int \sigma_y \, d\zeta \\
N_{xy} &= N_{yx} = \int \tau_{xy} \, d\zeta \\
Q_x &= \int \tau_{xz} \, d\zeta \\
Q_y &= \int \tau_{yz} \, d\zeta \\
M_x &= \int \sigma_x \, \zeta \, d\zeta \\
M_y &= \int \sigma_y \, \zeta \, d\zeta \\
M_{xy} &= M_{yx} = \int \tau_{xy} \, \zeta \, d\zeta
\end{aligned} \tag{2.29}$$

Therefore when the bending moments are referred to unit vectors along the axes (x',y') rather than along the axes (x,y), the approximation which leads to $N_{xy} = N_{yx}$

also leads to $M_{xy} = M_{yx}$. Henceforth, these notational differences will be dropped, the inplane shear being referred to as N_{xy} and the twisting moment as M_{xy}. When $\chi = \frac{\pi}{2}$, the axes (x',y') coincide with the axes (x,y) and the above definitions reduce to those for the orthogonal case. The scalar components N_x, N_y, N_{xy}, Q_x, Q_y, M_x, M_y and M_{xy} then agree with the sign conventions given in Sec. 2.3 and Fig. 2.

The transformation expressing the relation between membrane stresses in the oblique and orthogonal systems is identical to that for the bending stress resultants. This is to be expected from an examination of Eqs. (2.29). These transformations may be easily derived by considering the equilibrium of differential elements of the shell bounded by mixed combinations of coordinate lines (see, for example, Flügge (16)). The transformations are

$$\begin{bmatrix} N_{\bar{x}} \\ N_{\bar{y}} \\ N_{\bar{x}\bar{y}} \end{bmatrix} = \begin{bmatrix} \csc\chi & \cos\chi\cot\chi & 2\cot\chi \\ 0 & \sin\chi & 0 \\ 0 & \cos\chi & 1 \end{bmatrix} \begin{bmatrix} N_x \\ N_y \\ N_{xy} \end{bmatrix} \tag{2.30}$$

or, in matrix notation

$$\bar{\sigma}^m = T\sigma^m \tag{2.31}$$

where

$$T = \begin{bmatrix} \csc\chi & \cos\chi\cot\chi & 2\cot\chi \\ 0 & \sin\chi & 0 \\ 0 & \cos\chi & 1 \end{bmatrix} \tag{2.32}$$

Also,

$$\bar{\sigma}^b = T\sigma^b \tag{2.33}$$

2.5 Definitions of Displacements and Rotations in Oblique Coordinates

In order to keep invariant the form of the expression for work done by a force acting through a displacement or a moment acting through a rotation, which will in turn lead to a symmetrical stiffness matrix, displacements and rotations are defined in reference to the oblique coordinate system in the manner outlined in the following paragraphs.

Let $\vec{q}$ denote the displacement vector of a point on the middle surface. The displacement components u, v, w are defined by

$$\begin{aligned} u &= \vec{q} \cdot \hat{e}_x \\ v &= \vec{q} \cdot \hat{e}_y \\ w &= \vec{q} \cdot \hat{n} \end{aligned} \tag{2.34}$$

That is, the quantities u, v, and w are the orthogonal projections of $\vec{q}$ on the unit vectors $\hat{e}_x$, $\hat{e}_y$ and $\hat{n}$ respectively.

The invariance of the expression for the work done by a force acting through a displacement is easily verified.

The displacement vector $\vec{q}$ may be expressed as a linear combination of the unit vectors $\hat{e}_x$, $\hat{e}_y$, and $\hat{n}$ in the form,

$$\begin{aligned} \vec{q} = &[u \csc^2 \chi - v \cos \chi \cot \chi] \hat{e}_x \\ &+ [v \csc^2 \chi - u \csc \chi \cot \chi] \hat{e}_y + w\hat{n} \end{aligned} \tag{2.35}$$

This expression is used to obtain the relationship between displacements in the oblique and orthogonal coordinate systems.

Let $\vec{\theta}$ denote the rotation vector, defined on the middle surface. Then the quantities θ_x, θ_y, and θ_n are defined by

$$\begin{aligned} \theta_x &= \vec{\theta} \cdot \hat{e}_{x'} \\ \theta_y &= \vec{\theta} \cdot \hat{e}_{y'} \\ \theta_n &= \vec{\theta} \cdot \hat{n} \end{aligned} \tag{2.36}$$

Therefore, the quantities θ_x, θ_y, and θ_n are the orthogonal projections of $\vec{\theta}$ on the unit vectors $\hat{e}_{x'}$, $\hat{e}_{y'}$ and $\hat{n}$. Again the invariance of the work expression is easily verified. In a manner similar to that used to obtain Eq. (2.35), the rotation vector $\vec{\theta}$ may be expressed as a linear combination of the unit vectors $\hat{e}_{x'}$, $\hat{e}_{y'}$ and $\hat{n}$, in the form

$$\begin{aligned} \vec{\theta} = &(\theta_x \csc^2 \chi + \theta_y \csc \chi \cot \chi)\, \hat{e}_{x'} \\ &+ (\theta_x \csc \chi \cot \chi + \theta_y \csc^2 \chi)\, \hat{e}_{y'} + \theta_n \hat{n} \end{aligned} \tag{2.37}$$

The representations of $\vec{q}$ and $\vec{\theta}$ in terms of (u,v,w) and $(\theta_x, \theta_y, \theta_n)$ respectively are shown in Fig. 7.

The rotation and displacement quantities referred to the oblique coordinate system may be expressed in terms of corresponding quantities in an orthogonal coordinate system (Fig. 8). If, as before, barred quantities refer to the orthogonal system, the displacement and rotation vectors may be written as

$$\vec{q} = \bar{u}\,\hat{e}_x + \bar{v}\,\hat{e}_{y'} + \bar{w}\hat{n} \tag{2.38}$$

and

$$\vec{\theta} = \theta_{\bar{x}}\,\hat{e}_x + \theta_{\bar{y}}\,\hat{e}_{y'} + \theta_{\bar{n}}\,\hat{n} \tag{2.39}$$

Since

$$\begin{aligned} \hat{e}_{x'} &= \sin\chi\,\hat{e}_x - \cos\chi\,\hat{e}_{y'} \\ \hat{e}_y &= \cos\chi\,\hat{e}_x + \sin\chi\,\hat{e}_{y'} \quad , \end{aligned} \tag{2.40}$$

Eqs. (2.35) and (2.37) may be rewritten as

$$\vec{q} = u\,\hat{e}_x + [\,-u\cot\chi + v\csc\chi\,]\,\hat{e}_{y'} + w\hat{n} \tag{2.41}$$

and

$$\vec{\theta} = [\,\theta_x \csc\chi + \theta_y \cot\chi\,]\,\hat{e}_x + \theta_y\,\hat{e}_{y'} + \theta_n\,\hat{n} \tag{2.42}$$

Comparison of Eq. (2.41) with Eq. (2.38) yields the desired relation between displacement components in the oblique and orthogonal systems, namely,

$$\begin{aligned} \bar{u} &= u \\ \bar{v} &= -u\cot\chi + v\csc\chi \\ \bar{w} &= w \end{aligned} \tag{2.43}$$

Similarly, a comparison of Eq. (2.42) with Eq. (2.39) yields

$$\begin{aligned} \theta_{\bar{x}} &= \theta_x \csc\chi + \theta_y \cot\chi \\ \theta_{\bar{y}} &= \theta_y \\ \theta_{\bar{n}} &= \theta_n \end{aligned} \tag{2.44}$$

To the degree of approximation involved in shallow shell theory, the rotations and displacements are related by the expressions

$$\begin{aligned} \theta_{\bar{x}} &= \bar{w},_{\bar{y}} \\ \theta_{\bar{y}} &= -\bar{w},_{\bar{x}} \end{aligned} \tag{2.45}$$

in orthogonal coordinates. Terms involving curvatures and

twists multiplied by inplane displacements have been discarded from more exact expressions to yield Eq. (2.45).

Use of Eqs. (2.2), (2.43) and (2.44) yields the corresponding relations in oblique coordinates,

$$\begin{aligned} \theta_x &= w_{,y} \\ \theta_y &= - w_{,x} \end{aligned} \tag{2.46}$$

2.6 Strain Energy and Definition of Strains in Oblique Coordinates

The strains referred to the oblique coordinate system are defined here in such a manner as to retain formal correspondence between the governing equations in oblique and orthogonal coordinates. It must be emphasized that the definition of strain is completely arbitrary, as long as consistency is observed in subsequent manipulations. Therefore, let the membrane and bending strains in the oblique system be defined by the equations

$$\bar{\sigma}^{m,T}\,\bar{\varepsilon}^{m} = \sigma^{m,T}\,\varepsilon^{m} \tag{2.47}$$

and

$$\bar{\sigma}^{b,T}\,\bar{\varepsilon}^{b} = \sigma^{b,T}\,\varepsilon^{b} \tag{2.48}$$

where

$$\varepsilon^{m} = \begin{bmatrix} \varepsilon_x \\ \varepsilon_y \\ \gamma_{xy} \end{bmatrix} \tag{2.49}$$

and

$$\varepsilon^{b} = \begin{bmatrix} \kappa_x \\ \kappa_y \\ 2\kappa_{xy} \end{bmatrix} \tag{2.50}$$

With the use of Eq. (2.31), Eq. (2.47) may be rewritten as

$$\bar{\sigma}^{m,T}\ {}_{T}{}^{-1,T}\ \varepsilon^{m} = \bar{\sigma}^{m,T}\ \bar{\varepsilon}^{m} \tag{2.51}$$

Therefore since Eq. (2.47) is to be regarded as an identity,

$$\varepsilon^{m} = {}_{T}{}^{T}\ \bar{\varepsilon}^{m} \tag{2.52}$$

Similarly,

$$\varepsilon^{b} = {}_{T}{}^{T}\ \bar{\varepsilon}^{b} \tag{2.53}$$

Equations (2.52) and (2.53) define ε^{m} and ε^{b} in terms of displacements and curvatures relative to the orthogonal system, through the strain displacement relations Eqs. (2.7) and (2.8). The strain displacement relations in the oblique coordinate system are obtained from Eqs. (2.52) and (2.53), with the use of Eqs. (2.2), (2.6), (2.7), (2.8), (2.32) and (2.43).

Thus,

$$\begin{aligned} \varepsilon_{x} &= (u_{,x} - rw)\ \csc\chi \\ \varepsilon_{y} &= (v_{,y} - tw)\ \csc\chi \\ \gamma_{xy} &= (u_{,y} + v_{,x} - 2\ sw)\ \csc\chi \end{aligned} \tag{2.54}$$

and

$$\begin{aligned} \kappa_{x} &= -\ w_{,xx}\ \csc\chi \\ \kappa_{y} &= -\ w_{,yy}\ \csc\chi \\ 2\kappa_{xy} &= -\ 2\ w_{,xy}\ \csc\chi \end{aligned} \tag{2.55}$$

With the exception of the constant factor "csc χ", Eqs. (2.54) and (2.55) are formally the same as Eqs. (2.7) and (2.8). The factor "csc χ" could have been, of course, absorbed in the defining equations, Eqs. (2.47) and (2.48).

The stress-strain relations in the oblique coordinate system are now easily derived using the

stress-strain relations in orthogonal coordinates, Eqs. (2.11) and (2.12), and the transformations for stresses, Eqs. (2.31) and (2.33), and strains, Eqs. (2.52) and (2.53). Therefore,

$$\sigma^m = E^m \varepsilon^m \tag{2.56}$$

and

$$\sigma^b = E^b \varepsilon^b \tag{2.57}$$

where

$$E^m = T^{-1,T} \bar{E}^m T^{-1} \tag{2.58}$$

and

$$E^b = T^{-1,T} \bar{E}^b T^{-1} \tag{2.59}$$

Since $\bar{E}^m$ and $\bar{E}^b$ are symmetrical, E^m and E^b are also symmetrical. As will be seen later, this will lead to a symmetrical stiffness matrix, which is very desirable. When the matrix operations indicated in Eqs. (2.58) and (2.59) are performed, the explicit forms of E^m and E^b are found to be

$$E^m = \frac{Eh}{1-\nu^2} \begin{bmatrix} \csc^2\chi & \nu + \cot^2\chi & -\csc\chi\cot\chi \\ \nu + \cot^2\chi & \csc^2\chi & -\csc\chi\cot\chi \\ -\csc\chi\cot\chi & -\csc\chi\cot\chi & \frac{1-\nu}{2} + \cot^2\chi \end{bmatrix} \tag{2.60}$$

$$E^b = \frac{Eh^3}{12(1-\nu^2)} \begin{bmatrix} \csc^2\chi & \nu + \cot^2\chi & -\csc\chi\cot\chi \\ \nu + \cot^2\chi & \csc^2\chi & -\csc\chi\cot\chi \\ -\csc\chi\cot\chi & -\csc\chi\cot\chi & \frac{1-\nu}{2} + \cot^2\chi \end{bmatrix} \tag{2.61}$$

Finally, the expressions for the membrane strain energy U^m and the bending strain energy U^b are,

$$U^m = \tfrac{1}{2} \int\int \sigma^{m,T}\ \varepsilon^m \sin\chi\ dxdy =$$

$$= \tfrac{1}{2} \int\int \varepsilon^{m,T}\ E^{m,T}\ \varepsilon^m \sin\chi\ dxdy \qquad (2.62)$$

and

$$U^b = \tfrac{1}{2} \int\int \sigma^{b,T}\ \varepsilon^b \sin\chi\ dxdy =$$

$$= \tfrac{1}{2} \int\int \varepsilon^{b,T}\ E^{b,T}\ \varepsilon^b \sin\chi\ dxdy \qquad (2.63)$$

where the integrations extend over the middle surface of the shell. The total strain energy is, as before,

$$U = U^m + U^b \qquad (2.64)$$

U^m and U^b are of course, identical to $\bar{U}^m$ and $\bar{U}^b$ respectively, as given by Eqs. (2.19), (2.20) and (2.21). In fact, the strains referred to the oblique coordinate system were defined by equating the strain energy densities (see Eqs. (2.47) and (2.48)) in the two coordinate systems.

In Chapter 3, the expressions for membrane and bending strain energy will be utilized in the application of the finite element method.

3. METHOD OF ANALYSIS

3.1 General

The idealization of continuous structures as assemblages of individual pieces or elements has often been used as a device for obtaining approximate solutions to problems which are insoluble in their original form (25). This discretization of the structure results in the replacement of the original governing ordinary or partial differential equations by a set of linear algebraic equations. With the general availability of high-speed electronic computers, this reduction of the problem is significant, since the solution of large systems of linear algebraic equations poses no difficulty. When two or three dimensional elements are employed, the method is generally referred to as the "finite-element" method.

The finite element method historically has been visualized by supposing the structure to be "cut up" or divided into a number of sub-regions or elements, which are interconnected at a finite number of points, or "nodes". The force-deformation properties for an individual element, expressing relationships between nodal forces and displacements are established usually by employing a variational principle. Once this relationship is determined, the remainder of the analysis follows the usual procedure of the stiffness method of structural analysis. Therefore, it

is the determination of the nodal force-deformation relations for the element, or "element stiffness matrix" which is the significant portion of the analysis.

If the displacements of the structure are regarded as the fundamental unknown quantities, the principle of minimum total potential energy may be employed to obtain the element stiffness matrix. Other variational principles can be employed in the finite element method (38, 18, 24), however the potential energy principle is most often used (47, 30) and is used here.*

In any numerical approach to a given problem questions of convergence are very important. A great deal of attention has been focussed on such questions in the case of the finite element method (30, 18, 6), and much remains to be done in this area. Most of the early investigations of convergence simply involved successive refinements of grid size and comparisons with existing analytical solutions. While this procedure certainly does not prove convergence it at least allows one to gain some confidence in the method in the absence of theoretical assurances of convergence.

Melosh (30) formulated the finite element method in terms of the principle of minimum potential energy, and set forth some criteria for selecting displacement fields. He

---

* It may be mentioned here that the finite element method is not restricted to problems of structural analysis. It may be applied to any field problem which is formulated in variational terms.

distinguished between three types of errors which can occur:

1) Idealization errors, such as those involved in replacing a shell structure by an assemblage of flat elements.
2) Discretization errors, such as those involved in assuming the form of the displacements within an element.
3) Manipulation or round-off errors in the arithmetical operations.

Variational principles can, at best, guarantee the convergence of the discretization error to zero as the grid size is refined. Thus, in order to relate the finite element method directly to variational methods, the idealization error should be eliminated if possible. In the present case, the use of curved elements achieves this end.

The admissibility criterion of the coordinate functions in the conventional Rayleigh Ritz method is equivalent to the criterion of "sufficient" continuity* of the assumed displacements, together with the imposition of the forced boundary conditions at a later stage in the analysis. Likewise, the usual "completeness" criterion of the Rayleigh-Ritz method is analogous to the inclusion of rigid body displacements and constant strain states in the assumed displacements. Melosh (30), and Bazely et. al. (6) have

---

* "Sufficient" continuity here means that u, v, w, $w_{,x}$, and $w_{,y}$ are continuous over the entire structure.

enunciated these requirements. It must be remarked, however, that the above conditions guarantee monotonic convergence only to the true value of the potential energy. Uniform convergence to the true displacements and derivatives of displacements (i.e. stresses) does not necessarily follow. It is interesting to note that omission of terms representing a constant strain state has apparently resulted in convergence to incorrect results in applications to plate bending problems (12).

Bazely et. al. (6) have presented the argument that the only necessary requirements for convergence to the true energy level are the inclusion of a complete rigid body motion and all constant strain states, although convergence is no longer monotonic in this case. The conclusion that these requirements are sufficient to guarantee convergence is reasonable since successive refinements of grid size lead to ever-increasing satisfaction of continuity between elements, thus producing, in the limit, an admissible displacement field. In support of this argument, results of plate-bending analyses comparing "conforming" and "non-conforming" displacement assumptions were presented (6) and showed, in almost all cases and for all grid sizes, that the so-called "non-conforming" displacement field produced superior, although not monotonically converging, results.

Herein, displacement functions are selected in this spirit; continuity is sacrificed for completeness. As will be seen later, for one of the displacement functions employed,

a choice arises between achieving inter-element continuity and including a complete rigid body displacement. The latter is chosen. In practice, it may be true that neither is all-important, as Haisler and Stricklin (22) have shown that omission of rigid body terms for shells of revolution does not affect convergence. This conclusion is borne out by results, not reported herein, of comparative studies using element stiffness matrices derived subsequently, with and without inclusion of complete rigid body motions. However when the finite element method is regarded as a physical idealization rather than a mathematical one it is more satisfying to deal with a stiffness matrix which is "equilibrated", that is, one which gives rise to self-equilibrating nodal forces due to nodal displacements, and this is achieved through the inclusion of a complete rigid body motion in the assumed displacements.

In principle, it is possible to include Lagrangian multiplier terms to take into account the effect of discontinuities (26). However, this significantly increases the computational effort involved in obtaining a solution. It seems preferable instead to refine the grid size in order to obtain greater accuracy.

3.2 Review of Method of Derivation of Element Stiffness Matrix

For the sake of completeness, and in order to introduce notation used later, a brief account is given in

this section of the method of derivation of the element stiffness matrix. For fuller details, reference may be made to any of a number of works, for example, Clough (11) or Gallagher (19). The notation used by Gallagher (19) is, for the most part, used here.

The form of the displacements within the kth subregion or element is assumed to be

$$\begin{bmatrix} u \\ v \\ w \end{bmatrix} = M\alpha_{(k)} \qquad (3.1)$$

where M is a (3x20) matrix, which is a function of position within the element and $\alpha_{(k)}$ is a (20x1) column vector of, as yet, undetermined constants. It is assumed at this stage that the displacements defined by Eq. (3.1) give rise to a sufficiently continuous displacement field over the entire structure, as discussed in Sec. 3.1, since no account will be taken of discontinuities in computing the approximate total potential energy of the structure.

The projection of the kth element on the horizontal plane is shown in Fig. 9. The local coordinates of the element are (x,y). The element has projected lengths of 2a and 2b along the x and y axes respectively, and a skew angle of χ.

The (5x1) column vector,

$$q_{(k)} = \begin{Bmatrix} u \\ v \\ w \\ w,_y \\ -w,_x \end{Bmatrix} \tag{3.2}$$

is computed from Eq. (3.1), with the result that

$$q_{(k)} = M' \alpha_{(k)} \tag{3.3}$$

in which M' is a (5x20) matrix, the first three rows of which are identical to M. The last two rows of M' are obtained by differentiating the third row of M in accordance with Eq. (3.2).

The nodal values of $q_{(k)}$ are denoted by q_I, q_{II}, q_{III}, and q_{IV}, in accordance with the numbering scheme shown in Fig. 9. The (20x1) nodal displacement vector of the kth element is then

$$u_{(k)} = \begin{Bmatrix} q_I \\ q_{II} \\ q_{III} \\ q_{IV} \end{Bmatrix} \tag{3.4}$$

A relationship may now be found between the undetermined constants $\alpha_{(k)}$ and the nodal displacements $u_{(k)}$, since

$$u_{(k)} = B \alpha_{(k)} \tag{3.5}$$

where

$$B = \begin{Bmatrix} M'_I \\ M'_{II} \\ M'_{III} \\ M'_{IV} \end{Bmatrix}$$

and M'_I, M'_{II}, M'_{III}, M'_{IV}, indicates insertion of the local coordinates of nodes I, II, III and IV respectively in the matrix M'. B is thus a constant matrix containing the coordinates of the four nodes of the kth element. The constants $\alpha_{(k)}$ could have been retained as the generalized coordinates of the problem, however it is desirable to express them in terms of the new set of generalized coordinates $u_{(k)}$, since the forced boundary conditions, which must be imposed later, are stated directly in terms of $u_{(k)}$. In contrast to the conventional Rayleigh Ritz method in which the coordinate functions are chosen to satisfy the forced boundary conditions a priori, in the finite element method, no distinction is made between an element in the interior of the region and an element on the boundary in the initial derivation. The forced boundary conditions are imposed when the structure stiffness matrix is assembled, thus producing an admissible displacement field. The great advantage of the finite element method is that it is formulated independently of boundary conditions, and the mere specification of appropriate boundary nodal displacements produces a displacement field satisfying the forced boundary conditions of the problem.

If the matrix B is non-singular, which must be regarded as an additional restriction on M, Eq. (3.5) may be inverted to yield,

$$\alpha_{(k)} = B^{-1} u_{(k)} \tag{3.6}$$

which, with Eq. (3.1) gives

$$q_{(k)} = M' B^{-1} u_{(k)} \tag{3.7}$$

An examination of Eq. (3.7) reveals whether or not the continuity conditions are satisfied. In general, if a quantity, defined according to Eq. (3.7), along a given boundary of the element depends only on nodal values of generalized displacement at nodes on that boundary, it is continuous between elements.

The strains $\varepsilon^m_{(k)}$ and $\varepsilon^b_{(k)}$ may now be computed from Eq. (3.1), by employing the strain - displacement relations, Eqs. (2.54) and (2.55), as

$$\varepsilon^m_{(k)} = D^m \alpha_{(k)}$$

and

$$\varepsilon^b_{(k)} = D^b \alpha_{(k)} \tag{3.8}$$

or, with the use of Eq. (3.6), as

$$\varepsilon^m_{(k)} = D^m B^{-1} u_{(k)}$$

and

$$\varepsilon^b_{(k)} = D^b B^{-1} u_{(k)} \tag{3.9}$$

Approximations to the strain energy are now obtained by inserting Eqs. (3.9) in Eqs. (2.62) and (2.63) to yield

$$U^{*}_{(k)} = U^{*m}_{(k)} + U^{*b}_{(k)} \tag{3.10}$$

where

$$U^{*m}_{(k)} = \tfrac{1}{2}\, u^{T}_{(k)} B^{-1,T} \left\{ \iint D^{m}, T_E^{m}, T_D^{m} \sin \chi \, dxdy \right\} B^{-1} u_{(k)} \tag{3.11}$$

and

$$U^{*b}_{(k)} = \tfrac{1}{2}\, u^{T}_{(k)} B^{-1,T} \left\{ \iint D^{b}, T_E^{b}, T_D^{b} \sin \chi \, dxdy \right\} B^{-1} u_{(k)} \tag{3.12}$$

The stars indicate that the values are computed from approximate displacement modes.

The vector $\vec{p}$ of distributed external loading is resolved into components along the x and y axes and normal to the shell, so that

$$\vec{p} = p_u \hat{e}_x + p_v \hat{e}_y + p_w \hat{n} \tag{3.13}$$

As a result, the approximate potential of the external distributed loading is

$$\Omega^{*}_{(k)} = - \left\{ \int \int p^{T} M \sin \chi \, dxdy \right\} B^{-1} u_{(k)} \tag{3.14}$$

where

$$p = \begin{Bmatrix} p_u \\ p_v \\ p_w \end{Bmatrix}$$

Concentrated loads are resolved in the same manner as the distributed loading to yield

$$\Omega^{*\,c}_{(k)} = - p_c^{T} M_c B^{-1} u_{(k)} \tag{3.15}$$

where

$$P_c = \begin{Bmatrix} P_u \\ P_v \\ P_w \end{Bmatrix}$$

and M_c is obtained by inserting into M the local coordinates of the point at which the concentrated load acts. Let the (Nx1) column vector of structure displacements be denoted by u. Then the relation between the nodal displacements of the kth element and the structure displacements is expressed by the (20xN) "localizing" matrix $L_{(k)}$, such that

$$u_{(k)} = L_{(k)}\, u \tag{3.16}$$

When no transformation of coordinates is required in order to impose the forced boundary conditions, $L_{(k)}$ consists of zeroes and ones. When transformations are required, $L_{(k)}$ contains the appropriate transformation matrix.

The approximate total potential of the kth element is

$$\begin{aligned} V^*_{(k)} = \tfrac{1}{2}\, u^T L^T_{(k)} B^{-1,T} \Big\{ \iint [& D^m, T_E{}^m, T_D{}^m \\ & + D^b, T_E{}^b, T_D{}^b]\ \sin\chi\ dxdy \Big\} B^{-1} L_{(k)} u \\ & - \Big[\iint p^T M \sin\chi\ dxdy \Big] B^{-1} L_{(k)} u \\ & - \Big[P_c^T M_c \Big] B^{-1} L_{(k)} u \end{aligned} \tag{3.17}$$

The approximate total potential of the entire structure is computed by summing over the M elements or

regions. Therefore

$$V^* = \sum_{k=1}^{M} \left[\tfrac{1}{2} u^T L_{(k)}^T K_{(k)} L_{(k)} u - P_{(k)}^T L_{(k)} U \right] \tag{3.18}$$

where

$$K_{(k)} = B^{-1,T} \left[\iint (D^m, T_E^m, T_D^m + D^b, T_E^b, T_D^b) \sin \chi \, dxdy \right] B^{-1} \tag{3.19}$$

and

$$P_{(k)}^T = \left[P_C^T M_C + \iint p^T M \sin \chi \, dxdy \right] B^{-1} \tag{3.20}$$

V^* is now minimized with respect to the N generalized coordinates u, yielding

$$\sum_{k=1}^{M} \left[L_{(k)}^T \, K_{(k)} \, L_{(k)} \, u - L_{(k)}^T \, P_{(k)} \right] = 0 \tag{3.21}$$

since $K_{(k)}$ is symmetric.

If the notation

$$K = \sum_{k=1}^{M} L_{(k)}^T \, K_{(k)} \, L_{(k)} \tag{3.22}$$

$$P = \sum_{k=1}^{M} L_{(k)}^T \, P_{(k)} \tag{3.23}$$

is introduced, Eq. (3.21) may be rewritten as

$$K u = P \tag{3.24}$$

where K is called the structure stiffness matrix, and $K_{(k)}$ as given by Eq. (3.19) is the element stiffness matrix, which may be decomposed into a "bending" stiffness matrix

$K^{b}_{(k)}$ and a "membrane" stiffness matrix, $K^{m}_{(k)}$. Therefore

$$K_{(k)} = K^{m}_{(k)} + K^{b}_{(k)} \tag{3.25}$$

where

$$K^{m}_{(k)} = B^{-1,T}\left\{ \iint D^{m},T_{E}{}^{m},T_{D}{}^{m} \sin\chi \; dxdy \right\} B^{-1} \tag{3.26}$$

and

$$K^{b}_{(k)} = B^{-1,T}\left\{ \iint D^{b},T_{E}{}^{b},T_{D}{}^{b} \sin\chi \; dxdy \right\} B^{-1} \tag{3.27}$$

The same result is obtained by first minimizing the potential energy of the kth element or region and then assembling the element stiffness matrices to form the structure stiffness matrix.

It is to be emphasized that the actual generation of the structure stiffness matrix is not carried out in this way since much more efficient algorithms are available (45). The above approach, however, permits a convenient symbolic formulation of the procedure.

Eq. (3.24) is a set of linear algebraic equations which are solved to yield the values of the structure displacements (or generalized coordinates) u. Several methods of solution are available. The method used herein is the "Choleski" or "square-root" method (15) which is very efficient for positive-definite symmetric band matrices.

The column vector $P_{(k)}$ given by Eq. (3.20) is normally designated as the "generalized loading vector" for the kth element. In order to consistently apply the

variational method the generalized loads should be computed, rather than simply "lumping" the external distributed loads at the nodes to produce a statically equivalent set. This point has been noted by several writers (47, 5).

The stress resultants at a general location (x,y) in the kth element may be computed using Eqs. (2.56), (2.57), and (3.9), so that

$$\sigma^{m}_{(k)} = E^{m} D^{m} B^{-1} u_{(k)} \tag{3.28}$$

and

$$\sigma^{b}_{(k)} = E^{b} D^{b} B^{-1} u_{(k)}$$

or

$$\sigma_{(k)} = E D B^{-1} u_{(k)} \tag{3.29}$$

where

$$\sigma_{(k)} = \left\{ \begin{array}{c} \sigma^{m}_{(k)} \\ \hline \sigma^{b}_{(k)} \end{array} \right\}$$

and

$$E D = \left[\begin{array}{cc} E^{m} & D^{m} \\ \hline E^{b} & D^{b} \end{array} \right]$$

The matrix EDB^{-1} is termed the stress matrix, and $E^{m}D^{m}B^{-1}$ and $E^{b}D^{b}B^{-1}$ the membrane and bending stress matrices respectively.

Other procedures for computing stresses from the nodal displacements have been proposed (34), however Eqs. (3.28) and (3.29) are used herein, since it is desired to formulate the method in a manner which emphasizes as much as possible its relationship with the Rayleigh - Ritz method.

In the following sections, explicit forms will be given for the various matrices used above in symbolic form.

The equilibrium equations for the shallow shell do not appear in the derivation, and to solve the problem by the finite element method, knowledge of them is not required. However, they can easily be obtained by first substituting the strain-displacement relations, Eqs. (2.54) and (2.55) into the strain energy expressions, Eqs. (2.62) and (2.63), adding the potential of externally distributed loads and setting equal to zero the first variation of the potential energy. This procedure yields the natural boundary conditions as well as the equilibrium equations. The equilibrium equations so obtained are given in Appendix A, since they will be specialized for various cases and used for the comparison analytical solutions discussed in Chapter 4.

3.3 Rigid Body Motion

In this section, the expression for a rigid body motion of a shallow shell is determined.* The displacements u^R, v^R, and w^R corresponding to a rigid body motion are defined as the solutions of the homogeneous Eqs. (2.54) and (2.55). That is,

---

* Under an exact rigid body motion, the shallow shell equations yield non-vanishing stresses due to the approximations which are made. What is desired here is an expression for a "rigid body motion" within the accuracy of the theory.

$$u^R_{,x} - rw^R = 0$$
$$v^R_{,y} - tw^R = 0 \qquad (3.30)$$
$$u^R_{,y} + v^R_{,x} - 2\,sw^R = 0$$

$$w^R_{,xx} = 0$$
$$w^R_{,yy} = 0 \qquad (3.31)$$
$$w^R_{,xy} = 0$$

Integration of Eqs. (3.31) immediately yields

$$w^R = \alpha_9 + \alpha_{10}\,x + \alpha_{11}\,y \qquad (3.32)$$

where α_9, α_{10}, α_{11} are constants.

Substitution of Eq. (3.32) into Eq. (3.30) and integration yields

$$u^R = \alpha_1 + \alpha_9\,(rx + sy) + \alpha_{10}\,(\frac{rx^2}{2} - \frac{ty^2}{2}) + \alpha_{11}\,(rxy + sy^2) \qquad (3.33)$$

and

$$v^R = \alpha_5 + \alpha_9\,(sx + ty) + \alpha_{10}\,(sx^2 + txy) + \alpha_{11}\,(\frac{ty^2}{2} - \frac{rx^2}{2}) \qquad (3.34)$$

The rigid body displacement

$$u = ky$$
$$v = -kx$$

has been dropped from Eqs. (3.33) and (3.34) since it corresponds to the enforcement of equilibrium of moments about

the normal to the middle surface, which is violated by the assumptions of shallow shell theory.

The inclusion of the five rigid body motions represented in Eqs. (3.32), (3.33) and (3.34) in the assumed displacement functions guarantees that the stiffness matrix will be such that self-equilibrating nodal forces are produced by arbitrary nodal displacements.* As will be seen later, the price that is paid for the inclusion of all five rigid body degrees of freedom is the introduction of some inter-element in-plane discontinuities due to the presence of the α_9, α_{10} and α_{11} terms in the u and v displacements.

3.4 Choice of Displacement Functions

The choice of displacement functions is the crucial step in the finite element method. With this in mind, two separate stiffness matrices are presented, using different displacement assumptions. Both represent adaptations to shallow shell analysis of displacement functions which have been used in plate bending and plane stress analyses.

3.4.1. Melosh - Zienkiewicz Polynomial

The first of the displacement shapes is obtained from the twelve-parameter polynomial expression for w used by Melosh (30), Zienkiewicz (47) and many others in plate bending analyses. It is combined with the usual plane stress

---

* This is equivalent to the statement that no strain energy is produced by a rigid body displacement of the element.

functions for u and v, augmented to include the rigid body motion discussed in Sec. 3.3. Therefore,

$$u = \alpha_1 + \alpha_2 x + \alpha_3 y + \alpha_4 xy + \alpha_9 (rx + sy) + \alpha_{10} \left(\frac{rx^2}{2} - \frac{ty^2}{2}\right) + \alpha_{11} (rxy + sy^2) \qquad (3.35)$$

$$v = \alpha_5 + \alpha_6 x + \alpha_7 y + \alpha_8 xy + \alpha_9 (sx + ty) + \alpha_{10} (sx^2 + txy) + \alpha_{11} \left(\frac{ty^2}{2} - \frac{rx^2}{2}\right)$$

$$w = \alpha_9 + \alpha_{10} x + \alpha_{11} y + \alpha_{12} xy + \alpha_{13} x^2 + \alpha_{14} y^2 + \alpha_{15} x^3 + \alpha_{16} x^2 y + \alpha_{17} xy^2 + \alpha_{18} y^3 + \alpha_{19} x^3 y + \alpha_{20} xy^3$$

The matrix B^{-1} for this case is shown in Table 1. It is well known (47) that the above form for the normal displacement gives rise to discontinuities of derivatives of w normal to the boundaries between elements. The explicit form for the in-plane displacement u may be obtained from Eq. (3.35) and Table 1. It is

$$u = \left[\tfrac{1}{4} \left(1 - \frac{x}{a}\right)\left(1 - \frac{y}{b}\right)\right] u_1 + \left[\tfrac{1}{4} \left(1 - \frac{x}{a}\right)\left(1 + \frac{y}{b}\right)\right] u_2 + \left[\tfrac{1}{4} \left(1 + \frac{x}{a}\right)\left(1 - \frac{y}{b}\right)\right] u_3 + \left[\tfrac{1}{4} \left(1 + \frac{x}{a}\right)\left(1 + \frac{y}{b}\right)\right] u_4 + \left(1 - \frac{x^2}{a^2}\right) \left[\frac{3ar}{16} (w_1 + w_2 - w_3 - w_4) + \frac{abr}{16} (\theta_{x_1} - \theta_{x_2} - \theta_{x_3} + \theta_{x_4}) - \frac{a^2 r}{16} (\theta_{y_1} + \theta_{y_2} + \theta_{y_3} + \theta_{y_4})\right] \qquad (3.36)$$

$$+ \left(1 - \frac{y^2}{b^2}\right) \left[\frac{3b^2t}{16a} \left(-w_1 - w_2 + w_3 + w_4\right) + \frac{3sb}{8} \left(w_1 - w_2 + w_3 - w_4\right) \right.$$

$$+ \frac{b^3t}{16a} \left(-\theta_{x_1} + \theta_{x_2} + \theta_{x_3} - \theta_{x_4}\right) + \frac{sb^2}{8} \left(\theta_{x_1} + \theta_{x_2} + \theta_{x_3} + \theta_{x_4}\right)$$

$$\left. + \frac{b^2t}{16} \left(\theta_{y_1} + \theta_{y_2} + \theta_{y_3} + \theta_{y_4}\right) + \frac{abs}{8} \left(-\theta_{y_1} + \theta_{y_2} + \theta_{y_3} - \theta_{y_4}\right) \right]$$

where $\theta_x = w,_y$ and $\theta_y = -w,_x$ and the subscripts refer to the appropriate nodes. From Eq. (3.36) it can be seen that unless r, s and t are all zero, the value of u along an edge of the element is not defined solely by the generalized displacements at the nodes on that edge. Obviously, the situation is the same for v. Thus, due to the inclusion of the α_9, α_{10} and α_{11} terms in the expressions for u and v given in Eq. (3.35), discontinuities in the in-plane displacements appear.

In order to simplify the tables, the notation

$$\begin{aligned} c_1 &= \csc^2 \chi \\ c_2 &= \frac{1-\nu}{2} + \cot^2 \chi \\ c_3 &= \nu + \cot^2 \chi \\ c_4 &= -\cot \chi \csc \chi \end{aligned} \tag{3.37}$$

is introduced for the elements of the E^m and E^b matrices. Also introduced are

$$\begin{aligned} f_1 &= rc_1 + tc_3 + 2sc_4 \\ f_2 &= rc_3 + tc_1 + 2sc_4 \\ f_3 &= rc_4 + tc_4 + 2sc_2 \\ g_1 &= rf_1 + tf_2 + 2sf_3 \end{aligned} \tag{3.38}$$

The matrices

$$\left[\int\int D^{m,T}\, E^{m,T}\, D^{m} \sin\chi \; dxdy\right] ,$$

and

$$\left[\int\int D^{b,T}\, E^{b,T}\, D^{b} \sin\chi \; dxdy\right]$$

for the case of the constant thickness element are presented in Tables 2 and 3 respectively. The matrices $E^m D^m$, and $E^b D^b$ used in computing the stresses are given in Table 4.

3.4.2. Birkhoff - Garabedian Interpolation Formula

The second displacement shape used is obtained from a 12-parameter "compatible" interpolation formula developed by Birkhoff and Garabedian (7), which has been applied to plate bending problems by Deák and Pian (14). Three of the twelve functions are defined in a piecewise fashion throughout the region in order to obtain compatible normal derivatives of the lateral displacement. The use of Hermitian polynomials has been proposed (8) in order to achieve this continuity, however it appears that to include all constant strain states additional nodal degrees of freedom must be introduced, which is a computational disadvantage. Therefore, the 12-parameter form for w is used here.

It is convenient in this case to use dimensionless local coordinates (ξ, η) defined by

$$\begin{aligned} \xi &= x/a \\ \eta &= y/b \end{aligned} \qquad (3.39)$$

The displacements of the "compatible" element are now assumed to be

$$u = \tilde{\alpha}_1 + \tilde{\alpha}_2\xi + \tilde{\alpha}_3\eta + \tilde{\alpha}_4\xi\eta + \tilde{\alpha}_9 (ar\xi + sb\eta)$$
$$+ \tilde{\alpha}_{10} \left(\frac{ar\xi^2}{2} - \frac{b^2t\eta^2}{2a}\right) + \tilde{\alpha}_{11} (ar\xi\eta + bs\eta^2)$$

$$v = \tilde{\alpha}_5 + \tilde{\alpha}_6\xi + \tilde{\alpha}_7\eta + \tilde{\alpha}_8\xi\eta + \tilde{\alpha}_9 (as\xi + bt\eta) \qquad (3.40)$$
$$+ \tilde{\alpha}_{10} (as\xi^2 + bt\xi\eta) + \tilde{\alpha}_{11} \left(\frac{bt\eta^2}{2} - \frac{a^2r\xi^2}{2b}\right)$$

$$w = \tilde{\alpha}_9 + \tilde{\alpha}_{10}\xi + \tilde{\alpha}_{11}\eta + \tilde{\alpha}_{12}\xi\eta + \tilde{\alpha}_{13}\xi^2 + \tilde{\alpha}_{14}\eta^2 + \tilde{\alpha}_{15}\xi^3$$
$$+ \tilde{\alpha}_{16}F_6 + \tilde{\alpha}_{17}F_9 + \tilde{\alpha}_{18}\eta^3 + \tilde{\alpha}_{19}F_{11} + \tilde{\alpha}_{20}F_{12}$$

Eight of the twelve functions given by Birkhoff and Garabedian are the same as those used in Eq. (3.35).

To define the functions F_6, F_9, F_{11} and F_{12} the region $|\xi| \leq 1$, $|\eta| \leq 1$ is divided into subregions (a), (b), (c), and (d) as shown in Fig. 10. F_{11} is defined throughout the entire region as

$$F_{11} = \xi\eta \left[3 (\xi^2 + \eta^2) - \xi^2 \eta^2 - 5\right] \qquad (3.41)$$

The three remaining functions F_6, F_9, and F_{12} are defined in the four sub-regions as follows

Sub-Region (a): $F_6 = \xi^2 - 2\xi + \eta^2$

$F_9 = 2\eta (\xi - 1)$

$F_{12} = \frac{1}{4}\eta (\xi^3 - 3\xi) (\eta^2 - \xi^2)$

Sub-Region (b):
$$F_6 = 2\xi\,(\eta - 1)$$
$$F_9 = \eta^2 - 2\eta + \xi^2 \qquad (3.42)$$
$$F_{12} = \tfrac{1}{4}\xi\,(\eta^3 - 3\eta)\,(\eta^2 - \xi^2)$$

Sub-Region (c):
$$F_6 = -\,(\xi^2 + 2\xi + \eta^2)$$
$$F_9 = -\,2\eta\,(\xi + 1)$$
$$F_{12} = \tfrac{1}{4}\eta\,(\xi^3 - 3\xi)\,(\eta^2 - \xi^2)$$

Sub-Region (d):
$$F_6 = -\,2\xi\,(\eta + 1)$$
$$F_9 = -\,(\eta^2 + 2\eta + \xi^2)$$
$$F_{12} = \tfrac{1}{4}\xi\,(\eta^3 - 3\eta)\,(\eta^2 - \xi^2)$$

It can be shown (7) that the twelve displacement functions given in the third of Eqs. (3.40) are such that they vary at most cubically along a given boundary, and the normal derivative has, at most, a linear variation. Thus w, $w_{,\xi}$ and $w_{,\eta}$ are continuous between elements. From an examination of the definitions of the functions F_6, F_9, and F_{12}, it is apparent that w, $w_{,\xi}$ and $w_{,\eta}$ are continuous within an element but discontinuities in the second partial derivatives occur along the boundaries of the sub-regions in Fig. 10. Therefore, in evaluating the curvatures at a node, for example, an average is taken of the values defined in the two separate sub-regions common to that particular node.

The matrix $\overset{\gamma}{B}^{-1}$ for this displacement assumption is shown in Table 5. An examination of the in-plane displacement forms expressed in terms of nodal displacements yields

$$u = \tfrac{1}{4}\left[(1-\xi)(1-\eta)\right]u_1 + \tfrac{1}{4}\left[(1-\xi)(1+\eta)\right]u_2 + \tfrac{1}{4}\left[(1+\xi)(1-\eta)\right]u_3$$
$$+ \tfrac{1}{4}\left[(1+\xi)(1+\eta)\right]u_4$$
$$+ \frac{3}{16a}\left[a^2r(1-\xi^2) - b^2t(1-\eta^2) + 2sab(1-\eta^2)\right](w_1-w_4)$$
$$+ \frac{3}{16a}\left[a^2r(1-\xi^2) - b^2t(1-\eta^2) - 2sab(1-\eta^2)\right](w_2-w_3) \qquad (3.43)$$
$$+ \frac{sb^2}{8}(1-\eta^2)\left(\theta_{x_1}+\theta_{x_2}+\theta_{x_3}+\theta_{x_4}\right) + \frac{1}{16}\Big[-a^2r(1-\xi^2)$$
$$+ b^2t(1-\eta^2)\Big]\left(\theta_{y_1}+\theta_{y_2}+\theta_{y_3}+\theta_{y_4}\right)$$

and a similar expression for v. Again the inclusion of the complete rigid body displacement has led to in-plane discontinuities unless r, s, and t are all zero, in which case the skewed shell degenerates to a skewed flat plate. Thus, for a skewed plate, the displacement functions, Eqs. (3.40) satisfy the continuity requirements and should yield a solution which converges monotonically to the true energy level. If the coupling effect between the in-plane and normal displacements were disregarded as far as the rigid body motion is concerned, that is, if the $\tilde{\alpha}_9$, $\tilde{\alpha}_{10}$ and $\tilde{\alpha}_{11}$ terms were omitted from the expressions for u and v in Eq. (3.40), the continuity requirements would be fulfilled for non-zero r, s, and t as well. In fact, comparative studies, referred to earlier, have shown that solutions are insensitive to whether this is done or not. In all examples presented in this study, however, the complete rigid body motion is included.

The matrices

$$\left[\int\int \tilde{D}^{m,T} E^{m,T} \tilde{D}^{m} \sin\chi \; dxdy \right] ,$$

and

$$\left[\int\int \tilde{D}^{b,T} E^{b,T} \tilde{D}^{b} \sin\chi \; dxdy \right]$$

are presented in Tables 6 and 7, once again for the case of uniform thickness. In Table 8, the matrix $E\tilde{D}$ is given. This matrix is valid only at the nodes of the element since, in place of the functions F_6, F_9, F_{12}, and their derivatives which have certain symmetry properties, simpler functions with the same symmetry properties have been inserted. For example, $F_{6,\xi\xi}$ is an odd-even function (an odd function of ξ and an even function of η), with averaged nodal values $\pm$ 1. Therefore, to give the same nodal values the function $1 \cdot \xi$ may be substituted for it. This simplifies the programming.

For simplicity, the two element stiffness matrices developed in this section will be referred to as "non-compatible" (Sec. 3.4.1) and "compatible" (Sec. 3.4.2) although strictly speaking the element displacement field used in Sec. 3.4.2 is completely compatible only when (r,s,t) are all zero (i.e. a skewed plate) or when the $\tilde{\alpha}_9$, $\tilde{\alpha}_{10}$, $\tilde{\alpha}_{11}$ terms are omitted from the expressions for u and v in Eq. (3.40) (i.e. a complete rigid body motion is not included).

3.5 Generalized Nodal Forces for Uniform Pressure Loading

For the case of uniform pressure loading, the matrix of external distributed loading reduces to

$$p = \left\{ \begin{array}{c} 0 \\ 0 \\ p_o \end{array} \right\} \tag{3.44}$$

The column vector of nodal loads for this case is the same for the two displacement shapes which were introduced in Secs. 3.4.1 and 3.4.2. It is

$$P^T_{(k)(unif.)} = \left\{ 0,0,1,\frac{b}{3}, \ -\frac{a}{3},0,0,1, \ -\frac{b}{3}, -\frac{a}{3},0,0,1,\frac{b}{3},\frac{a}{3},0,0,1, \ -\frac{b}{3},\frac{a}{3} \right\}$$

$$\cdot \ a \ b \ p_o \ \sin \chi \tag{3.45}$$

If statically equivalent loads were used instead, the nodal moments $\pm \frac{b}{3}$, $\pm \frac{a}{3}$ would not appear. However, it is apparent from Eq. (3.45) that when four similar elements are joined together at a node, the sum of the nodal couples is zero. Therefore, in the interior of the shell, there is no difference between generalized and statically equivalent nodal forces for the case of uniform normal pressure loading and the particular sets of displacement functions chosen. On a boundary, where two elements are connected to a node, the nodal couple vectors normal to the boundary cancel. However, the nodal couple vectors in the direction tangent to the boundary, i.e. bending moments normal to the boundary, do not. Consequently, unless the boundary condition on this edge is such that rotation in the direction of the nodal moment is not permitted, a difference does exist between generalized and statically equivalent nodal forces, in the special case under discussion.

3.6 Stiffness Matrices for Edge Beams and Tie Rods

The stiffness matrix for a straight edge beam* is given in Table 9. The beam axis has an eccentricity e relative to the shell middle surface. The stiffness matrix for the case of zero eccentricity may be found in any one of a number of references (29, 45, 23) and the eccentricity is taken into account merely by a transformation of coordinates as shown in Appendix B. The stiffness matrix for an axial force member (the tie rod) is likewise readily available (29, 45, 23) and is not listed herein. The stiffness matrix for a curved edge beam** is listed in Table 10 and a brief account of its derivation is given in Appendix B. Eccentricity of the beam axis with respect to the shell middle surface is again considered.

3.7 Transformation of Stiffness Matrices

In order to satisfy forced boundary conditions which are expressed in terms of linear combinations of u, v, w, θ_x, and θ_y rather than in terms of a single one of these quantities, it is necessary to transform coordinates. This is a standard operation, and is dealt with in many works on matrix structural analysis (23). However, a brief outline is included here for completeness.

---

* Applicable in the case of a hyperbolic paraboloid bounded by characteristics.

** As in the case of shells bounded by lines of principal curvature

In order to facilitate the transformations, the (20x20) shell stiffness matrix is expanded to a (24x24) matrix by inserting rows and columns of zeroes corresponding to the sixth (neglected) degree of freedom at each node. Let the expanded (24x24) shell stiffness matrix be denoted by $\underline{K}$. The column vectors of nodal displacements and forces are likewise expanded to dimensions (24x1). These are denoted by $\underline{P}$ and $\underline{u}$ respectively. Therefore, in the original coordinate system,

$$\underline{P} = \underline{K}\,\underline{u} \tag{3.46}$$

If $\underline{P}$ is now transformed to the new coordinate system by the relation

$$P^* = T_o\,\underline{P} \tag{3.47}$$

it follows from the equality of work done in the two coordinate systems that the nodal displacements transform according to the relation

$$\underline{u} = T_o^T\,u^* \tag{3.48}$$

where u^*, P^* are the nodal displacements and forces respectively, in the new coordinate system.

Equations (3.47) and (3.48), together with Eq. (3.46) yield the desired relation

$$P^* = K^*\,u^* \tag{3.49}$$

where

$$K^* = T_o\,\underline{K}\,T_o^T \tag{3.50}$$

Thus, Eq. (3.50) expresses the transformation law for the stiffness matrix.

Beam and tie rod stiffness matrices may be transformed in an analogous manner.

3.8 Boundary Conditions

Several types of boundary conditions are defined in this section. It is to be emphasized that only forced boundary conditions are specified in the analysis. The natural boundary conditions, together with the equilibrium equations are satisfied approximately as part of the minimization procedure.* Thus, for example, on a free edge the nodal force in the direction of $\hat{n}$ is not to be set equal to zero in an attempt to satisfy the natural boundary condition of zero effective shear. In fact, for the free edge case, a uniform normal load would require such a nodal force (together with moments if generalized loads are used). It might be expected therefore that convergence would be superior for those problems in which all or most of the boundary conditions are of the forced type. Also, the extent to which the natural boundary conditions are satisfied for a given problem can be used as a means of assessing whether or not convergence is satisfactory in a practical sense.

Boundary conditions are defined below for an edge x = constant. Both forced and natural boundary conditions

---

* This, of course, is in agreement with the conventional Rayleigh-Ritz method in which the natural boundary conditions need not be satisfied by the coordinate functions.

are given for each case, together with the appropriate nodal displacements which are to be specified in the finite element analysis.

3.8.1. Simple Supports

The term "simple supports" is often used in the literature to signify quite different types of boundary conditions. Three types of simple supports are used herein, and are

3.8.1.1 Hinge Support

The boundary conditions for an edge x = constant are:

$$\begin{aligned} u &= 0 \\ v &= 0 \\ w &= 0 \\ M_x &= 0 \end{aligned} \tag{3.51}$$

The nodal displacements which are specified are

$$\begin{aligned} u &= 0 \\ v &= 0 \\ w &= 0 \\ \theta_x &= 0 \end{aligned} \tag{3.52}$$

The specification of $w = 0$ and $\theta_x = 0$ at the nodes are together equivalent to the condition $w = 0$ along the entire edge.

3.8.1.2 Roller Support

The boundary conditions for roller supports are

$$\begin{aligned} v &= 0 \\ w &= 0 \\ N_x &= 0 \\ M_x &= 0 \end{aligned} \tag{3.53}$$

and the specified nodal displacements are

$$\begin{aligned} v &= 0 \\ w &= 0 \\ \theta_x &= 0 \end{aligned} \tag{3.54}$$

3.8.1.3 Knife Edge Support

This type of support arises when Levy-type solutions are sought in the case of the hyperbolic paraboloid bounded by characteristics. The boundary conditions are

$$\begin{aligned} u &= 0 \\ w &= 0 \\ N_{xy} &= 0 \\ M_x &= 0 \end{aligned} \tag{3.55}$$

The specified nodal displacements are

$$\begin{aligned} u &= 0 \\ w &= 0 \\ \theta_x &= 0 \end{aligned} \tag{3.56}$$

3.8.2 Clamped Support

In this case, all of the boundary conditions are of the forced type. They are

$$\begin{aligned} u &= 0 \\ v &= 0 \\ w &= 0 \\ \theta_y &= 0 \end{aligned} \tag{3.57}$$

and the corresponding specified nodal displacements are

$$\begin{aligned} u &= 0 \\ v &= 0 \\ w &= 0 \\ \theta_x &= 0 \\ \theta_y &= 0 \end{aligned} \tag{3.58}$$

3.8.3 Free Edge

In contrast to the previous case, the boundary conditions here are all of the natural type. They are

$$\begin{aligned} N_x &= 0 \\ N_{xy} &= 0 \\ M_x &= 0 \\ R_x &= 0 \end{aligned} \tag{3.59}$$

where $R_x = Q_x + \frac{\partial Mxy}{\partial y}$

is the effective transverse edge shear, analogous to that occurring in Lagrange's plate theory.

In this case, no specification of nodal displacements is made.

3.8.4 Symmetry

For this case transformations are required. The boundary conditions are then

$$\begin{aligned} u^* &= 0 \\ \theta_y^* &= 0 \\ N_{xy}^* &= 0 \\ R_x^* &= 0 \end{aligned} \tag{3.60}$$

where the stars indicate transformation of the coordinate system; and u^* is the displacement normal to the plane of

symmetry, θ_y^* is the rotation vector in the plane of symmetry perpendicular to $\hat{n}$, and N_{xy}^* and R_x^* are the membrane shear and effective transverse shear respectively, in the plane of symmetry.

3.8.5 Corner Conditions

Several different boundary conditions at the shell corners are referred to in the numerical examples.

3.8.5.1 Pin Support

This signifies that no displacements are allowed, but the corner is free to rotate. The specified nodal displacements are then

$$\begin{aligned} u &= 0 \\ v &= 0 \\ w &= 0 \end{aligned} \qquad (3.61)$$

3.8.5.2 Horizontal Roller Support

The nodal displacement in the vertical direction is restrained. This also requires a coordinate transformation. The specification of nodal displacements is therefore

$$w_{vertical} = 0 \qquad (3.60)$$

3.8.5.3 Buttress Support

The buttress corner support is identical to the clamped support. Therefore the nodal displacements to be specified at the corner are

$$
\begin{aligned}
u &= 0 \\
v &= 0 \\
w &= 0 \\
\theta_x &= 0 \\
\theta_y &= 0
\end{aligned}
\tag{3.61}
$$

Once again the formal correspondence between quantities defined with respect to the oblique and orthogonal coordinate systems is apparent. The boundary conditions given above for the general (oblique) case have exactly the same form as the corresponding boundary conditions for the orthogonal case, $\chi = \pi/2$. Such is not the case if, for example, the bending moment vectors, as well as the in plane stress resultant vectors are referred to the unit vectors $\hat{e}_x$ and $\hat{e}_y$.

In the following chapter several numerical examples are presented and discussed.

4. NUMERICAL RESULTS

4.1 General

The examples presented in this chapter are of two main types. First, a variety of plate and shell problems for which analytical or other numerical solutions are available are analyzed. These problems are intended to substantiate the finite element method as applied to shallow shells and to enable one to evaluate in a limited sense the convergence characteristics of the two element stiffness matrices presented. Second, a group of problems of more practical interest are dealt with, in order to investigate the effects of skewedness, tie rods, and eccentric edge beams on the behaviour of hyperbolic paraboloids bounded by characteristics.

Three shells of fixed dimensions are chosen in order to isolate the effects of the various boundary conditions imposed on them. For ease of reference, they will be designated as Shell I, Shell II, and Shell III in the remainder of this chapter. The dimensions of the shells are given in Fig. 11.

Shell I is a square elliptical paraboloid with equal radii of curvature, for which considerable numerical data is presented in Reference (21).

Shell II is a square hyperbolic paraboloid bounded by lines of principal curvature. It is similar in dimensions

to Shell I except that the positive radius of curvature is approximately twice that of the negative radius of curvature.*

Shell III is a square hyperbolic paraboloid bounded by characteristics, for which numerical results obtained by a variational method have been given (10). The first main group of problems, comparisons with analytical and numerical results, are now discussed.

4.2 Skewed Plates

4.2.1 Simply-Supported Skewed Plate Under Central Concentrated Load

A simply supported rhombic plate of side length a with a skew angle of 72° is subjected to a concentrated central load -P. Analyses using both the compatible and non-compatible elements for grid sizes of (2x2), (4x4), and (8x8) over the entire plate were carried out. The central deflection vs. grid size is plotted in Fig. 13. The reference value of $w_c = -.01067\ Pa^2/D$ is taken from results presented by Aggarwala (3).

This problem illustrates the trend noted by Bazely et al. (6). For all grid sizes for which results have been obtained, the non-compatible element gives superior results,

---

* According to the sign convention used herein, positive curvature (i.e. positive r or t) is concave in the positive z direction.

although the convergence is not monotonic. However the inference that the non-compatible element always produces superior results is not correct as is shown by the next series of examples.

4.2.2 Clamped Skewed Plates Under Uniform Normal Load

A series of clamped rhombic plates of side length a, under uniform normal load $-p_o$ and with varying skew angles are analyzed. The central deflection, and the bending moments on diametral sections are given in Table 11 for skew angles of 75°, 60°, and 45° and compared with results given by Morley (33). The bending moments M_{ad} and M_{bc} are computed from the quantities M_x, M_y and M_{xy} by the formulae:

$$M_{bc} = \tfrac{1}{2} \cot \tfrac{\chi}{2} (M_x+2M_{xy}+M_y)$$

$$M_{ad} = \tfrac{1}{2} \tan \tfrac{\chi}{2} (M_x-2M_{xy}+M_y)$$

which are easily obtained by consideration of the equilibrium of differential elements of the plate.

Grid sizes of (8x8) over the entire plate are used for each element and for each skew angle. In addition, for the 60° skew plate, results of analyses using (12x12) grids over the entire plate are given.

Although the difference is not marked, for this series of plates the compatible element does produce more accurate results in most instances. For a given grid size, the accuracy of the central deflection and bending moment M_{bc} given by the compatible element analysis decreases as the

skew angle decreases. This difficulty has been noted by Morley (33) in his series solutions. The non-compatible element, on the other hand, is unpredictable, in some cases exhibiting decreasing accuracy as the skew angle decreases and in some cases not.

Generalized nodal loads must be used with the compatible element in order to consistently apply the variational procedure. However, with the non-compatible element it appears that statically equivalent nodal loads lead to greater accuracy than do the generalized nodal loads. The examples presented in Sections 4.2.1 and 4.2.2 were selected so that comparisons could be made between the two element stiffness matrices under the same nodal loads, since for the two problems analyzed in these Sections, the generalized and statically equivalent nodal loads are identical.

In the analysis of shell problems, complete compatibility is no longer achieved, so that it might appear that there is now nothing to be gained by employing generalized nodal loads. However, in some cases more accurate results are obtained when this more consistent procedure is followed, as will be shown in Section 4.3.2.1.

4.3 Simply Supported Shells: Comparisons with Series Solutions

4.3.1 Roller Supported Elliptical Paraboloid Under Central Concentrated Load: Comparison of Compatible and Non-Compatible Elements

Shell I, the square, equal radii-of-curvature elliptical paraboloid is roller supported on all edges, and subjected to a central concentrated load $-P_o$. Advantage is taken of symmetry, with grids of (6x6) being used on one quadrant of the shell. Fig. 14 shows the normal deflection $\bar{w}$, and the membrane stress resultant $N_{\bar{x}}$ across the section $\bar{x} = 0$ as given by the compatible and non-compatible element analyses. A Navier solution (3600 terms) is also plotted. No bending moments are shown since the double series for the moments are extremely poorly convergent and in fact are divergent under the concentrated load.

As expected, the deflections are highly localized near the point of application of the concentrated load. At this point, the deflection $\bar{w}$ computed using the non-compatible element is closest to the series solution. However, the compatible element results for $\bar{w}$ at all other points and for $N_{\bar{x}}$ across the entire section agree more closely with the "exact" series solution.

When sharp variations of displacements and stresses are expected, as is the case here because of the concentrated load, finer grids would normally be employed. The relatively

coarse (6x6) grids are used for purposes of illustration so that some distinction can be shown graphically between the two finite element analyses. As the grid size is further refined, the two finite element analyses agree more closely.

4.3.2 Roller Supported Elliptical Paraboloid Under Uniform Normal Load

The square equal radii-of-curvature elliptical paraboloid (Shell I) is roller supported on all edges and subjected to a uniform normal load of intensity $-p_o$. For this case, and for all cases investigated in which a shallow shell is subjected to a uniform normal load, the compatible and non-compatible element analyses agree to approximately three significant figures for grid sizes of (6x6) or finer. Therefore, since all shells treated subsequently are subjected to uniform normal loads, only the results of the compatible element analyses are given.

4.3.2.1 Comparison of Results Using Statically Equivalent and Generalized Nodal Loads

Grids of (6x6) are used on one quadrant of the shell. The normal deflection $\bar{w}$, the membrane stresses $N_{\bar{x}}$ and $N_{\bar{y}}$ across the mid-section $\bar{x} = 0$, and the membrane shear $N_{\bar{x}\bar{y}}$ across the end-section, $\bar{y} = L_y/2$ are shown in Figures 15 and 16, for statically equivalent and generalized nodal loads.

The maximum normal deflection occurs at a distance of approximately $L_y/9$ from the roller support, then decreases

slightly and remains essentially constant in the central region of the shell. Both nodal loadings produce close agreement with the exact solution near the center. Near the edge however, the generalized loading results in superior accuracy. As should be expected the agreement with the exact solution is much better for the uniform load case than for the concentrated load case discussed in Section 4.3.1.

The membrane force $N_{\bar{y}}$ across the mid-section $\bar{x} = 0$ is insensitive to the type of nodal loading used. The finite element results agree very well with the series solution in the central region of the shell where $N_{\bar{y}}$ is largest. Near the edge the finite element $N_{\bar{y}}$ force "dips" and underestimates the exact $N_{\bar{y}}$ force. As will be seen in further examples this occurs frequently and appears to be due to the lack of satisfaction of the natural boundary condition.

The plot of the membrane force $N_{\bar{x}}$ across the mid-section $\bar{x} = 0$ also demonstrates the superior accuracy achieved through use of generalized nodal loads in this particular case.

The most sensitive membrane force is $N_{\bar{x}\bar{y}}$ along the support $\bar{x} = L_x/2$. As the corner is approached, $N_{\bar{x}\bar{y}}$ rises to a maximum and in the region within a distance of approximately $L_y/9$ from the corner the finite element $N_{\bar{x}\bar{y}}$ force underestimates the exact $N_{\bar{x}\bar{y}}$. Once again the generalized nodal loads produce superior accuracy.

The bending moments vary extremely rapidly, and are large only in the region of the shell near the boundary. Therefore, in order to adequately approximate the bending moments, grid sizes of (9x9) on one quadrant of the shell are used. The bending moments $M_{\bar{x}}$ across the mid-section $\bar{y} = 0$ are shown in Fig. 17.

A reversal of the relative accuracy due to the two types of nodal loadings occurs here, the statically equivalent nodal loads producing the superior results. This may once again be traced to the degree of satisfaction of the natural boundary conditions. The computed values of $M_{\bar{x}}$ on the boundary are shown in Fig. 17, and it can be seen that the use of statically equivalent nodal loads results in more complete satisfaction of the natural boundary condition on the normal bending moment. Convergence of natural boundary conditions is discussed in Section 4.3.2.2.

The finite element results using the (6x6) grid for the normal deflection $\bar{w}$ and the membrane forces $N_{\bar{x}}$ and $N_{\bar{y}}$ are certainly accurate enough for practical purposes. A finer grid, for example (9x9), must be used to obtain accurate bending moment curves, and the shear $N_{\bar{x}\bar{y}}$ on the end-section $\bar{y} = L_y/2$ can also be obtained with a greater degree of accuracy by use of finer grids. The effect of grid size on the finite element results is discussed in the following section.

4.3.2.2 Effect of Grid Size

Grids of (3x3), (6x6) and (9x9) on one quadrant of the shell are used, for the case of generalized nodal loads only. The membrane shear force $N_{\bar{x}\bar{y}}$ across the end-section $\bar{y} = L_y/2$ and the membrane force $N_{\bar{y}}$ across the mid-section $\bar{x} = 0$ are shown in Figures 18 and 19. As expected, the use of finer grid sizes substantially increases the accuracy of the finite element results.

The shear at the corner of the shell using a (9x9) grid underestimates the exact value by more than 10%. However, since the membrane theory predicts an infinite shear at the corner, it is not surprising that the convergence to the true value using the bending theory is slow.

As increasing numbers of terms are taken in a series solution, the convergence trend is similar to that exhibited by the finite element results shown in Fig. 18.

4.3.2.3 Convergence of Natural Boundary Conditions

Some of the deviations of the finite element solutions from the exact values may be attributed to the fact that the assumed displacement field does not satisfy the natural boundary conditions. For the roller-supported elliptical paraboloid, the natural boundary conditions on the edge $\bar{x} = L_x/2$ are

$$N_{\bar{x}} = 0$$

$$M_{\bar{x}} = 0$$

Table 12 shows the computed value of $N_{\bar{x}}$ and $M_{\bar{x}}$ at the point $\bar{x} = L_x/2$, $\bar{y} = 0$ for grid sizes of (3x3), (6x6) and (9x9) for each of the two types of nodal loads.

As the grid size is refined, the computed values of $N_{\bar{x}}$ and $M_{\bar{x}}$ on the edge decrease and in the limit should approach zero if the method is convergent. For finite grid sizes the use of generalized nodal loads leads to closer satisfaction of the condition $N_{\bar{x}} = 0$ for this particular case, and also produces more accurate membrane forces. The statically equivalent nodal loads satisfy more closely the condition $M_{\bar{x}} = 0$ and produce more accurate bending moments. More intensive investigations are required before any general rule can be stated, but it seems likely that a comparison of the computed values of boundary stress resultants with the natural boundary conditions can be used as a practical measure of the adequacy of convergence.

4.3.3 Roller Supported Hyperbolic Paraboloid Bounded by Lines of Curvature Under Uniform Normal Load

A comparison of finite element results with the series solution for Shell II, the hyperbolic paraboloid bounded by lines of curvature, is given here so that the validity of the finite element method may be demonstrated for the three main types of shells considered herein.

The normal deflection $\bar{w}$ across the mid-section $\bar{x} = 0$ and the bending moment $M_{\bar{x}}$ across the mid-section $\bar{y} = 0$ are shown in Fig. 20. The membrane forces $N_{\bar{x}}$ and $N_{\bar{y}}$

and the bending moments $M_{\bar{x}}$ and $M_{\bar{y}}$ across the mid-section $\bar{x} = 0$ are shown in Fig. 21.

The agreement with the series solution is excellent for all quantities and is slightly better than for the elliptical paraboloid discussed in Section 4.3.2.

A comparison of the results given in Figs. 20 and 21 with the results given in the previous sections clearly points out the comparative disadvantages of the hyperbolic paraboloid bounded by lines of curvature. The central deflection is approximately 25 times that of the elliptical paraboloid analyzed in the previous section, and while the membrane forces are lower, the bending moments are larger and do not rapidly damp out away from the roller support. Thus the roller-supported hyperbolic paraboloid bounded by lines of curvature carries load primarily by bending rather than by membrane forces, and is therefore comparatively inefficient structurally.

4.3.4 Knife-Edge Supported Hyperbolic Paraboloid Bounded by Characteristics Under Uniform Normal Load

Shell III, the square hyperbolic paraboloid bounded by characteristics is knife-edge supported on all edges and subjected to a uniform normal load of - 1.0 lb/in^2. A grid of (12x12) over the entire shell is used in the analysis.

The normal deflection $\bar{w}$ and the membrane shear $N_{\bar{x}\bar{y}}$ across the mid-section $\bar{x} = 0$ are shown in Fig. 22 and the

membrane force $\bar{N}_x$ and the bending moment $\bar{M}_y$ across the mid-section $\bar{x} = 0$ are shown in Fig. 23.

All quantities plotted agree with the series solutions to within 2%. The membrane theory predicts a constant $\bar{N}_{xy}$ of 16.0 lb/in. throughout the shell, while the bending theory yields a value of $\bar{N}_{xy} = 21.8$ lb/in. at the center of the shell. The bending moment $\bar{M}_y$ is fairly large, producing bending stresses of the same order of magnitude as the membrane stresses, and dies out slowly toward the center of the shell.

4.4 Comparisons with Other Numerical Results

4.4.1 Clamped Hyperbolic Paraboloid Bounded by Characteristics Under Uniform Normal Load

Shell III is clamped on all edges and subjected to a uniform normal load of -1.0 lb/in^2. This shell has been analyzed by Chetty and Tottenham (10) using a variational method. Figure 24 shows the comparison of the finite element results for a grid of (10x10) over the entire shell with the results given in Ref. (10). The agreement is quite good considering the coarseness of the grid used in the finite element analysis. This is in agreement with what has been stated previously regarding the expected improvement of accuracy when the boundary conditions are all of the forced type.

It is interesting to note that the agreement is better for the bending moment $M_{\bar{x}}$ than for the membrane shear force $N_{\bar{x}\bar{y}}$. It must be remembered however, that the comparison here is with another approximate solution rather than with the exact solution as has been the case in previous examples.

The membrane shear $N_{\bar{x}\bar{y}}$ exceeds the membrane value of 16.0 lb/in.^{2} by only a slight amount at the center of the shell, but the bending moment propagates into the central region of the shell, producing fairly large bending stresses.

4.4.2 Clamped Elliptical Paraboloid Under Uniform Normal Load

Shell I is clamped on all edges and subjected to a uniform normal load of $-p_o$. A grid of (9x9) on one quadrant of the shell is used in the analysis.

Figure 25 shows the normal deflection $\bar{w}$ and the membrane force $N_{\bar{x}}$ across the mid-section $\bar{x} = 0$, as compared with results given by Gustafson and Schnobrich (21). Figure 26 shows a similar comparison for the membrane force $N_{\bar{y}}$ and the bending moment $M_{\bar{y}}$ across the mid-section $\bar{x} = 0$.

The results of Ref. (21) were obtained using a discrete model approximation and thus the comparison made here is with another approximate solution rather than with the exact solution.

In this case, the finite element solution does not agree with the comparison approximate solution as closely as

was the case in the previous section, Section 4.4.1.

There is a difference of approximately 10% in the two values for the central deflection. The membrane stresses $N_{\bar{x}}$ and $N_{\bar{y}}$ agree very closely at the center of the shell but diverge near the boundary. The bending moments $M_{\bar{x}}$ damp out within approximately the same distance from the support, but the finite element analysis predicts higher bending moments in the boundary region. From a practical standpoint the discrepancy between the two sets of results is not serious, but it is doubtful that this amount of disagreement can be attributed to coarseness of grid. Some of the difference may be due to the fact that the discrete model used in Ref. (21) includes the effect of inplane displacements on the bending moments, a factor which is neglected in shallow shell theory.

For the roller supported case, comparative studies have shown that the inclusion of the inplane terms has virtually no effect on the results, so that if the discrepancy is due to this factor, it is a result of the particular boundary conditions, and not of the shallowness of the shell.

4.5 Hyperbolic Paraboloid Bounded by Characteristics Under Uniform Normal Load

Shell III, the square hyperbolic paraboloid analyzed previously, is buttressed at one low corner and supported on a horizontal roller at the other low corner. One of the high corners is supported on a horizontal roller and the remaining high corner is free. The shell is subjected to a uniform

normal load of -1.0 lb/in.^{2} as before, and a (12x12) grid over the entire shell is used in the following series of analyses which are carried out to determine the effect of a tie rod and edge beams on the behaviour of the shell. The results are intended for comparison purposes only, since for these particular boundary conditions the (12x12) grid is fairly coarse.

4.5.1 Effect of Tie Rod Connecting Low Corners

A non-dimensional parameter λ, which is a measure of the tie rod stiffness relative to that of the shell, is defined as

$$\lambda = \frac{(EA)_{\text{tie rod}}}{EhL_x}$$

where $(EA)_{\text{tie rod}}$ is the axial stiffness of the tie rod.

Analyses are carried out for values of λ equal to 0, 0.04, and ∞.

The normal deflection $\bar{w}$ across the diagonal connecting the high corners is shown in Fig. 27. The effect of the tie rod is very pronounced as can be seen from the figure, and for even a moderate value of λ, a marked reduction in the deflection results. The actual numerical values for deflections are rather large compared to the thickness of the shell, which is ¼ in.; however this is not of major importance since the example is intended only to show the relative effect of the tie rod.

The membrane force $\bar{N}_y$ across the mid-section $\bar{y} = 0$ is shown in Fig. 28 and the membrane shear $\bar{N}_{xy}$ and the bending

moment $M_{\bar{x}}$ across the mid-section y = 0 are shown in Fig. 29. The "arching force" N across the diagonal connecting the low corners is shown in Fig. 30. Once again the tie rod has a very beneficial effect on the stress distribution in the shell. It is important to note that a relatively small tie rod produces, in this case at least, nearly all the benefits of fully restraining the low corner, that is placing the low corner on a pin support rather than a roller support.

4.5.2 Effect of Edge Beam Eccentricity

Edge beams 3/4 in. wide by 2 in. deep are placed on each edge of the shell. Analyses are carried out for values of eccentricity, e, equal to $-\frac{1}{2}$ in., 0 and $+\frac{1}{2}$ in. Young's Modulus and Poisson's Ratio for the beam are the same as those of the shell. All the stiffness properties of the beam are taken into account in the analyses as well as the eccentricity and transverse slope of the shell middle surface with respect to the beam. Although the cross sectional dimensions of the edge beams are reasonable in comparison with the thickness of the shell, the (length/depth) ratios of the edge beams are relatively small due to the large (thickness/span) ratio of the shell.

The deflection $\bar{w}$ across the diagonal connecting the high corners is shown in Fig. 31. Also plotted is the deflection from Section 4.5.2 for the case $\lambda = 0$. In this case the fact that edge beams are present is much more important than whether they are eccentric or not.

The deflection $\bar{w}$ is re-plotted on a larger scale in Fig. 32 together with the membrane shear $N_{\bar{x}\bar{y}}$ across the mid-section $\bar{y} = 0$. In Fig. 33 are shown the membrane force $N_{\bar{y}}$ and the bending moment $M_{\bar{x}}$ across the mid-section $\bar{y} = 0$. The "arching force" N across the diagonal is plotted in Fig. 34.

In the region near the supported high corner, the upstanding edge beam reduces the deflection as compared to the other two edge beams, while in the region near the unsupported high corner the upstanding edge beam produces the largest deflection.

The membrane forces $N_{\bar{x}\bar{y}}$ and $N_{\bar{y}}$ show the same effect: the upstanding edge beam is most beneficial in the region near the boundary but is least beneficial in the central region of the shell.

The upstanding edge beam results in a more symmetrical distribution of bending moment $M_{\bar{x}}$ than does the downstanding beam, but the concentric edge beam is superior to both. Near the low corners where the compressive arching force is the greatest, the concentric edge beam yields the lowest stresses.

An overall assessment favours the concentric beam for these particular boundary conditions. The results of an experimental investigation (40) on a hyperbolic paraboloid of different dimensions and with different corner supports prompted the conclusion that upstanding edge beams were more beneficial than either concentric or downstanding ones. The

effect of eccentricity appears, however, to be dependent on the type of support provided at the corners.

4.6 Skewed Hyperbolic Paraboloid Bounded by Characteristics Under Uniform Normal Load

Shell III is converted into a skewed hyperbolic paraboloid with a skew angle of 60°. The side lengths and relative elevations of the corners remain the same. The shell is clamped on two adjacent edges and the two remaining edges, intersecting at one of the high corners, are free. A uniform normal load of -1.0 lb/in.^{2} is applied.

The normal deflection $\bar{w}$ across the diagonal from the clamped high corner to the free high corner is plotted in Fig. 35 as is the membrane shear $N_{\bar{x}\bar{y}}$ along the fixed edge. All stresses are converted from skew quantities to orthogonal quantities so that $N_{\bar{x}\bar{y}}$ is the actual shear on the edge. The $N_{\bar{x}\bar{y}}$ is shown dotted near the corner since it is uncertain whether the computed value at the corner is accurate.

The force $N_{\bar{y}}$ across the section $\bar{y} = L_y/2$ and the bending moment $M_{\bar{y}}$ across the section $\bar{x} = L_x/2$ are shown in Fig. 36.

The direct membrane force $N_{\bar{y}}$ is relatively small near the clamped edge but rises to a large (compressive) value along the free edge. The bending moment $M_{\bar{y}}$ decreases away from the clamped edge but rises in the region near the free edge to a value which is approximately two-thirds of the clamping moment at the fixed edge.

The direct stress N and the normal bending moment M across the diagonal connecting the clamped low corners are shown in Fig. 37. The distribution of N resembles the distribution of fibre stress in a deep cantilevered beam. The bending moment M is considerably reduced due to the curvature of the shell, being an order of magnitude smaller than in the corresponding plate structure.

4.7 Effect of Valley Beams on Umbrella Hyperbolic Paraboloid

An umbrella shell is constructed from four hyperbolic paraboloid units, each of the dimensions of Shell III. Normally, when such shells are built, valley beams are included along the boundaries between the four separate units.

To determine the effect of the valley beams two analyses are carried out, one with the valley beams and one without. Grids of (12x12) are used on one quadrant of the total umbrella shell. The valley beam used is of the same dimensions as the edge beams used in Section 4.5.2, and are concentric. The value of Young's Modulus for the edge beam is 10,000 lb/in.^{2} and Poisson's Ratio is 0.39.

The normal deflection $\bar{w}$ across the diagonal from the column support to the free corner is shown in Fig. 38. The beam has little effect on the deflection except near the column support where the deflection is small anyway.

Figure 40 shows $N_{\bar{x}}$ and $M_{\bar{y}}$ across the section $\bar{x} = L_x/2$. The reduction of the $N_{\bar{x}}$ force due to the valley

beam is much less pronounced away from the valley, although the bending moment $M_{\bar{y}}$ is reduced significantly by the valley beams even in the central region away from the beam.

Thus it may be concluded that while the valley beam is not effective in reducing the maximum deflection, it has a beneficial effect on the stress distribution and prevents large direct stresses from developing in the shell along the boundaries between the four separate units.

5. CONCLUSIONS AND RECOMMENDATIONS FOR FURTHER STUDY

5.1 Conclusions

The finite element method as herein applied to shallow shells, using elements of the same shape as the shell middle surface rather than a series of flat elements, has been shown to give results in good agreement with exact solutions. Agreement with other numerical solutions is also good, although some discrepancies are noted. The most advantageous feature of the method is its versatility and the ease with which, for example, edge beams and tie rods can be included.

The two displacement assumptions used in this study produce almost exactly the same numerical results when applied to uniformly pressure-loaded shallow shells, although this may not always be the case for other loading conditions. Therefore it is concluded that the continuity of derivatives of the displacement w across inter-element boundaries is not essential. The inclusion of a complete rigid body motion in the displacement assumption may also be nonessential, as a recent study (22) has suggested, and numerical results, not reported herein, have tended to confirm. However, all results presented in this report are obtained with the complete rigid body motion included.

The use of generalized nodal loads as opposed to statically equivalent nodal loads produces some desirable and

some undesirable features. In the example presented, and for the displacement shapes used here, the generalized nodal loads resulted in superior accuracy for deflections and membrane forces and the statically equivalent nodal loads led to more accurate bending moments.

Some of the peculiarities of the finite element results, notably the underestimation of the membrane forces near the boundary, may be traced to the fact that the natural boundary conditions are not satisfied exactly for a finite grid size. In a problem for which the exact solution is unknown, the degree of satisfaction of the natural boundary conditions may be used as a practical method of assessing whether or not a fine enough grid has been used in the analysis.

The numerical examples presented have shown the extreme sensitivity of corner supported hyperbolic paraboloids to horizontal movement of the corners,* and the beneficial effects of even a relatively small tie rod connecting the low corners.

The effect of edge beam eccentricity was not marked in the particular case treated, the presence of the edge beam being much more important than its location with respect to the shell middle surface. However, it is not to be concluded that such is the case for all boundary conditions.

---

* Elliptical paraboloids are also very sensitive to corner movement, (3), (21) and tie rods are desirable for them also.

The umbrella shell analysis showed that while valley beams do not significantly reduce the maximum deflection or the membrane forces away from the valley, they do prevent the development of large direct stresses along the valley and reduce bending moments throughout the shell.

5.2 Recommendations for Further Study

Further studies of shell behavior in which several parameters such as (rise/span) and (thickness/radius of curvature) ratios are varied would be of interest.

Improvement of the rate of convergence of the finite element analysis is desirable. Some possibilities for doing this are:

(1) The use of a graded mesh near the boundaries or wherever rapid variations of displacement or stresses are expected. Since a fairly large number of elements is required to adequately approximate the bending moments when uniform meshes are used, graded meshes may allow the use of coarser grids for the same accuracy.

(2) The improvement of the satisfaction of the natural boundary conditions. Displacement shapes which are capable of satisfying, for example, the membrane natural boundary conditions might be used. This, however, would result in an increased number of generalized coordinates per element and thus for the same computational effort, not as fine a mesh could be used. Therefore, whether or not improved accuracy should be sought by using more refined displacement

assumptions, or by using relatively crude assumptions together with fine grids is answerable only by actual numerical comparisons.

Alternative methods of satisfying the natural boundary conditions are the use of Lagrangian multipliers (26) or a reformulation as a mixed variational problem in which some of the displacements and some of the stresses are assumed in terms of generalized coordinates (24, 38).

Several extensions of the scope of this investigation suggest themselves. Temperature effects, non-uniform thickness, anisotropy, and flexible column supports could all be immediately included. Normally in the finite element technique, geometrical variations are handled in a stepwise fashion, which is appropriate to the type of analysis in which the curved shell is approximated by an assemblage of flat elements. In this case, since curved elements are used, it is preferable to express the thickness analytically in terms of x and y if possible and include it in the integrations which are performed in the process of obtaining the stiffness matrix. Anisotropy can be included by making the E^m and E^b matrices slightly more general, that is by not setting some of the elements of the matrices equal as has been done in this study. Flexible column supports require no modifications in the procedure.

Other extensions, such as to vibrations, buckling and plasticity could also be made, with the extension to plastic behavior requiring perhaps the most effort.

LIST OF REFERENCES

1. Abu-Sitta, S. H., "Finite Difference Solutions of the Bending Theory of the Elliptic Paraboloid," IASS Bulletin No. 20.

2. Abu-Sitta, S. H., "Experimental Studies of Shell Models," IASS-IMCYC Congreso Internacional Sobre La Aplicacion de Estructuras Laminares en Arquitectura, Mexico City, September, 1967.

3. Aggarwala, B. D., "Bending of Parallelogram Plates," Journal of the Engineering Mechanics Division, ASCE, August, 1967.

4. Apeland, K., "Stress Analysis of Translational Shells," Journal of the Engineering Mechanics Division, ASCE, February, 1961.

5. Archer, J. S., "Consistent Matrix Formulations for Structural Analysis Using Finite Element Techniques," AIAA Journal, October, 1965.

6. Bazely, G. P., Cheung, Y. K., Irons, B. M., and Zienkiewicz, O. C., "Triangular Elements in Plate Bending - Conforming and Non-Conforming Solutions," Conference on Matrix Methods in Structural Mechanics, Wright-Patterson AFB, Ohio, October, 1965.

7. Birkhoff, G., and Garabedian, H. L., "Smooth Surface Interpolation," Journal of Mathematics and Physics, Vol. 39, 1960.

8. Bogner, F. K., Fox, R. L., and Schmidt, L. A., "The Generation of Interelement Compatible Stiffness and Mass Matrices by the Use of Interpolation Formulas," Conference on Matrix Methods in Structural Mechanics, Wright-Patterson AFB, Ohio, October, 1965.

9. Bouma, A. L., "Some Applications of the Bending Theory Regarding Doubly Curved Shells," Proceedings of the Symposium on the Theory of Thin Elastic Shells, August, 1959.

10. Chetty, S. M. K., and Tottenham, H., "An Investigation into the Bending Analysis of Hyperbolic Paraboloid Shells," Indian Concrete Journal, July, 1964.

11. Clough, R. W., "The Finite Element Method in Structural Mechanics," Stress Analysis, edited by O. C. Zienkiewicz and G. S. Holister, Wiley, 1965.

12. Clough, R. W., and Tocher, J. L., "Finite Element Stiffness Matrices for Analysis of Plate Bending," Conference on Matrix Methods in Structural Mechanics, Wright-Patterson AFB, Ohio, October, 1965.

13. Das Gupta, N. C., "Edge Disturbances in a Hyperbolic Paraboloid," Civil Engineering and Public Works Review, February, 1963.

14. Deák, A. L., and Pian, T. H. H., "Application of the Smooth Surface Interpolation to the Finite Element Analysis," Technical Note, AIAA Journal, January, 1967.

15. Faddeeva, V. N., Computational Methods of Linear Algebra, Dover Publications, 1959.

16. Flügge, W., Stresses in Shells, Springer-Verlag, New York, 1966.

17. Flügge, W., and Conrad, D. A., "Singular Solutions in the Theory of Shallow Shells," Technical Report 101, Division of Engineering Mechanics, Stanford University, September, 1956.

18. Fraejis de Veubeke, B., "Bending and Stretching of Plates - Special Models for Upper and Lower Bounds," Conference on Matrix Methods in Structural Mechanics, Wright-Patterson AFB, Ohio, October, 1965.

19. Gallagher, R. H., A Correlation Study of Methods of Matrix Structural Analysis, AGARDograph 69, MacMillan, New York, 1964.

20. Gillies, D. C., "The Use of Interlacing Nets for the Application of Relaxation Methods to Problems Involving Two Dependent Variables," Proceedings, Royal Society, London, 1948.

21. Gustafson, W. C., and Schnobrich, W. C., "Multiple Translational Shells," IASS-IMCYC Congreso Internacional Sobre La Aplicacion de Estructuras Laminares en Arquitectura, Mexico City, September, 1967.

22. Haisler, W. E., and Stricklin, J. A., "Rigid Body Displacements of Curved Elements in the Analysis of Shells by the Matrix Displacement Method," Technical Note, AIAA Journal, August, 1967.

23. Hall, A. S., and Woodhead, R. W., Frame Analysis, Wiley, New York and London, 1961.

24. Herrmann, L. R., "A Bending Analysis for Plates," Conference on Matrix Methods in Structural Mechanics, Wright-Patterson AFB, Ohio, October, 1965.

25. Hrennikoff, A., "Solution of Problems of Elasticity by the Framework Method," Journal of Applied Mechanics, December, 1941.

26. Jones, R. E., "A Generalization of the Direct Stiffness Method of Structural Analysis," AIAA Journal, May, 1964.

27. Langhaar, H. L., Foundations of Practical Shell Analysis, Department of Theoretical and Applied Mechanics, University of Illinois, June, 1964.

28. Margeurre, K., "Zur Theorie der gekrümmten Platte grösser Formanderung," Proceedings, Fifth International Congress on Applied Mechanics, 1938.

29. Martin, H. C., Introduction to Matrix Methods of Structural Analysis, McGraw-Hill, New York, 1966.

30. Melosh, R. J., "Basis for Derivation of Matrices for the Direct Stiffness Method," AIAA Journal, July, 1963.

31. Mirza, J. F., "Stresses and Deformations in Umbrella Shells," Journal of the Structural Division, ASCE, April, 1967.

32. Mohraz, B., and Schnobrich, W. C., "The Analysis of Shallow Shell Structures by a Discrete Element System," Civil Engineering Studies, SRS 304, University of Illinois, March, 1966.

33. Morley, L. S. D., "Bending of Clamped Rectilinear Plates," Quarterly Journal of Mechanics and Applied Mathematics, Vol. 17, 1964.

34. Navaratna, D. R., "Computation of Stress Resultants in Finite Element Analyses," Technical Note, AIAA Journal, November, 1966.

35. Noor, A. K., and Veletsos, A. S., "A Study of Doubly Curved Shallow Shells," Civil Engineering Studies, SRS 274, University of Illinois, March, 1963.

36. Novozhilov, V., The Theory of Thin Shells, translated by P. G. Lowe, edited by J. R. M. Radok, P. Noordhoff, Groningen, 1959.

37. Parikh, K. S., "Analysis of Shells Using Framework Analogy," Sc. D. Thesis, Massachusetts Institute of Technology, June, 1962.

38. Pian, T. H. H., "Derivation of Element Stiffness Matrices by Assumed Stress Distributions," Technical Note, AIAA Journal, July, 1964.

39. Reissner, E., "On Some Aspects of the Theory of Thin Elastic Shells," Journal, Boston Society of Civil Engineers, 1955.

40. Rowe, R. E., "Modelling of Shells," IASS Conference, Leningrad, September, 1966.

41. Russell, R. R., and Gerstle, K. H., "Bending of Hyperbolic Paraboloid Structures," Journal of the Structural Division, ASCE, June, 1967.

42. Schnobrich, W. C., "A Physical Analogue for the Numerical Analysis of Cylindrical Shells," Ph.D. Thesis, University of Illinois, 1962.

43. Soare, M., "A Numerical Approach to the Bending Theory of Hypar Shells," Indian Concrete Journal, February-March, 1966.

44. Stricklin, J., Navaratna, D. R., and Pian, T. H. H., "Improvements on the Analysis of Shells of Revolution by the Matrix Displacement Method," Technical Note, AIAA Journal, November, 1966.

45. Tezcan, S. S., "Computer Analysis of Plane and Space Structures," Journal of the Structural Division, ASCE, April, 1966.

46. Vlasov, V. Z., General Theory of Shells and its Applications in Engineering, NASA Technical Translation F-99.

47. Zienkiewicz, O. C., and Cheung, Y. K., "The Finite Element Method for Analysis of Elastic Isotropic and Orthotropic Slabs," Proceedings, Institute of Civil Engineers, August, 1964.

$$
\begin{pmatrix}
\frac{1}{4} & . & \frac{3h_1}{16a} & \frac{bh_1}{16a} & -\frac{h_1}{16} & \frac{1}{4} & . & \frac{3h_2}{16a} & -\frac{bh_2}{16a} & -\frac{h_2}{16} & \frac{1}{4} & . & -\frac{3h_2}{16a} & -\frac{bh_2}{16a} & -\frac{h_2}{16} & \frac{1}{4} & . & -\frac{3h_1}{16a} & \frac{bh_1}{16a} & -\frac{h_1}{16} \\
-\frac{1}{4a} & . & -\frac{r}{4} & -\frac{br}{8} & \frac{ar}{8} & -\frac{1}{4a} & . & -\frac{r}{4} & \frac{br}{8} & \frac{ar}{8} & \frac{1}{4a} & . & -\frac{r}{4} & -\frac{br}{8} & -\frac{ar}{8} & \frac{1}{4a} & . & -\frac{r}{4} & \frac{br}{8} & -\frac{ar}{8} \\
-\frac{1}{4b} & . & -\frac{s}{4} & -\frac{bs}{8} & \frac{as}{8} & \frac{1}{4b} & . & -\frac{s}{4} & \frac{bs}{8} & \frac{as}{8} & -\frac{1}{4b} & . & -\frac{s}{4} & -\frac{bs}{8} & -\frac{as}{8} & \frac{1}{4b} & . & -\frac{s}{4} & \frac{bs}{8} & -\frac{as}{8} \\
\frac{1}{4ab} & . & \frac{3r}{8b} & \frac{r}{8} & -\frac{ar}{8b} & -\frac{1}{4ab} & . & -\frac{3r}{8b} & \frac{r}{8} & \frac{ar}{8b} & -\frac{1}{4ab} & . & \frac{3r}{8b} & \frac{r}{8} & \frac{ar}{8b} & \frac{1}{4ab} & . & -\frac{3r}{8b} & \frac{r}{8} & -\frac{ar}{8b} \\
. & \frac{1}{4} & -\frac{3h_2}{16b} & -\frac{h_2}{16} & \frac{ah_2}{16b} & . & \frac{1}{4} & \frac{3h_1}{16b} & -\frac{h_1}{16} & -\frac{ah_1}{16b} & . & \frac{1}{4} & -\frac{3h_1}{16b} & -\frac{h_1}{16} & -\frac{ah_1}{16b} & . & \frac{1}{4} & \frac{3h_2}{16b} & -\frac{h_2}{16} & \frac{ah_2}{16b} \\
. & -\frac{1}{4a} & -\frac{s}{4} & -\frac{bs}{8} & \frac{as}{8} & . & -\frac{1}{4a} & -\frac{s}{4} & \frac{bs}{8} & \frac{as}{8} & . & \frac{1}{4a} & -\frac{s}{4} & -\frac{bs}{8} & -\frac{as}{8} & . & \frac{1}{4a} & -\frac{s}{4} & \frac{bs}{8} & -\frac{as}{8} \\
. & -\frac{1}{4b} & -\frac{t}{4} & -\frac{bt}{8} & \frac{at}{8} & . & \frac{1}{4b} & -\frac{t}{4} & \frac{bt}{8} & \frac{at}{8} & . & -\frac{1}{4b} & -\frac{t}{4} & -\frac{bt}{8} & -\frac{at}{8} & . & \frac{1}{4b} & -\frac{t}{4} & \frac{bt}{8} & -\frac{at}{8} \\
. & \frac{1}{4ab} & \frac{3t}{8a} & \frac{bt}{8a} & -\frac{t}{8} & . & -\frac{1}{4ab} & \frac{3t}{8a} & -\frac{bt}{8a} & -\frac{t}{8} & . & -\frac{1}{4ab} & -\frac{3t}{8a} & -\frac{bt}{8a} & -\frac{t}{8} & . & \frac{1}{4ab} & -\frac{3t}{8a} & \frac{bt}{8a} & -\frac{t}{8} \\
. & . & \frac{1}{4} & \frac{b}{8} & -\frac{a}{8} & . & . & \frac{1}{4} & -\frac{b}{8} & -\frac{a}{8} & . & . & \frac{1}{4} & \frac{b}{8} & \frac{a}{8} & . & . & \frac{1}{4} & -\frac{b}{8} & \frac{a}{8} \\
. & . & -\frac{3}{8a} & -\frac{b}{8a} & \frac{1}{8} & . & . & -\frac{3}{8a} & \frac{b}{8a} & \frac{1}{8} & . & . & \frac{3}{8a} & \frac{b}{8a} & \frac{1}{8} & . & . & \frac{3}{8a} & -\frac{b}{8a} & \frac{1}{8} \\
. & . & -\frac{3}{8b} & -\frac{1}{8} & \frac{a}{8b} & . & . & \frac{3}{8b} & -\frac{1}{8} & -\frac{a}{8b} & . & . & -\frac{3}{8b} & -\frac{1}{8} & -\frac{a}{8b} & . & . & \frac{3}{8b} & -\frac{1}{8} & \frac{a}{8b} \\
. & . & \frac{1}{2ab} & \frac{1}{8a} & -\frac{1}{8b} & . & . & -\frac{1}{2ab} & \frac{1}{8a} & \frac{1}{8b} & . & . & -\frac{1}{2ab} & -\frac{1}{8a} & -\frac{1}{8b} & . & . & \frac{1}{2ab} & -\frac{1}{8a} & \frac{1}{8b} \\
. & . & . & . & \frac{1}{8a} & . & . & . & . & \frac{1}{8a} & . & . & . & . & -\frac{1}{8a} & . & . & . & . & -\frac{1}{8a} \\
. & . & . & -\frac{1}{8b} & . & . & . & . & \frac{1}{8b} & . & . & . & . & -\frac{1}{8b} & . & . & . & . & \frac{1}{8b} & . \\
. & . & \frac{1}{8a^3} & . & -\frac{1}{8a^2} & . & . & \frac{1}{8a^3} & . & -\frac{1}{8a^2} & . & . & -\frac{1}{8a^3} & . & -\frac{1}{8a^2} & . & . & -\frac{1}{8a^3} & . & -\frac{1}{8a^2} \\
. & . & . & . & -\frac{1}{8ab} & . & . & . & . & \frac{1}{8ab} & . & . & . & . & \frac{1}{8ab} & . & . & . & . & -\frac{1}{8ab} \\
. & . & . & \frac{1}{8ab} & . & . & . & . & -\frac{1}{8ab} & . & . & . & . & -\frac{1}{8ab} & . & . & . & . & \frac{1}{8ab} & . \\
. & . & \frac{1}{8b^3} & \frac{1}{8b^2} & . & . & . & -\frac{1}{8b^3} & \frac{1}{8b^2} & . & . & . & \frac{1}{8b^3} & \frac{1}{8b^2} & . & . & . & -\frac{1}{8b^3} & \frac{1}{8b^2} & . \\
. & . & -\frac{1}{8a^2b} & . & \frac{1}{8a^2b} & . & . & \frac{1}{8a^2b} & . & -\frac{1}{8a^2b} & . & . & \frac{1}{8a^2b} & . & \frac{1}{8a^2b} & . & . & -\frac{1}{8a^2b} & . & -\frac{1}{8a^2b} \\
. & . & -\frac{1}{8ab^2} & -\frac{1}{8ab^2} & . & . & . & \frac{1}{8ab^2} & -\frac{1}{8ab^2} & . & . & . & \frac{1}{8ab^2} & \frac{1}{8ab^2} & . & . & . & -\frac{1}{8ab^2} & \frac{1}{8ab^2} & .
\end{pmatrix}
$$

$$h_1 = a^2r - b^2t + 2sab$$

$$h_2 = a^2r - b^2t - 2sab$$

TABLE 1. B^{-1} Matrix for Non-Compatible Element

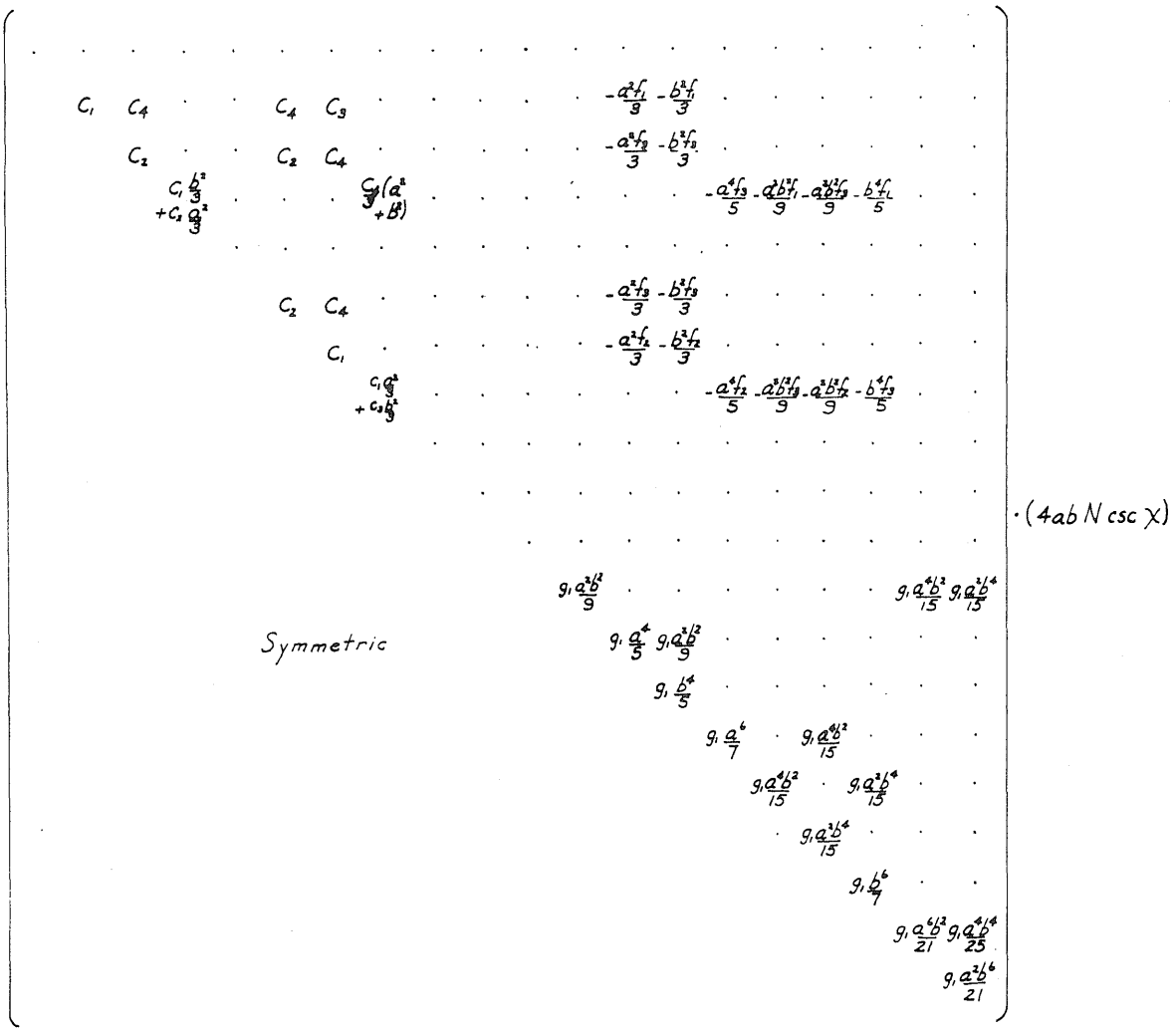

TABLE 2. $\left[\iint D^{m,T} E^{m,T} D^{m} \sin \chi \, dxdy \right]$ Matrix for Non-Compatible Element

$$
\begin{pmatrix}
[0]_{11\times 11} & [0]_{11\times 9} \\
\hline
[0]_{9\times 11} & \begin{array}{ccccccccc}
C_2 & C_4 & C_4 & \cdot & \cdot & \cdot & \cdot & C_2a^2 & C_2b^2 \\
 & C_1 & C_3 & \cdot & \cdot & \cdot & \cdot & C_4a^2 & C_4b^2 \\
 & & C_1 & \cdot & \cdot & \cdot & \cdot & C_4a^2 & C_4b^2 \\
 & & & 3C_1a^2 & 2C_4a^2 & C_3a^2 & \cdot & \cdot & \cdot \\
 & & & & \frac{C_1}{3}b^2 + \frac{4}{3}C_2a^2 & \frac{2}{3}C_4(a^2+b^2) & C_3b^2 & \cdot & \cdot \\
 & & & & & \frac{C_1}{3}a^2 + \frac{4}{3}C_2b^2 & 2C_4b^2 & \cdot & \cdot \\
 & & \text{Symmetric} & & & & 3C_1b^2 & \cdot & \cdot \\
 & & & & & & & C_1a^2b^2 + \frac{9}{5}C_2a^4 & C_2a^2b^2 + C_3a^2b^2 \\
 & & & & & & & & C_1a^2b^2 + \frac{9}{5}C_2b^4
\end{array}
\end{pmatrix}
\cdot (16ab\,D\csc\chi)
$$

TABLE 3. $\left[\iint D^{b,T}\, E^{b,T}\, D^{b} \sin\chi \, dxdy\right]$ Matrix for Non-Compatible Element

·	C_1	C_4	C_1y+C_4x	·	C_4	C_3	C_3x+C_4y	·	·	·	$-xyf_1$	$-x^2f_1$	$-y^2f_1$	$-x^3f_1$	$-x^2yf_1$	$-xy^2f_1$	$-y^3f_1$	$-x^3yf_1$	$-xy^3f_1$	
·	C_3	C_4	C_3y+C_4x	·	C_4	C_1	C_1x+C_4y	·	·	·	$-xyf_2$	$-x^2f_2$	$-y^2f_2$	$-x^3f_2$	$-x^2yf_2$	$-xy^2f_2$	$-y^3f_2$	$-x^3yf_2$	$-xy^3f_2$	$\cdot(Ncscy)$
·	C_4	C_2	C_4y+C_2x	·	C_2	C_4	C_4x+C_2y	·	·	·	$-xyf_3$	$-x^2f_3$	$-y^2f_3$	$-x^3f_3$	$-x^2yf_3$	$-xy^2f_3$	$-y^3f_3$	$-x^3yf_3$	$-xy^3f_3$	
·	·	·	·	·	·	·	·	·	·	·	$-2C_4$	$-2C_1$	$-2C_3$	$-6xC_1$	$-2yC_1$ $-4xC_4$	$-2xC_3$ $-4yC_4$	$-6yC_3$	$-6xyC_1$ $-6x^2C_4$	$-6xyC_3$ $-6y^2C_4$	
·	·	·	·	·	·	·	·	·	·	·	$-2C_4$	$-2C_3$	$-2C_1$	$-6xC_3$	$-2yC_3$ $-4xC_4$	$-2xC_1$ $-4yC_4$	$-6yC_1$	$-6xyC_3$ $-6x^2C_4$	$-6xyC_1$ $-6y^2C_4$	$\cdot(Dcscy)$
·	·	·	·	·	·	·	·	·	·	·	$-2C_2$	$-2C_4$	$-2C_4$	$-6xC_4$	$-2yC_4$ $-4xC_2$	$-2xC_4$ $-4yC_2$	$-6yC_4$	$-6xyC_4$ $-6x^2C_2$	$-6xyC_4$ $-6y^2C_2$	

TABLE 4. E^mD^m and E^bD^b Matrices for Non-Compatible Element

$$
\begin{pmatrix}
\frac{1}{4} & . & \frac{3h_1}{16a} & \frac{b^2s}{8} & -\frac{(a^2r-b^2t)}{16} & \frac{1}{4} & . & \frac{3h_2}{16a} & \frac{b^2s}{8} & -\frac{(a^2r-b^2t)}{16} & \frac{1}{4} & . & -\frac{3h_1}{16a} & \frac{b^2s}{8} & -\frac{(a^2r-b^2t)}{16} & \frac{1}{4} & . & -\frac{3h_2}{16a} & \frac{b^2s}{8} & -\frac{(a^2r-b^2t)}{16} \\
-\frac{1}{4} & . & -\frac{ar}{4} & -\frac{abr}{8} & \frac{a^2r}{8} & -\frac{1}{4} & . & -\frac{ar}{4} & \frac{abr}{8} & \frac{a^2r}{8} & \frac{1}{4} & . & -\frac{ar}{4} & -\frac{abr}{8} & -\frac{a^2r}{8} & \frac{1}{4} & . & -\frac{ar}{4} & \frac{abr}{8} & -\frac{a^2r}{8} \\
-\frac{1}{4} & . & -\frac{bs}{4} & -\frac{b^2s}{8} & \frac{abs}{8} & \frac{1}{4} & . & -\frac{bs}{4} & \frac{b^2s}{8} & \frac{abs}{8} & -\frac{1}{4} & . & -\frac{bs}{4} & -\frac{b^2s}{8} & -\frac{abs}{8} & \frac{1}{4} & . & -\frac{bs}{4} & \frac{b^2s}{8} & -\frac{abs}{8} \\
\frac{1}{4} & . & \frac{3ar}{8} & \frac{abr}{8} & . & -\frac{1}{4} & . & -\frac{3ar}{8} & \frac{abr}{8} & . & -\frac{1}{4} & . & \frac{3ar}{8} & \frac{abr}{8} & . & \frac{1}{4} & . & -\frac{3ar}{8} & \frac{abr}{8} & . \\
. & \frac{1}{4} & -\frac{3h_2}{16b} & -\frac{(a^2r-b^2t)}{16} & -\frac{a^2s}{8} & . & \frac{1}{4} & \frac{3h_1}{16b} & -\frac{(a^2r-b^2t)}{16} & -\frac{a^2s}{8} & . & \frac{1}{4} & -\frac{3h_1}{16b} & -\frac{(a^2r-b^2t)}{16} & -\frac{a^2s}{8} & . & \frac{1}{4} & \frac{3h_2}{16b} & -\frac{(a^2r-b^2t)}{16} & -\frac{a^2s}{8} \\
. & -\frac{1}{4} & -\frac{as}{4} & -\frac{abs}{8} & \frac{a^2s}{8} & . & -\frac{1}{4} & -\frac{as}{4} & \frac{abs}{8} & \frac{a^2s}{8} & . & \frac{1}{4} & -\frac{as}{4} & -\frac{abs}{8} & -\frac{a^2s}{8} & . & \frac{1}{4} & -\frac{as}{4} & \frac{abs}{8} & -\frac{a^2s}{8} \\
. & -\frac{1}{4} & -\frac{bt}{4} & -\frac{b^2t}{8} & \frac{abt}{8} & . & \frac{1}{4} & -\frac{bt}{4} & \frac{b^2t}{8} & \frac{abt}{8} & . & -\frac{1}{4} & -\frac{bt}{4} & -\frac{b^2t}{8} & -\frac{abt}{8} & . & \frac{1}{4} & -\frac{bt}{4} & \frac{b^2t}{8} & -\frac{abt}{8} \\
. & \frac{1}{4} & \frac{3bt}{8} & . & -\frac{abt}{8} & . & -\frac{1}{4} & \frac{3bt}{8} & . & -\frac{abt}{8} & . & -\frac{1}{4} & -\frac{3bt}{8} & . & -\frac{abt}{8} & . & \frac{1}{4} & -\frac{3bt}{8} & . & -\frac{abt}{8} \\
. & . & \frac{1}{4} & \frac{b}{8} & -\frac{a}{8} & . & . & \frac{1}{4} & -\frac{b}{8} & -\frac{a}{8} & . & . & \frac{1}{4} & \frac{b}{8} & \frac{a}{8} & . & . & \frac{1}{4} & -\frac{b}{8} & \frac{a}{8} \\
. & . & -\frac{3}{8} & . & \frac{a}{8} & . & . & -\frac{3}{8} & . & \frac{a}{8} & . & . & \frac{3}{8} & . & \frac{a}{8} & . & . & \frac{3}{8} & . & \frac{a}{8} \\
. & . & -\frac{3}{8} & -\frac{b}{8} & . & . & . & \frac{3}{8} & -\frac{b}{8} & . & . & . & -\frac{3}{8} & -\frac{b}{8} & . & . & . & \frac{3}{8} & -\frac{b}{8} & . \\
. & . & \frac{1}{4} & . & . & . & . & -\frac{1}{4} & . & . & . & . & -\frac{1}{4} & . & . & . & . & \frac{1}{4} & . & . \\
. & . & . & . & \frac{a}{8} & . & . & . & . & \frac{a}{8} & . & . & . & . & -\frac{a}{8} & . & . & . & . & -\frac{a}{8} \\
. & . & . & -\frac{b}{8} & . & . & . & . & \frac{b}{8} & . & . & . & . & -\frac{b}{8} & . & . & . & . & \frac{b}{8} & . \\
. & . & \frac{1}{8} & . & -\frac{a}{8} & . & . & \frac{1}{8} & . & -\frac{a}{8} & . & . & -\frac{1}{8} & . & -\frac{a}{8} & . & . & -\frac{1}{8} & . & -\frac{a}{8} \\
. & . & . & \frac{b}{8} & . & . & . & . & -\frac{b}{8} & . & . & . & . & -\frac{b}{8} & . & . & . & . & \frac{b}{8} & . \\
. & . & . & . & -\frac{a}{8} & . & . & . & . & \frac{a}{8} & . & . & . & . & \frac{a}{8} & . & . & . & . & -\frac{a}{8} \\
. & . & \frac{1}{8} & \frac{b}{8} & . & . & . & -\frac{1}{8} & \frac{b}{8} & . & . & . & \frac{1}{8} & \frac{b}{8} & . & . & . & -\frac{1}{8} & \frac{b}{8} & . \\
. & . & -\frac{1}{16} & -\frac{b}{32} & \frac{a}{32} & . & . & \frac{1}{16} & -\frac{b}{32} & -\frac{a}{32} & . & . & \frac{1}{16} & \frac{b}{32} & \frac{a}{32} & . & . & -\frac{1}{16} & \frac{b}{32} & -\frac{a}{32} \\
. & . & . & \frac{b}{8} & \frac{a}{8} & . & . & . & \frac{b}{8} & -\frac{a}{8} & . & . & . & -\frac{b}{8} & \frac{a}{8} & . & . & . & -\frac{b}{8} & -\frac{a}{8}
\end{pmatrix}
$$

$$h_1 = a^2r - b^2t + 2sab$$

$$h_2 = a^2r - b^2t - 2sab$$

TABLE 5. $\tilde{B}^{-1}$ Matrix for Compatible Element

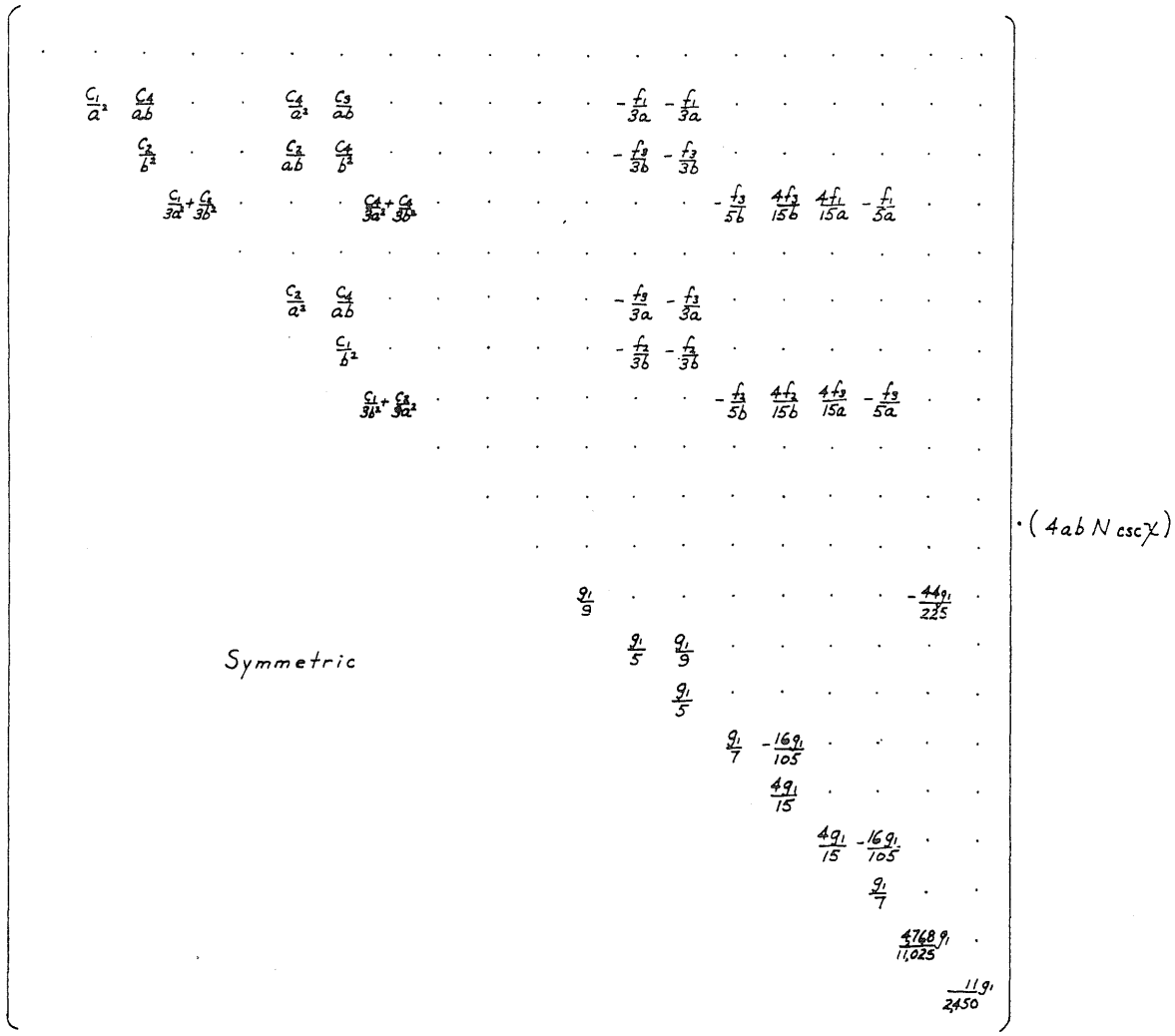

TABLE 6. $\left[\iint \tilde{D}^{m,T}\, E^{m,T}\, \tilde{D}^{m} \sin\chi\, dxdy\right]$ Matrix for Compatible Element

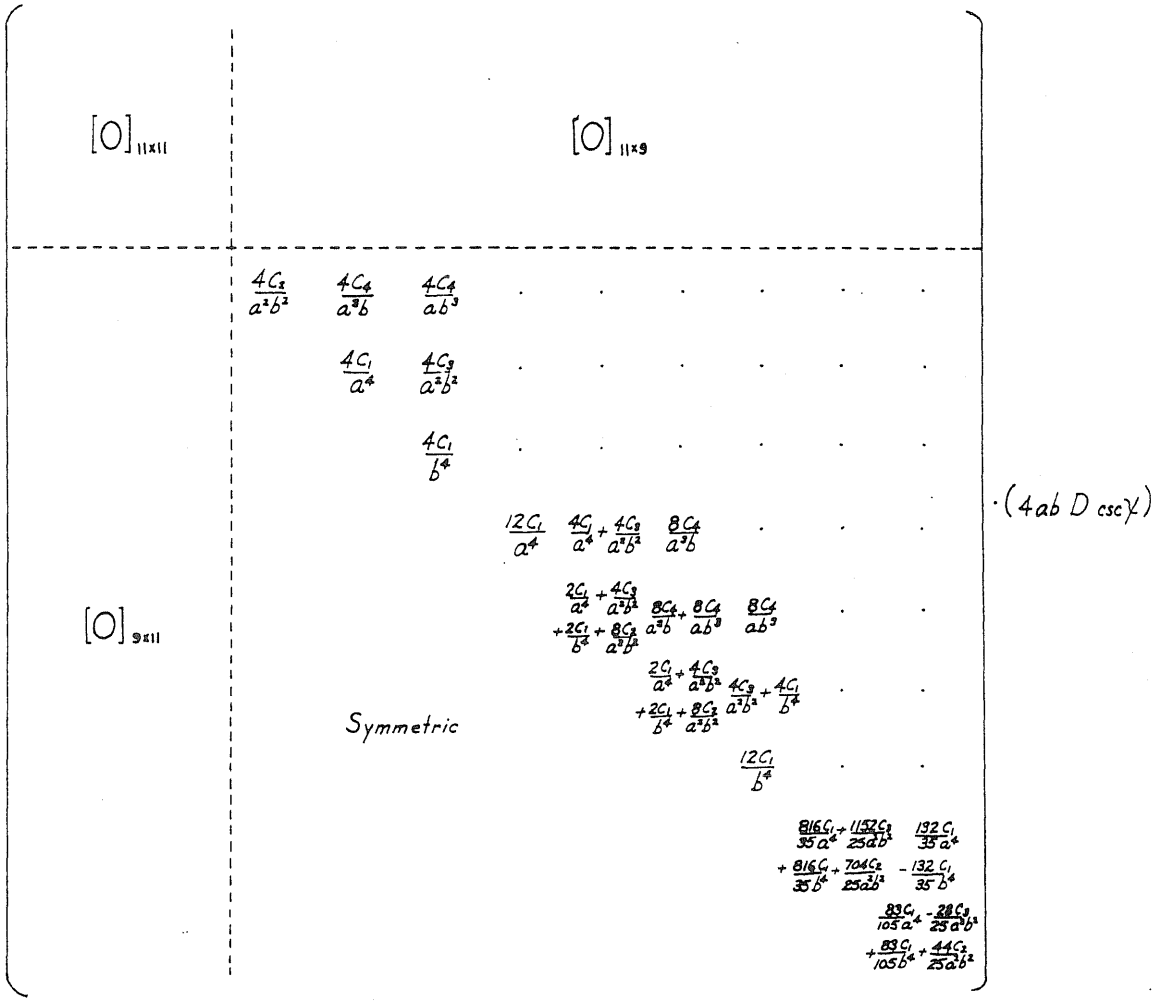

TABLE 7. $\left[\iint \tilde{D}^{b,T}\, E^{b,T}\, \tilde{D}^{b} \sin\chi \, dxdy\right]$ Matrix for Compatible Element

$$
\left(\begin{array}{cccccccccccccccccc}
\cdot & \frac{C_1}{a} & \frac{C_4}{b} & \eta\frac{C_1}{a}+\xi\frac{C_4}{b} & \cdot & \frac{C_4}{a} & \frac{C_2}{b} & \xi\frac{C_2}{b}+\eta\frac{C_4}{a} & \cdot & \cdot & \cdot & -\xi\eta f_1 & -\xi^2 f_1 & -\eta^2 f_1 & -\xi^3 f_1 & \cdot & \cdot & -\eta^3 f_1 & \cdot & \cdot \\
\cdot & \frac{C_3}{a} & \frac{C_4}{b} & \eta\frac{C_3}{a}+\xi\frac{C_4}{b} & \cdot & \frac{C_4}{a} & \frac{C_1}{b} & \xi\frac{C_1}{b}+\eta\frac{C_4}{a} & \cdot & \cdot & \cdot & -\xi\eta f_2 & -\xi^2 f_2 & -\eta^2 f_2 & -\xi^3 f_2 & \cdot & \cdot & -\eta^3 f_2 & \cdot & \cdot \\
\cdot & \frac{C_4}{a} & \frac{C_2}{b} & \eta\frac{C_4}{a}+\xi\frac{C_2}{b} & \cdot & \frac{C_2}{a} & \frac{C_4}{b} & \xi\frac{C_4}{b}+\eta\frac{C_2}{a} & \cdot & \cdot & \cdot & -\xi\eta f_3 & -\xi^2 f_3 & -\eta^2 f_3 & -\xi^3 f_3 & \cdot & \cdot & -\eta^3 f_3 & \cdot & \cdot \\
\hline
\cdot & \cdot & \cdot & \cdot & \cdot & \cdot & \cdot & \cdot & \cdot & \cdot & \cdot & -\frac{2C_4}{ab} & -\frac{2C_1}{a^2} & -\frac{2C_3}{b^2} & -\frac{6\xi C_1}{a^2} & \begin{array}{c}-\xi\frac{C_1}{a^2}\\ -\xi\frac{C_3}{b^2}\\ -2\eta\frac{C_4}{ab}\end{array} & \begin{array}{c}-\eta\frac{C_1}{a^2}\\ -\eta\frac{C_3}{b^2}\\ -2\xi\frac{C_4}{ab}\end{array} & -6\eta\frac{C_3}{b^2} & \begin{array}{c}-12\xi\eta\frac{C_1}{a^2}\\ -12\xi\eta\frac{C_3}{b^2}\\ -8\frac{C_4}{ab}\end{array} & \begin{array}{c}-2\xi\eta\frac{C_1}{a^2}\\ +2\xi\eta\frac{C_3}{b^2}\end{array} \\
\cdot & \cdot & \cdot & \cdot & \cdot & \cdot & \cdot & \cdot & \cdot & \cdot & \cdot & -\frac{2C_4}{ab} & -\frac{2C_3}{a^2} & -\frac{2C_1}{b^2} & -\frac{6\xi C_3}{a^2} & \begin{array}{c}-\xi\frac{C_3}{a^2}\\ -\xi\frac{C_1}{b^2}\\ -2\eta\frac{C_4}{ab}\end{array} & \begin{array}{c}-\eta\frac{C_3}{a^2}\\ -\eta\frac{C_1}{b^2}\\ -2\xi\frac{C_4}{ab}\end{array} & -6\eta\frac{C_1}{b^2} & \begin{array}{c}-12\xi\eta\frac{C_3}{a^2}\\ -12\xi\eta\frac{C_1}{b^2}\\ -8\frac{C_4}{ab}\end{array} & \begin{array}{c}-2\xi\eta\frac{C_3}{a^2}\\ +2\xi\eta\frac{C_1}{b^2}\end{array} \\
\cdot & \cdot & \cdot & \cdot & \cdot & \cdot & \cdot & \cdot & \cdot & \cdot & \cdot & -\frac{2C_2}{ab} & -\frac{2C_4}{a^2} & -\frac{2C_4}{b^2} & -\frac{6\xi C_4}{a^2} & \begin{array}{c}-\xi\frac{C_4}{a^2}\\ -\xi\frac{C_4}{b^2}\\ -2\eta\frac{C_2}{ab}\end{array} & \begin{array}{c}-\eta\frac{C_4}{a^2}\\ -\eta\frac{C_4}{b^2}\\ -2\xi\frac{C_2}{ab}\end{array} & -6\eta\frac{C_4}{b^2} & \begin{array}{c}-12\xi\eta\frac{C_4}{a^2}\\ -12\xi\eta\frac{C_4}{b^2}\\ -8\frac{C_2}{ab}\end{array} & \begin{array}{c}-2\xi\eta\frac{C_4}{a^2}\\ +2\xi\eta\frac{C_4}{b^2}\end{array}
\end{array}\right)
\begin{array}{l}\cdot(N\csc\gamma)\\ \\ \\ \cdot(D\csc\gamma)\end{array}
$$

(valid only at nodes of element)

TABLE 8. $E^{m}\tilde{D}^{m}$ and $E^{b}\tilde{D}^{b}$ Matrices for Compatible Element

$$
\begin{bmatrix}
\frac{AE}{L} & \cdot & \cdot & \cdot & -\frac{eAE}{L} & \cdot & -\frac{AE}{L} & \cdot & \cdot & \cdot & \frac{eAE}{L} & \cdot \\
\frac{12EI_z}{L^3} & \cdot & \frac{12eEI_z}{L^3} & \cdot & \frac{6EI_z}{L^2} & \cdot & -\frac{12EI_z}{L^3} & \cdot & -\frac{12eEI_z}{L^3} & \cdot & \frac{6EI_z}{L^2} & \\
\frac{12EI_y}{L^3} & \cdot & -\frac{6EI_y}{L^2} & \cdot & \cdot & \cdot & -\frac{12EI_y}{L^3} & \cdot & -\frac{6EI_y}{L^2} & \cdot & & \\
\frac{GJ}{L} + \frac{12e^2EI_z}{L^3} & \cdot & \frac{6eEI_z}{L^2} & \cdot & -\frac{12eEI_z}{L^3} & \cdot & -\frac{GJ}{L} - \frac{12e^2EI_z}{L^3} & \cdot & \frac{6eEI_z}{L^2} & & & \\
\frac{4EI_y}{L} + e^2\frac{AE}{L} & \cdot & \frac{eAE}{L} & \cdot & \frac{6EI_y}{L^2} & \cdot & \frac{2EI_y}{L} - e^2\frac{AE}{L} & \cdot & & & & \\
\frac{4EI_z}{L} & \cdot & -\frac{6EI_z}{L^2} & \cdot & -\frac{6eEI_z}{L^2} & \cdot & \frac{2EI_z}{L} & & & & & \\
\frac{AE}{L} & \cdot & \cdot & \cdot & -\frac{eAE}{L} & \cdot & & & & & & \\
\text{Symmetric} & & & & & & & & & & & \\
\frac{12EI_z}{L^3} & \cdot & \frac{12eEI_z}{L^3} & \cdot & -\frac{6EI_z}{L^2} & & & & & & & \\
\frac{12EI_y}{L^3} & \cdot & \frac{6EI_y}{L^2} & \cdot & & & & & & & & \\
\frac{GJ}{L} + 12e^2\frac{EI_z}{L^3} & \cdot & -\frac{6eEI_z}{L^2} & & & & & & & & & \\
\frac{4EI_y}{L} + e^2\frac{AE}{L} & \cdot & & & & & & & & & & \\
\frac{4EI_z}{L} & & & & & & & & & & &
\end{bmatrix}
$$

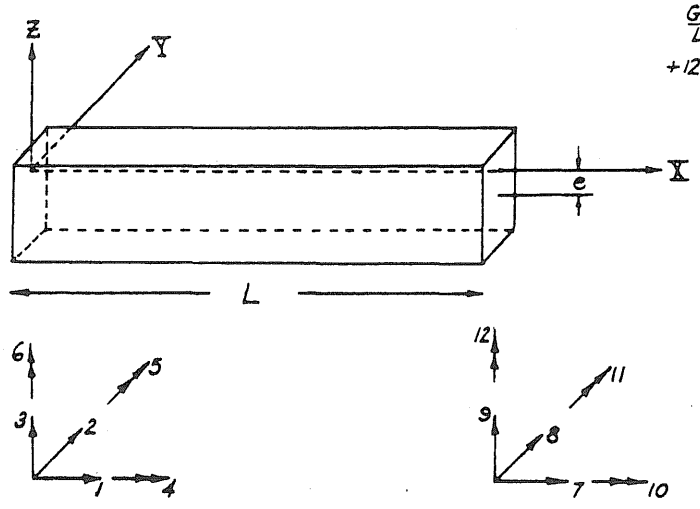

TABLE 9. Stiffness Matrix for Straight Beam with Respect to Eccentric Axes

$$
\begin{bmatrix}
k_1\bar{A} & \cdot & k_1\bar{B} & \cdot & k_1(\bar{C}-e\bar{A}) & \cdot & -k_1(\bar{A}\cos\beta + \bar{B}\sin\beta) & \cdot & k_1(\bar{A}\sin\beta - \bar{B}\cos\beta) & \cdot & k_1(\bar{A}R(1-\cos\beta) + \bar{A}e\cos\beta + \bar{B}e\sin\beta - \bar{B}R\sin\beta - \bar{C}) & \cdot \\
 & & k_2\bar{G} & \cdot & k_2(\bar{H}+e\bar{G}) & \cdot & k_2\bar{I} & \cdot & -k_2\bar{G} & \cdot & k_2(\bar{G}R(1-\cos\beta) - e\bar{G} - \bar{H}\cos\beta - \bar{I}\sin\beta) & k_2(\bar{G}R\sin\beta + \bar{H}\sin\beta - \bar{I}\cos\beta) \\
 & & & & k_1\bar{D} & \cdot & k_1(\bar{E}-e\bar{B}) & \cdot & -k_1(\bar{B}\cos\beta + \bar{D}\sin\beta) & \cdot & k_1(\bar{B}\sin\beta - \bar{D}\cos\beta) & k_1(\bar{B}R(1-\cos\beta) + \bar{B}e\cos\beta - \bar{D}R\sin\beta + \bar{D}e\sin\beta - \bar{E}) \\
 & & & & & & k_2(\bar{I} + 2e\bar{H} + e^2\bar{G}) & \cdot & k_2(\bar{K}+e\bar{I}) & \cdot & -k_1(\bar{H}+e\bar{G}) & \cdot \\
 & & & & & & & & & & k_2((\bar{H}+e\bar{G})R(1-\cos\beta) - e(\bar{H}+e\bar{G}) - (\bar{J}+e\bar{H})\cos\beta - (\bar{K}+e\bar{I})\sin\beta) & k_2(\bar{H}+e\bar{G})R\sin\beta + (\bar{J}+e\bar{H})\sin\beta - (\bar{K}+e\bar{I})\cos\beta \\
 & & & & & & & & & & & \\
 & & & & k_1(\bar{F} - 2e\bar{C} + e^2\bar{A}) & \cdot & -k_1((\bar{C}-e\bar{A})\cos\beta + (\bar{E}-e\bar{B})\sin\beta) & \cdot & k_1((\bar{C}-e\bar{A})\sin\beta - (\bar{E}-e\bar{B})\cos\beta) & \cdot & k_1((\bar{C}-e\bar{A})R(1-\cos\beta) + e(\bar{C}-e\bar{A})\cos\beta + e(\bar{E}-e\bar{B})\sin\beta - R(\bar{E}-e\bar{B})\sin\beta + e\bar{C}-\bar{F}) & \cdot \\
 & & & & & & & & & & k_2(\bar{I}R(1-\cos\beta) - e\bar{I} - \bar{K}\cos\beta - \bar{L}\sin\beta) & k_2(\bar{I}R\sin\beta + \bar{K}\sin\beta - \bar{L}\cos\beta) \\
 & & & & & & k_2\bar{L} & \cdot & -k_2\bar{I} & \cdot & & \\
 & & & & & & & & & & & \\
 & & & & & & k_1\bar{A} & \cdot & -k_1\bar{B} & \cdot & k_1(\bar{C}-e\bar{A}) & \cdot \\
 & & & & & & & & & & & \\
 & & & & & & & & k_2\bar{G} & \cdot & k_2(\bar{H}+e\bar{G}) & \cdot & -k_2\bar{I} \\
 & & & & & & & & & & & \\
 & & & & & & & & k_1\bar{D} & \cdot & -k_1(\bar{E}-e\bar{B}) & \cdot \\
 & & & & & & & & & & & \\
 & & & & & & & & & & k_2(\bar{J} + 2e\bar{H} + e^2\bar{G}) & \cdot & -k_2(\bar{K}+e\bar{I}) \\
 & & & & & & & & & & & \\
 & & & & & & & & & & k_1(\bar{F} - 2e\bar{C} + e^2\bar{A}) & \cdot \\
 & & & & & & & & & & & \\
 & & & & & & & & & & & k_2\bar{L}
\end{bmatrix}
$$

Symmetric

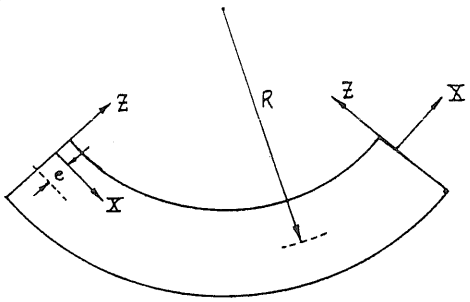

TABLE 10. Stiffness Matrix for Curved Beam with Respect to Eccentric Axes

Skew Angle, χ	$W_c = c \cdot 10^{-3}\frac{p_o a^4}{D}$			$M^+_{bc} = d \cdot 10^{-2} p_o a^2$			$M^+_{ad} = e \cdot 10^{-2} p_o a^2$		
	N-C*	C**	Morley***	N-C	C	Morley	N-C	C	Morley
75°	-1.159	-1.092	-1.123	-2.132	-1.924	-2.021	-2.398	-2.192	-2.280
60°	- .795	- .744	- .769	-1.642	-1.454	-1.544	-2.101	-1.909	-1.979
(12x12)	- .782	- .758		-1.592	-1.502		-2.034	-1.945	
45°	- .388	- .359	- .377	-1.025	- .897	- .976	-1.551	-1.396	-1.444

* Non-Compatible element

** Compatible element

*** Morley, Reference (33)

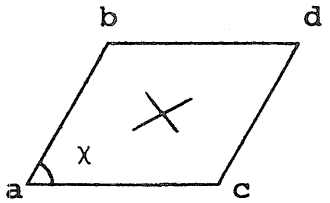

+ M_{bc} and M_{ad} denote normal bending moments at center of plate on diametral sections bc and ad respectively.

TABLE 11. Comparison of Deflections and Bending Moments in Uniformly Loaded Clamped Skewed Plates

Grid Size	$(N_{\bar{x}})_{\bar{x}=\frac{L_x}{2},\bar{y}=0}$		$(M_{\bar{x}})_{\bar{x}=\frac{L_x}{2},\bar{y}=0}$	
	St. Eq.*	Gen.**	St. Eq.	Gen.
3x3	-.461	.323	4.27	-4.30
6x6	-.088	.044	1.75	-3.18
9x9	-.042	-.011	-.67	-1.78

* Statically equivalent nodal loads

** Generalized nodal loads

$N_{\bar{x}}$ = (table entry) x $p_o L_x$

$M_{\bar{x}}$ = (table entry) x 10^{-4} $p_o L_x^2$

TABLE 12. Convergence of Natural Boundary Conditions for Uniformly Loaded Roller Supported Elliptical Paraboloid

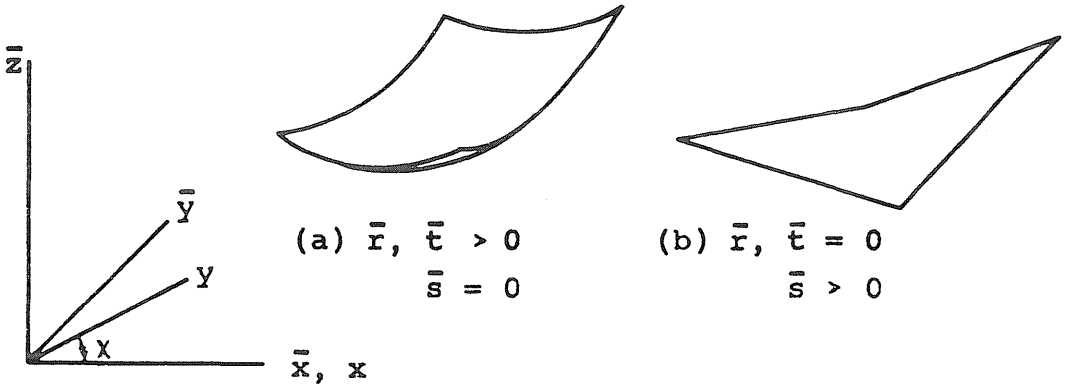

FIG. 1 SURFACES OF POSITIVE CURVATURE AND TWIST

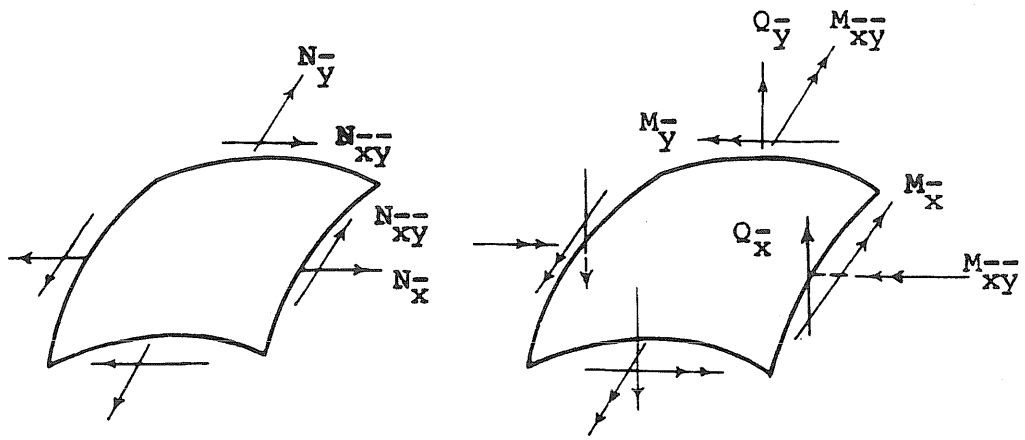

(a) Membrane Stress Resultants

(b) Bending Stress Resultants

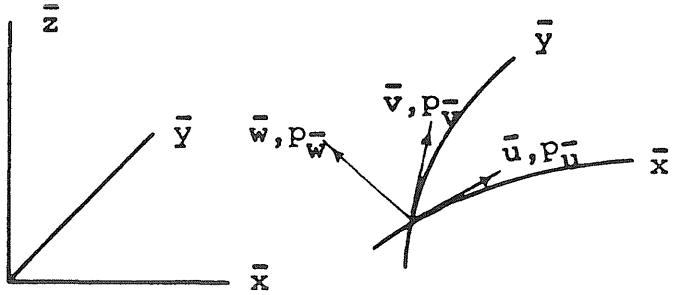

(c) Displacements and Loads

FIG. 2 SIGN CONVENTION FOR FORCES, MOMENTS AND DISPLACEMENTS IN ORTHOGONAL COORDINATES

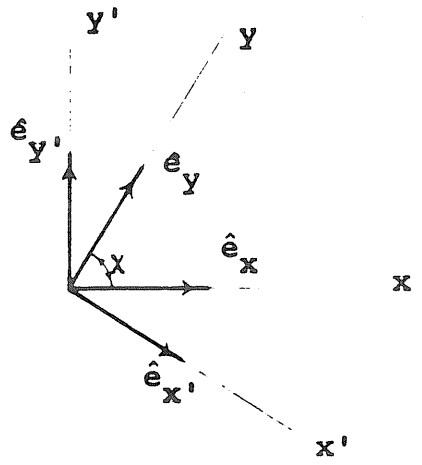

FIG. 3 UNIT VECTORS IN SHELL TANGENT PLANE

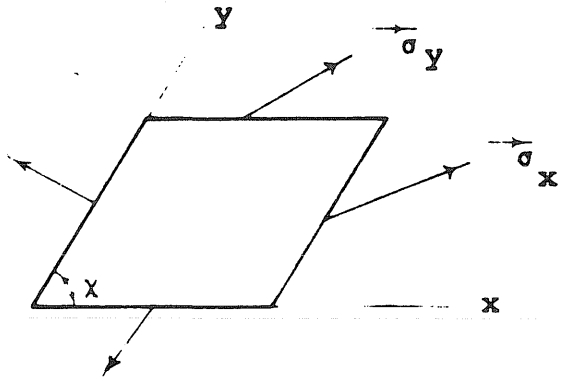

FIG. 4 STRESS VECTORS ACTING ON DIFFERENTIAL ELEMENT OF SHELL

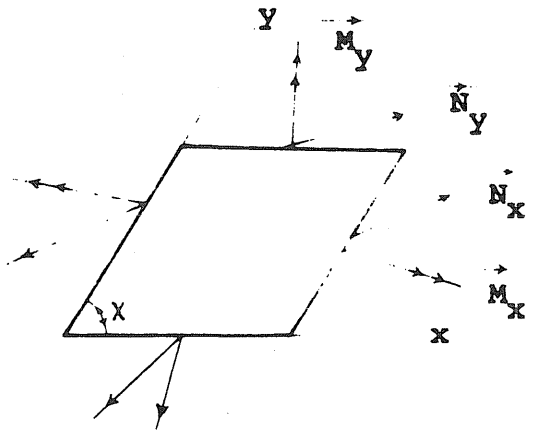

FIG. 5 STRESS RESULTANT AND MOMENT VECTORS ACTING ON DIFFERENTIAL ELEMENT OF SHELL

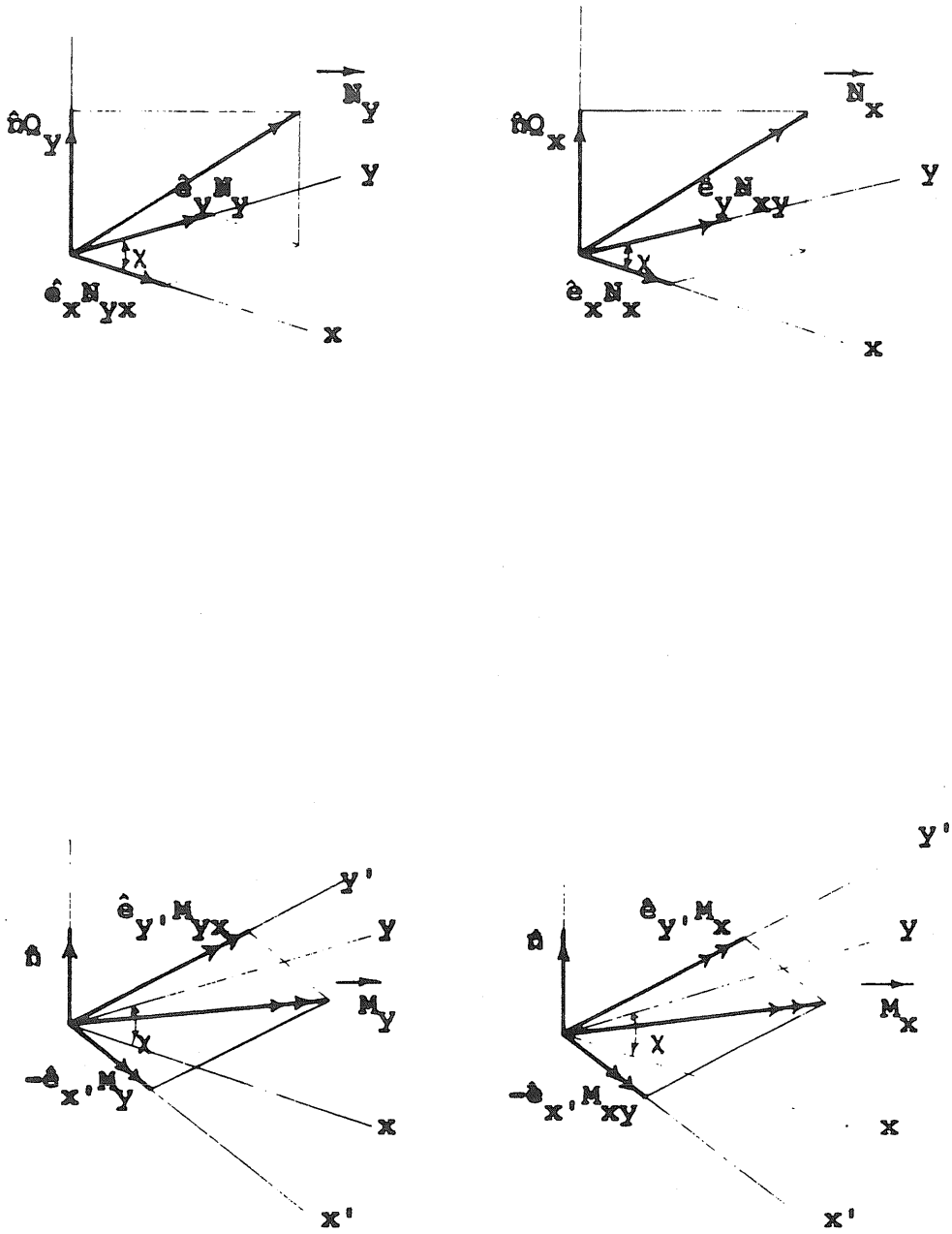

FIG. 6 REPRESENTATION OF STRESS RESULTANT AND MOMENT VECTORS IN OBLIQUE COORDINATES

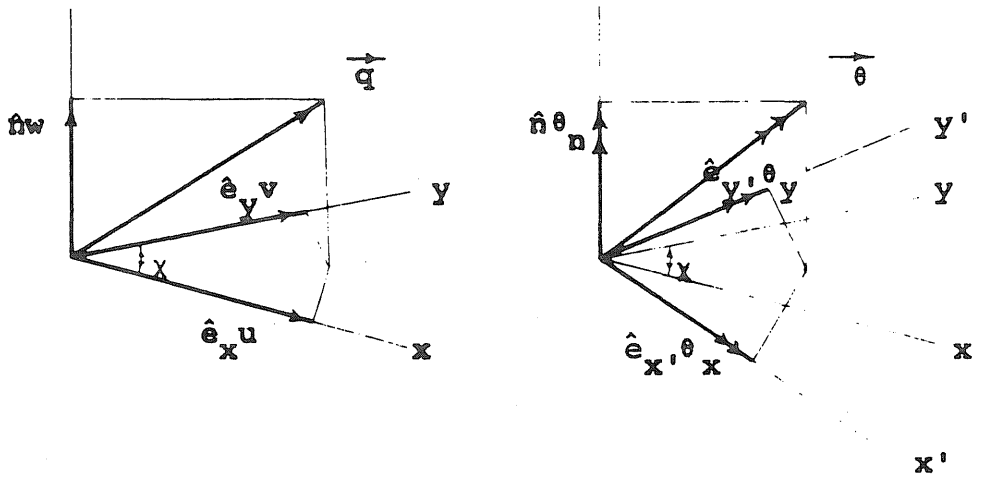

FIG. 7 REPRESENTATION OF DISPLACEMENT AND ROTATION VECTORS IN OBLIQUE COORDINATES

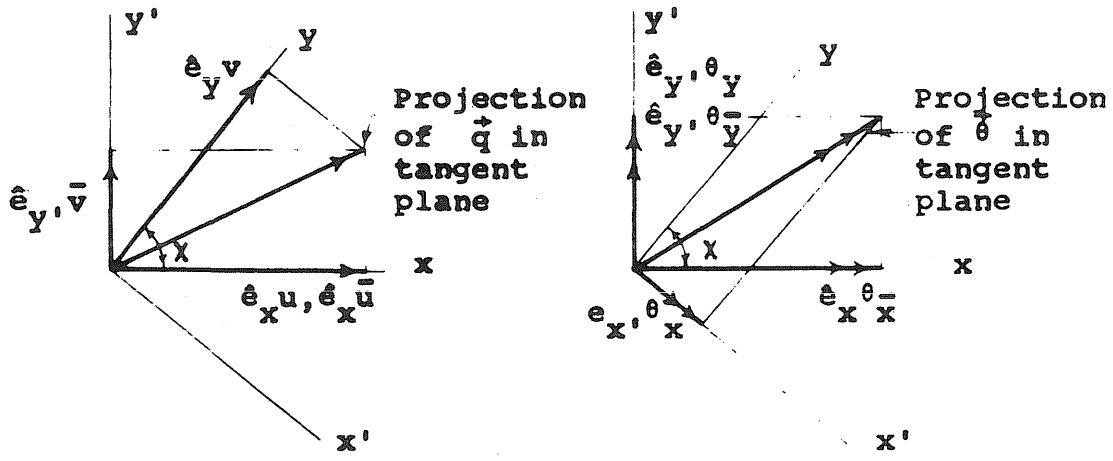

FIG. 8 RELATION BETWEEN ORTHOGONAL AND OBLIQUE COMPONENTS OF DISPLACEMENT AND ROTATION

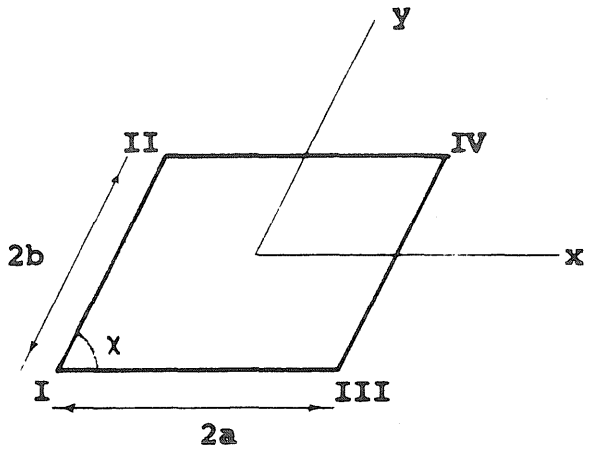

FIG. 9 GEOMETRY AND NODAL NUMBERING FOR SKEWED ELEMENT

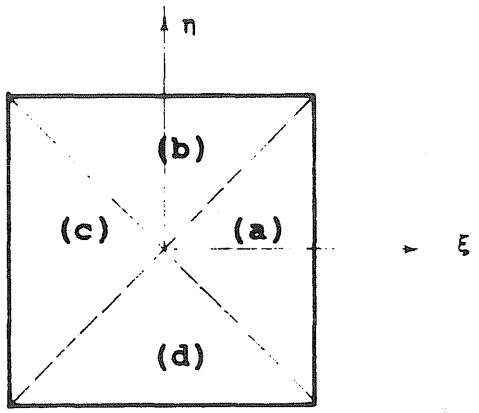

FIG. 10 SUB-REGIONS FOR FUNCTIONS F_6, F_9, F_{11}, F_{12}

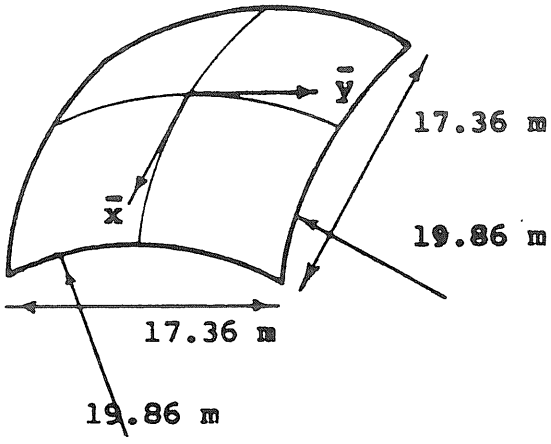

SHELL I

h = .07 m

ν = 0.0

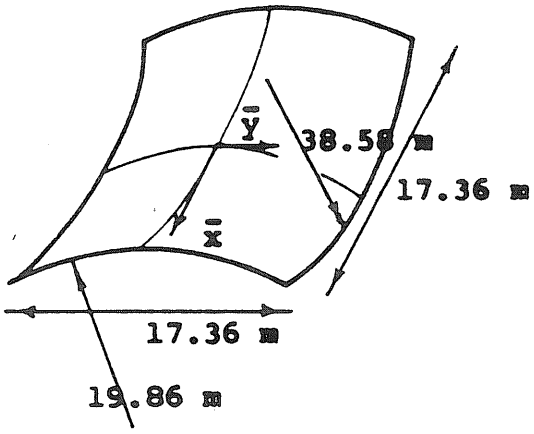

SHELL II

h = .07 m

ν = 0.0

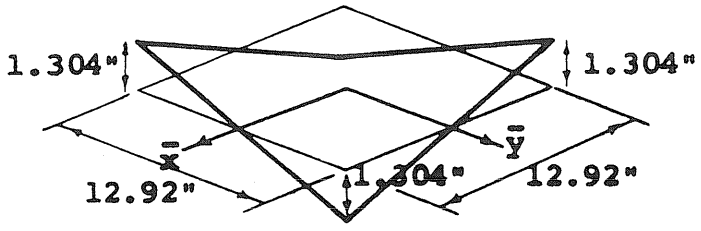

SHELL III

E = 5×10^5 lb/in^2

h = 0.25 in.

ν = 0.39

FIG. 11 SHELLS CONSIDERED IN NUMERICAL EXAMPLES

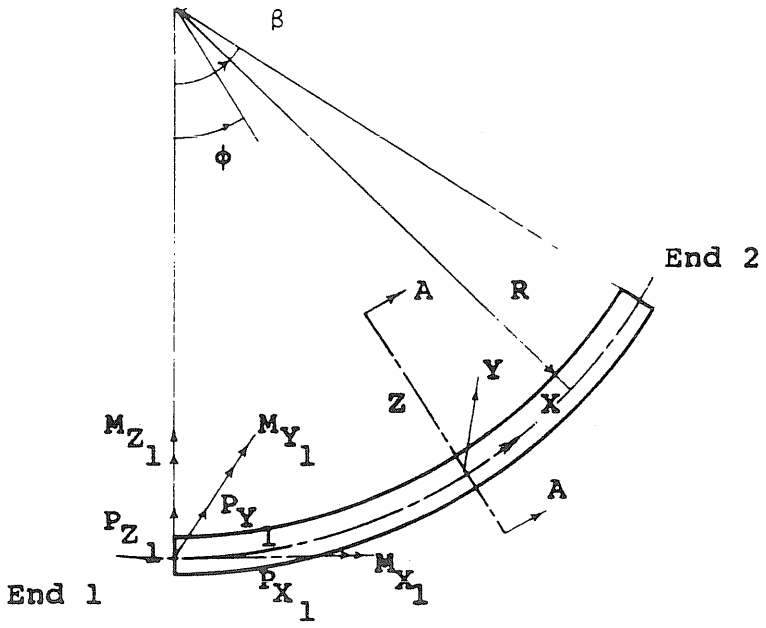

Section A-A

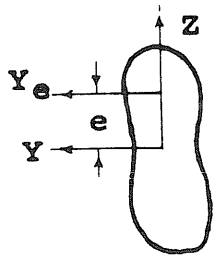

FIG. 12 CURVED EDGE BEAM

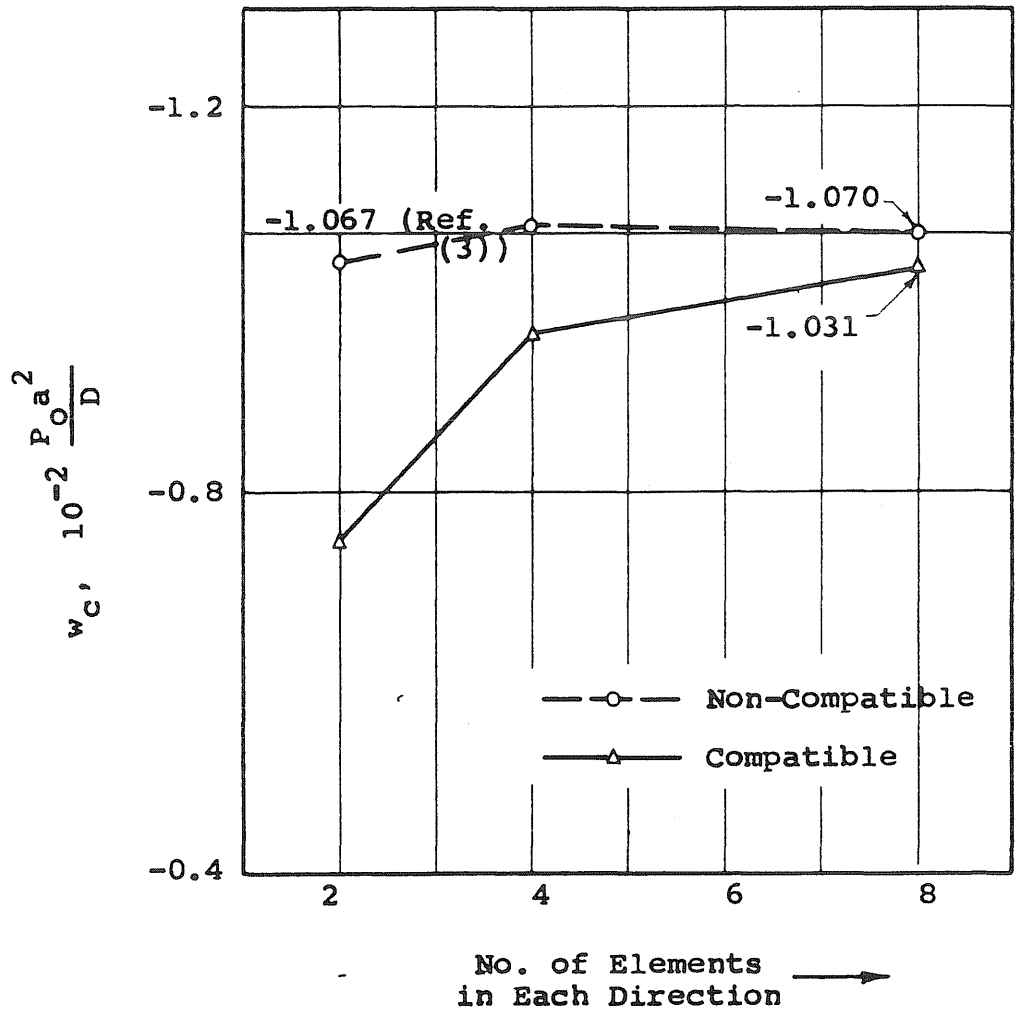

FIG. 13 CENTRAL DEFLECTION VS. GRID SIZE FOR SIMPLY SUPPORTED SKEWED PLATE UNDER CENTRAL CONCENTRATED LOAD

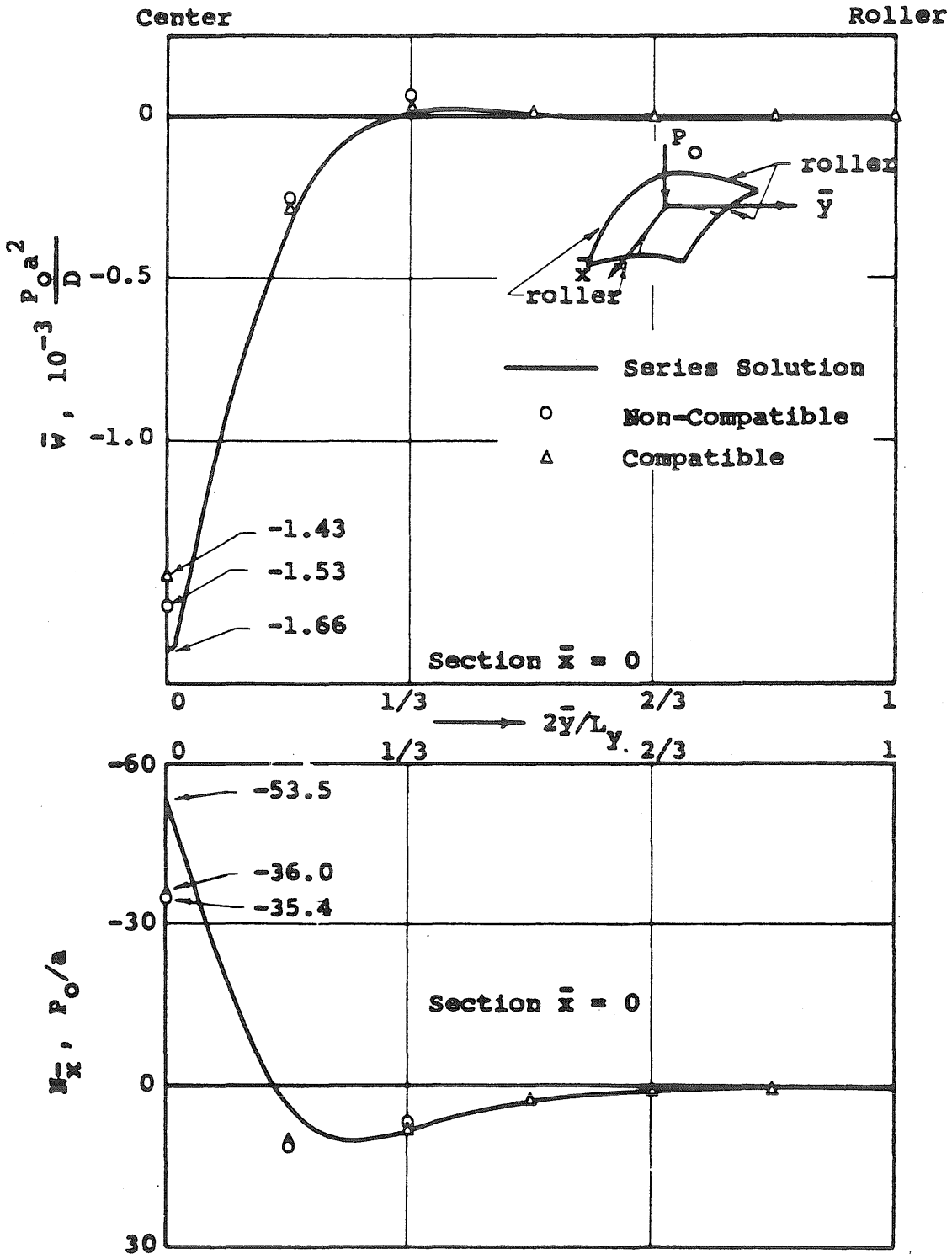

FIG. 14 DEFLECTION $\bar{w}$ AND FORCE $M_{\bar{x}}$ ACROSS MID-SECTION OF ROLLER SUPPORTED ELLIPTICAL PARABOLOID UNDER CENTRAL CONCENTRATED LOAD

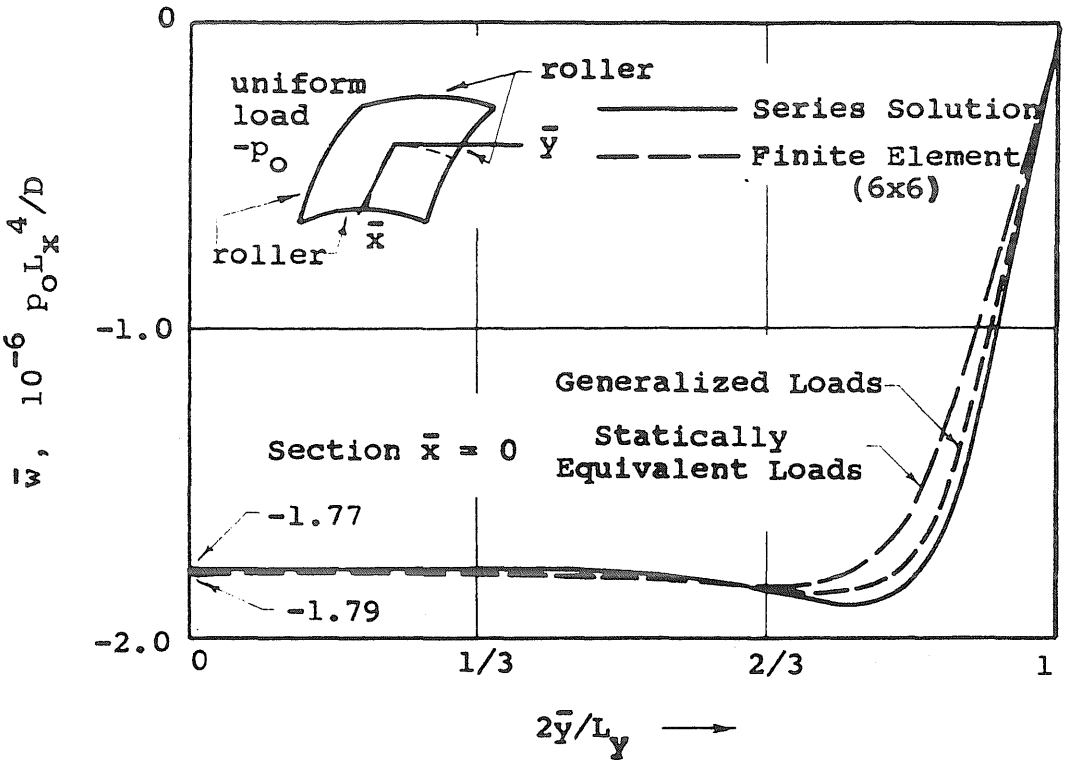

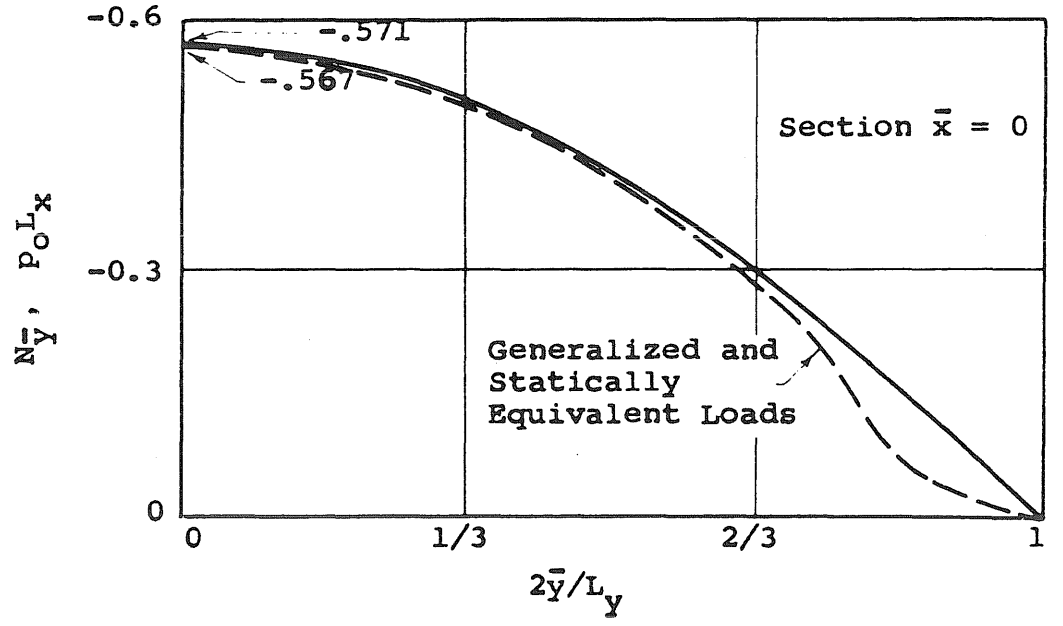

FIG. 15 DEFLECTION $\bar{w}$ AND FORCE $N_{\bar{y}}$ ACROSS MID-SECTION OF ROLLER SUPPORTED ELLIPTICAL PARABOLOID UNDER UNIFORM NORMAL LOAD

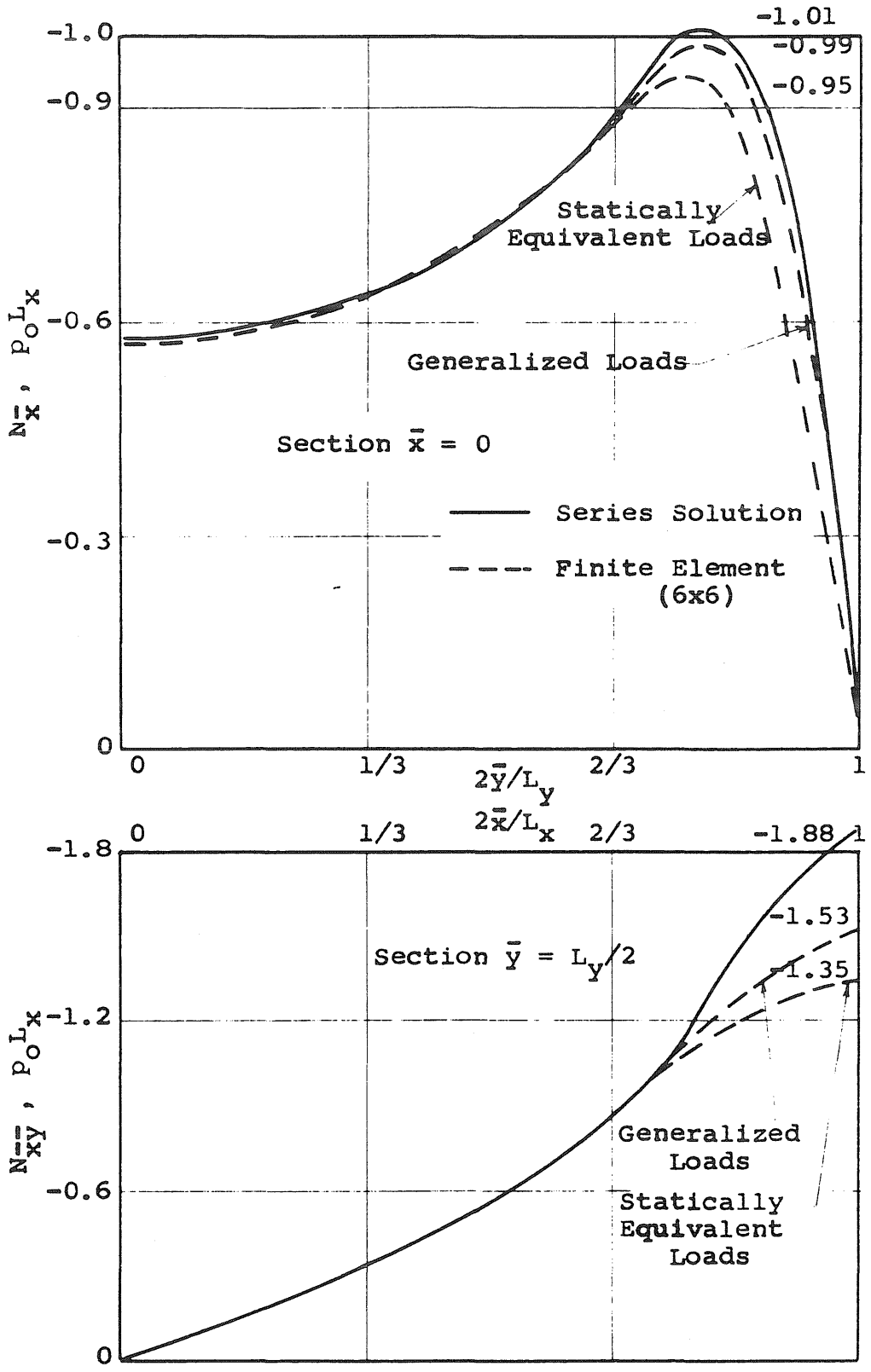

FIG. 16 FORCES $N_{\bar{x}}$ AND $N_{\bar{x}\bar{y}}$ IN ROLLER SUPPORTED ELLIPTICAL PARABOLOID UNDER UNIFORM NORMAL LOAD

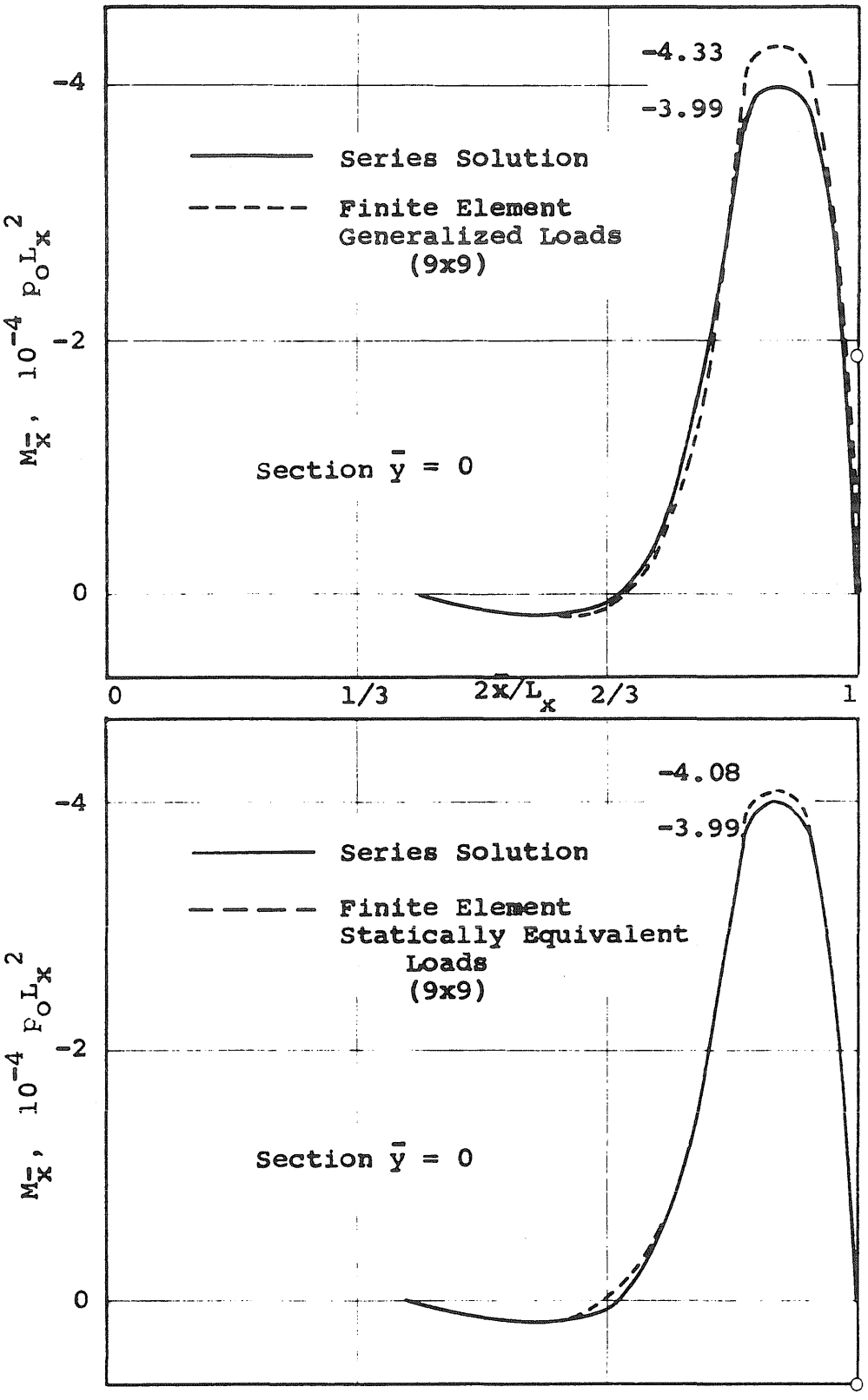

FIG. 17 BENDING MOMENT $M_{\bar{x}}$ ACROSS MID-SECTION OF ROLLER SUPPORTED ELLIPTICAL PARABOLOID UNDER UNIFORM NORMAL LOAD

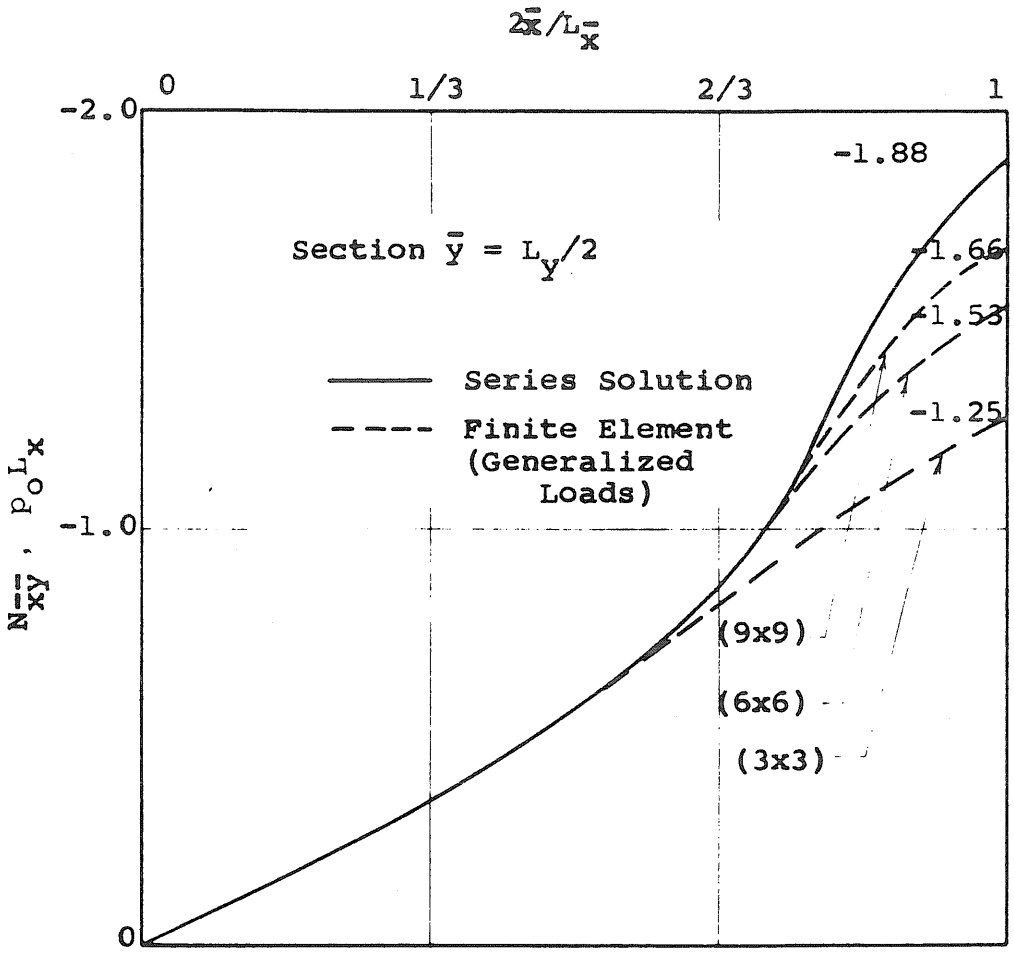

FIG. 18 FORCE $N_{\bar{x}\bar{y}}$ ACROSS SUPPORT OF ROLLER SUPPORTED ELLIPTICAL PARABOLOID UNDER UNIFORM NORMAL LOAD

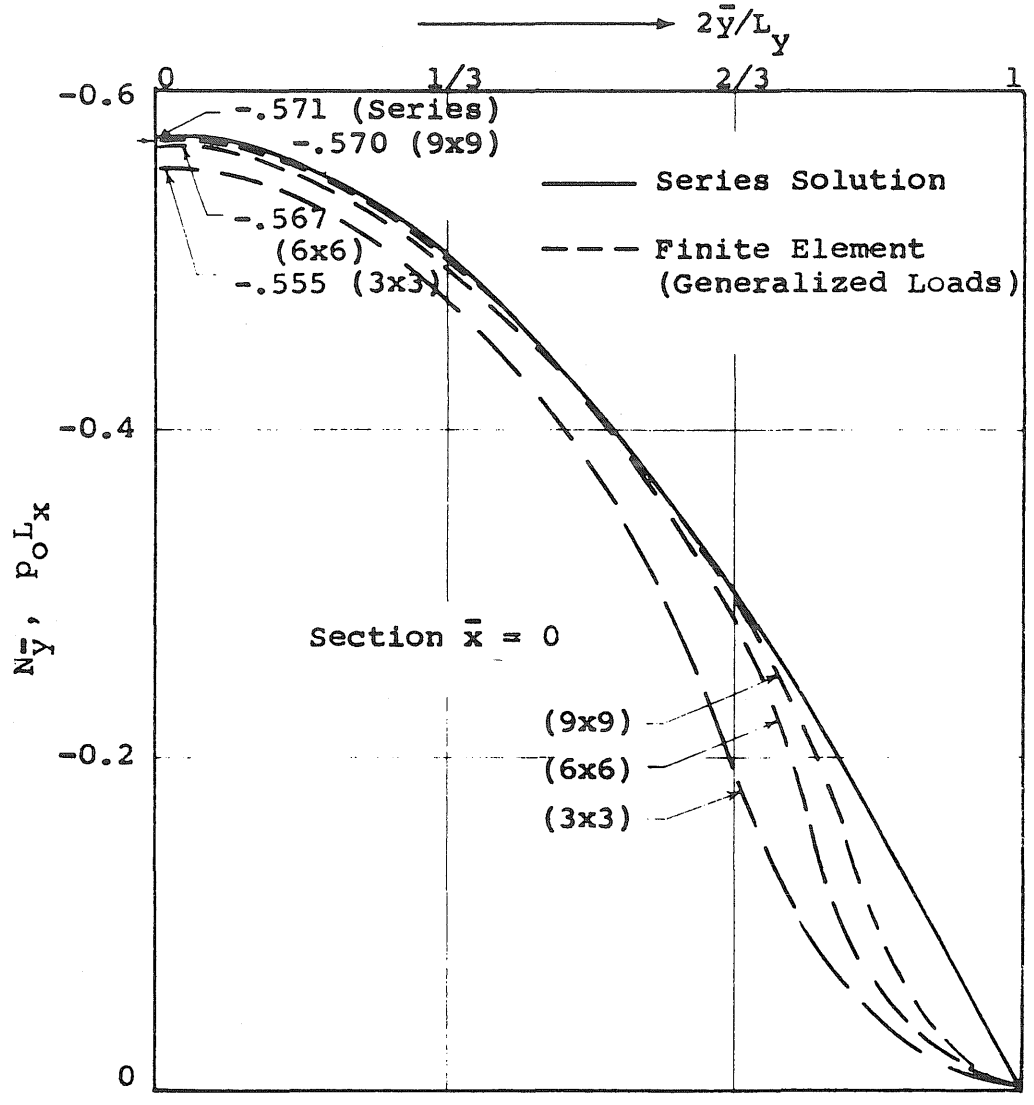

FIG. 19 FORCE $N_{\bar{y}}$ ACROSS MID-SECTION OF ROLLER SUPPORTED ELLIPTICAL PARABOLOID UNDER UNIFORM NORMAL LOAD

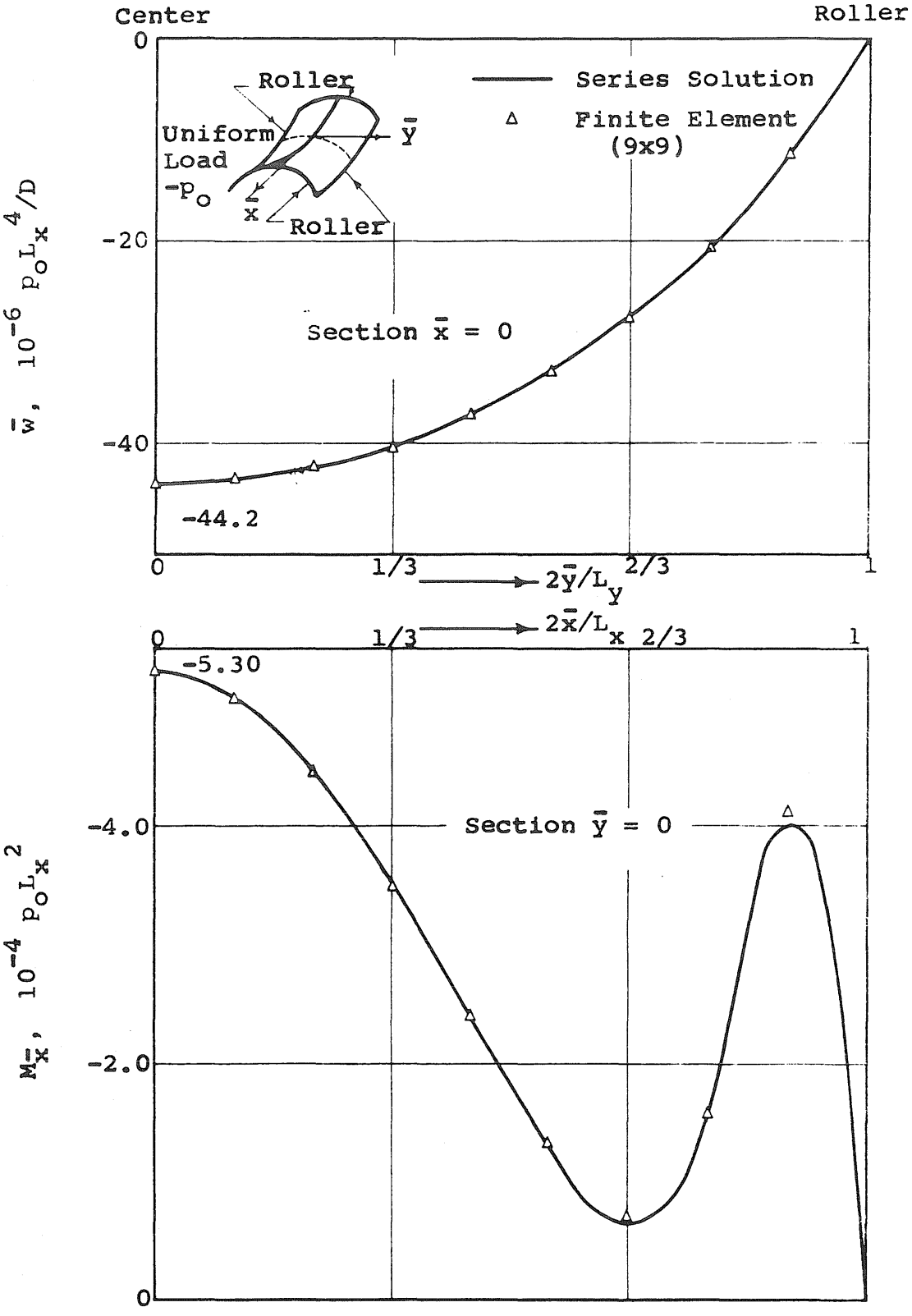

FIG. 20 DEFLECTION $\bar{w}$ AND BENDING MOMENT $M_{\bar{x}}$ IN ROLLER SUPPORTED HYPERBOLIC PARABOLOID BOUNDED BY LINES OF CURVATURE, UNDER UNIFORM NORMAL LOAD

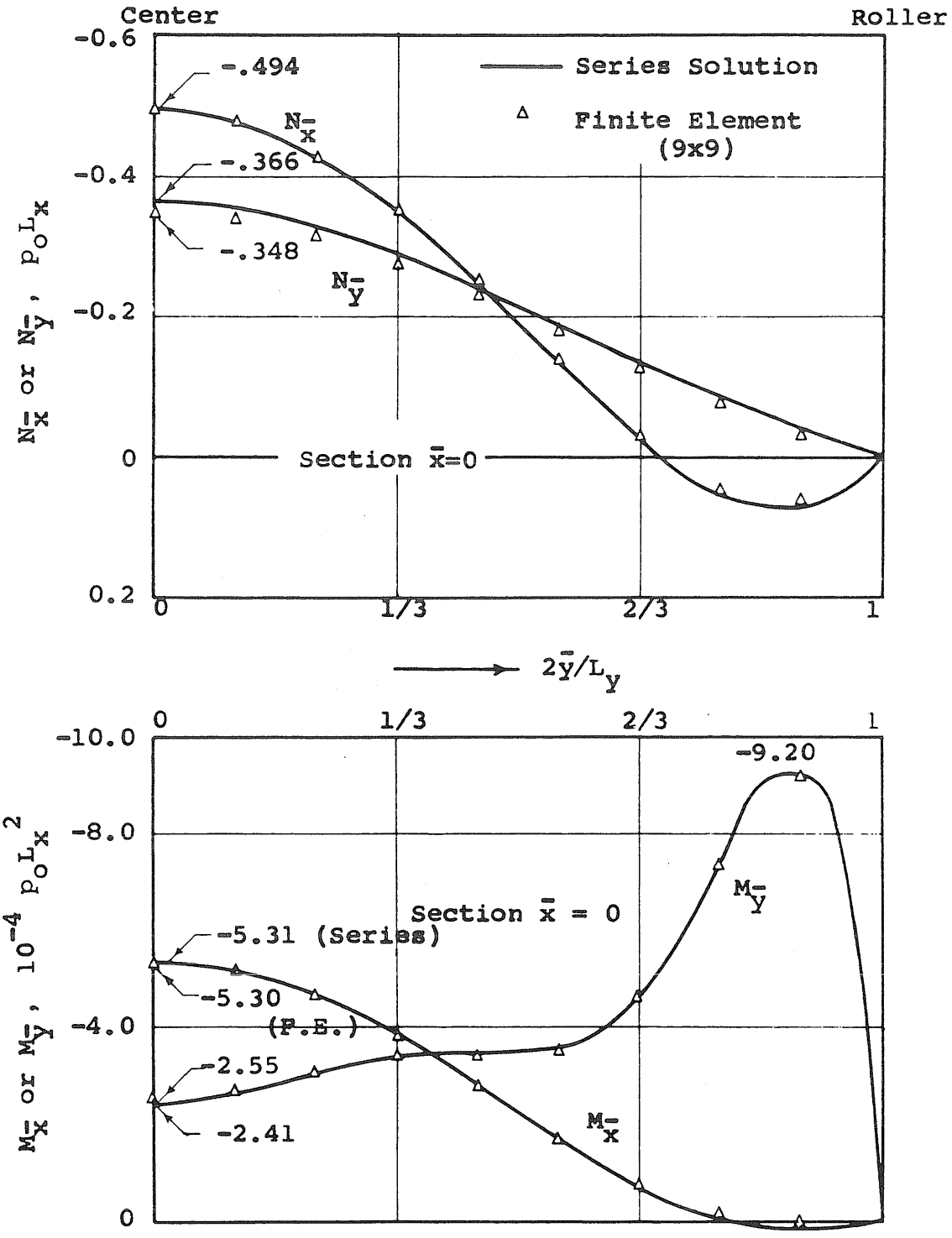

FIG. 21 FORCES $N_{\bar{x}}$, $N_{\bar{y}}$ AND BENDING MOMENTS $M_{\bar{x}}$, $M_{\bar{y}}$ ACROSS MID-SECTION OF ROLLER SUPPORTED HYPERBOLIC PARABOLOID BOUNDED BY LINES OF CURVATURE, UNDER UNIFORM NORMAL LOAD

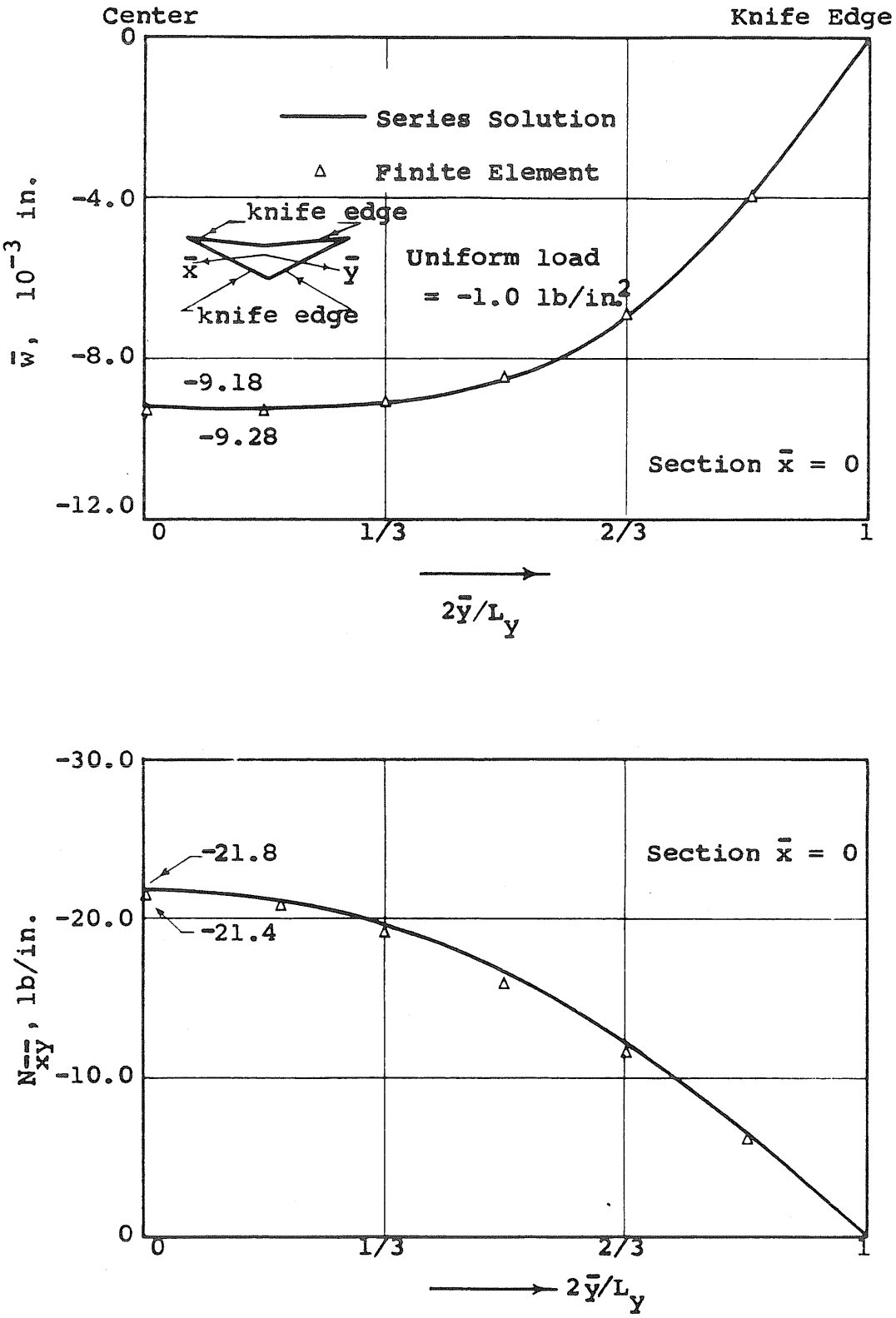

FIG. 22 DEFLECTION $\bar{w}$ AND FORCE $N_{\bar{x}\bar{y}}$ ACROSS MID-SECTION OF KNIFE-EDGE SUPPORTED HYPERBOLIC PARABOLOID BOUNDED BY CHARACTERISTICS, UNDER UNIFORM NORMAL LOAD

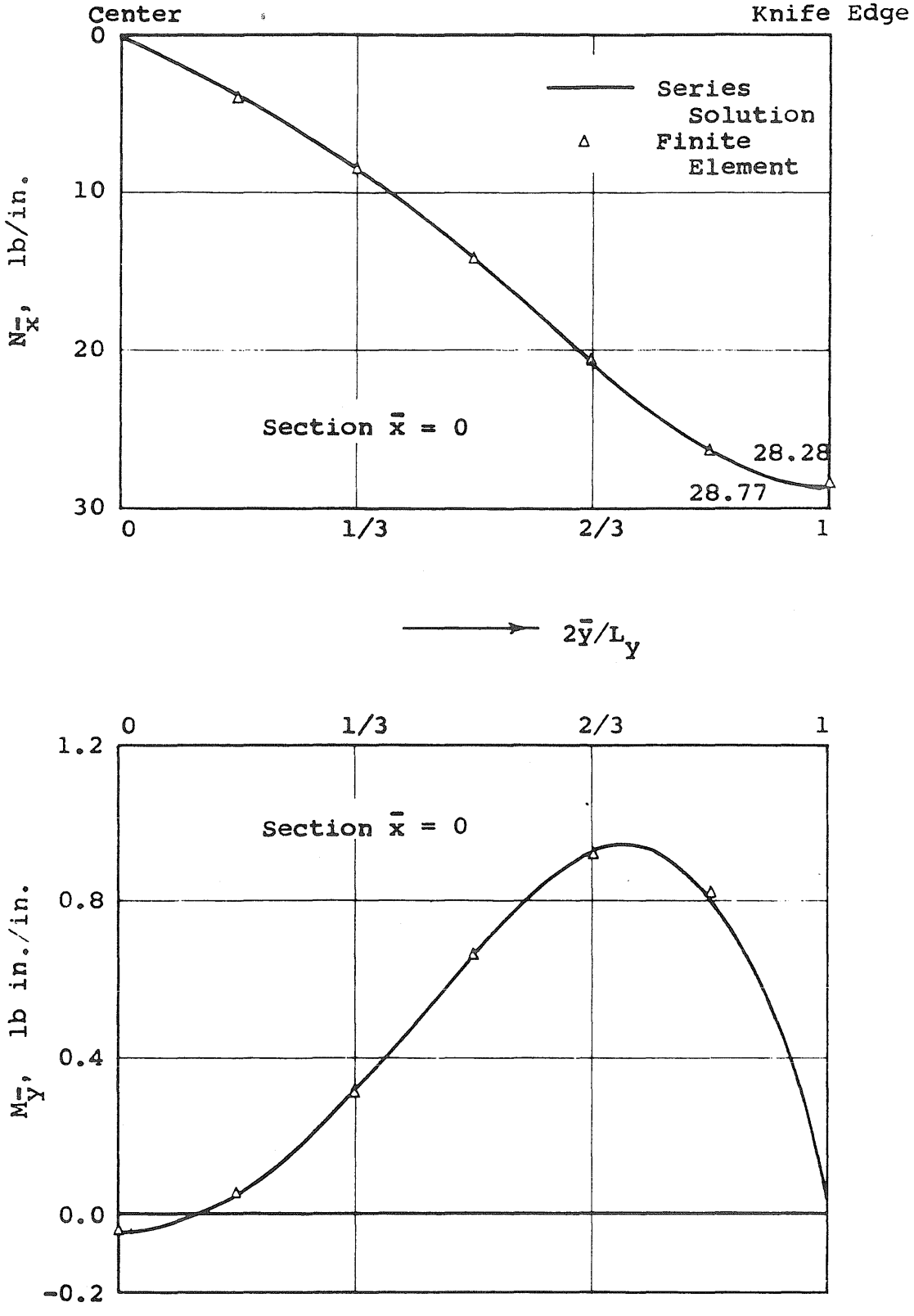

FIG. 23 FORCE $N_{\bar{x}}$ AND BENDING MOMENT $M_{\bar{y}}$ ACROSS MID-SECTION OF KNIFE-EDGE SUPPORTED HYPERBOLIC PARABOLOID BOUNDED BY CHARACTERISTICS, UNDER UNIFORM NORMAL LOAD

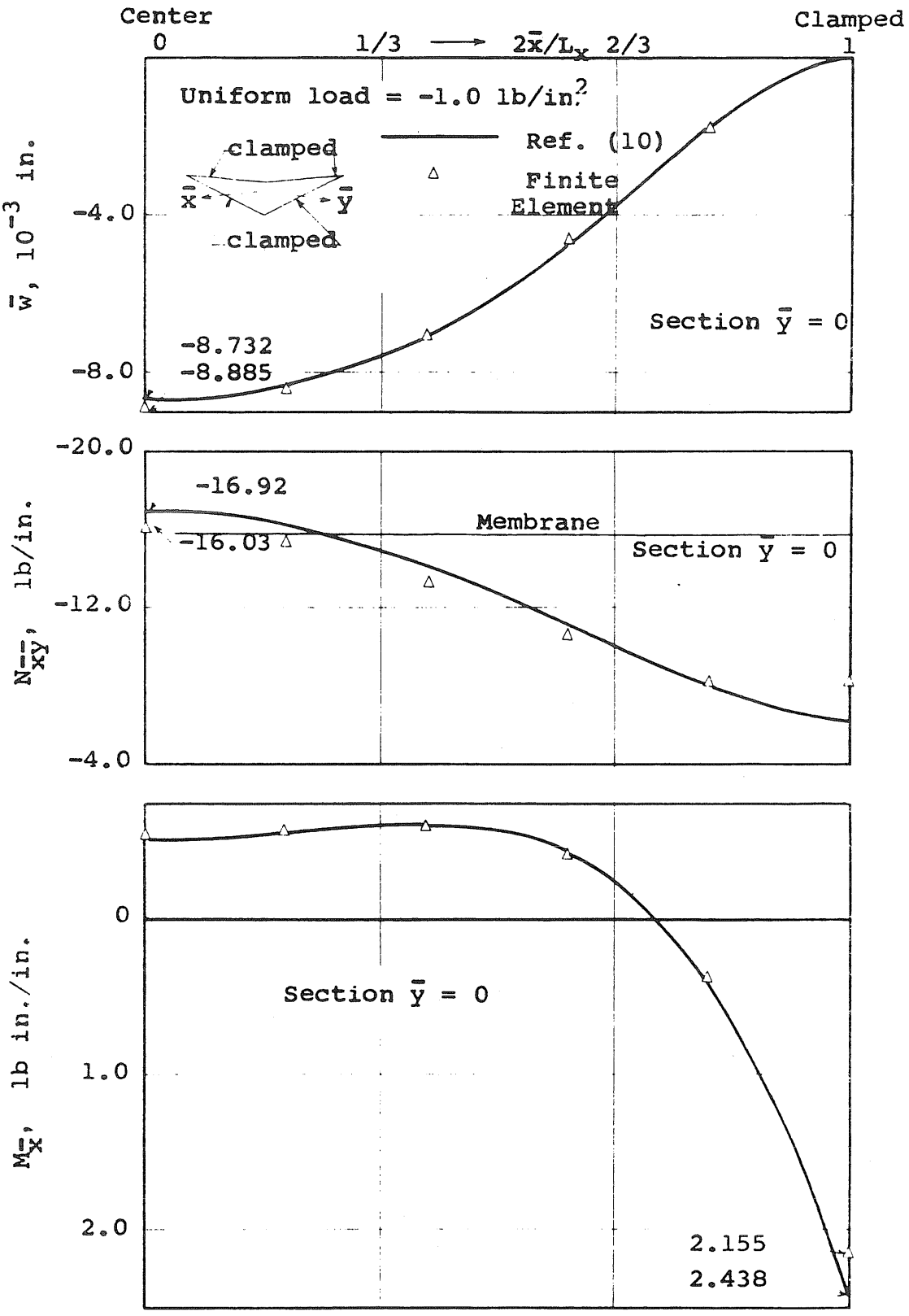

FIG. 24 DEFLECTION $\bar{w}$, FORCE $N_{\bar{x}\bar{y}}$ AND BENDING MOMENT $M_{\bar{x}}$ ACROSS MID-SECTION OF CLAMPED HYPERBOLIC PARABOLOID BOUNDED BY CHARACTERISTICS, UNDER UNIFORM NORMAL LOAD

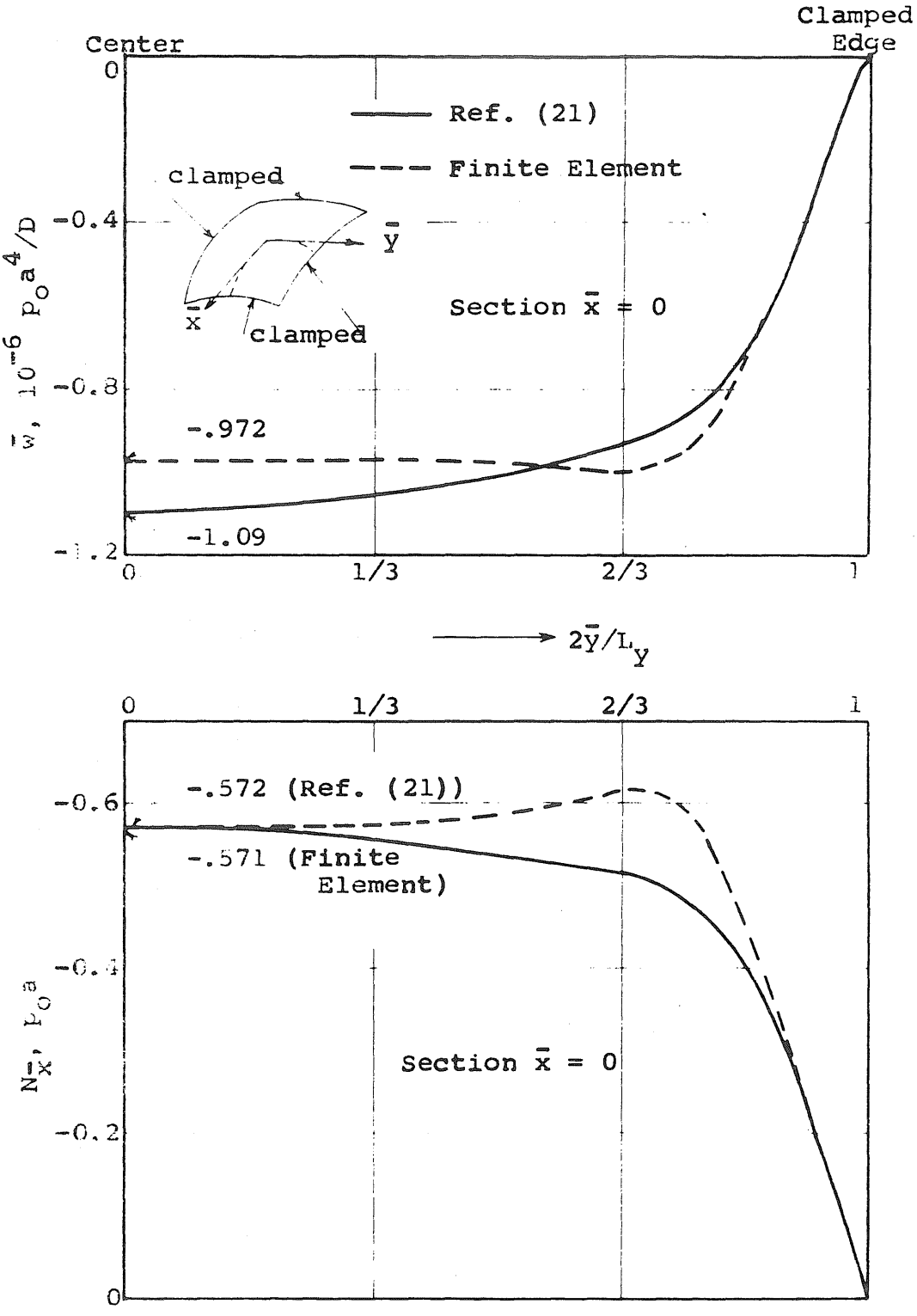

FIG. 25 DEFLECTION $\bar{w}$ AND FORCE $N_{\bar{x}}$ ACROSS MID-SECTION OF CLAMPED ELLIPTICAL PARABOLOID UNDER UNIFORM NORMAL LOAD

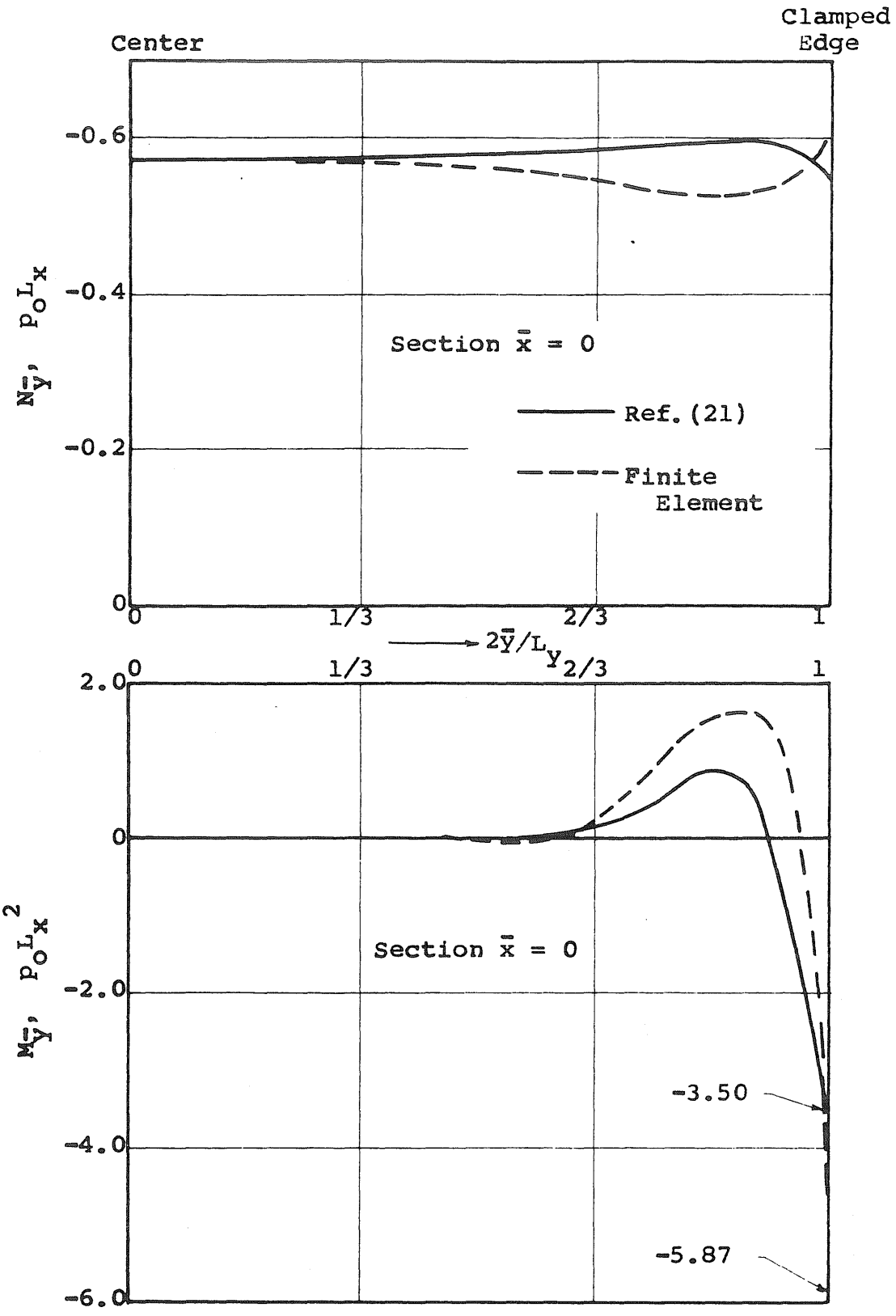

FIG. 26 FORCE $N_{\bar{y}}$ AND BENDING MOMENT $M_{\bar{y}}$ ACROSS MID-SECTION OF CLAMPED ELLIPTICAL PARABOLOID UNDER UNIFORM NORMAL LOAD

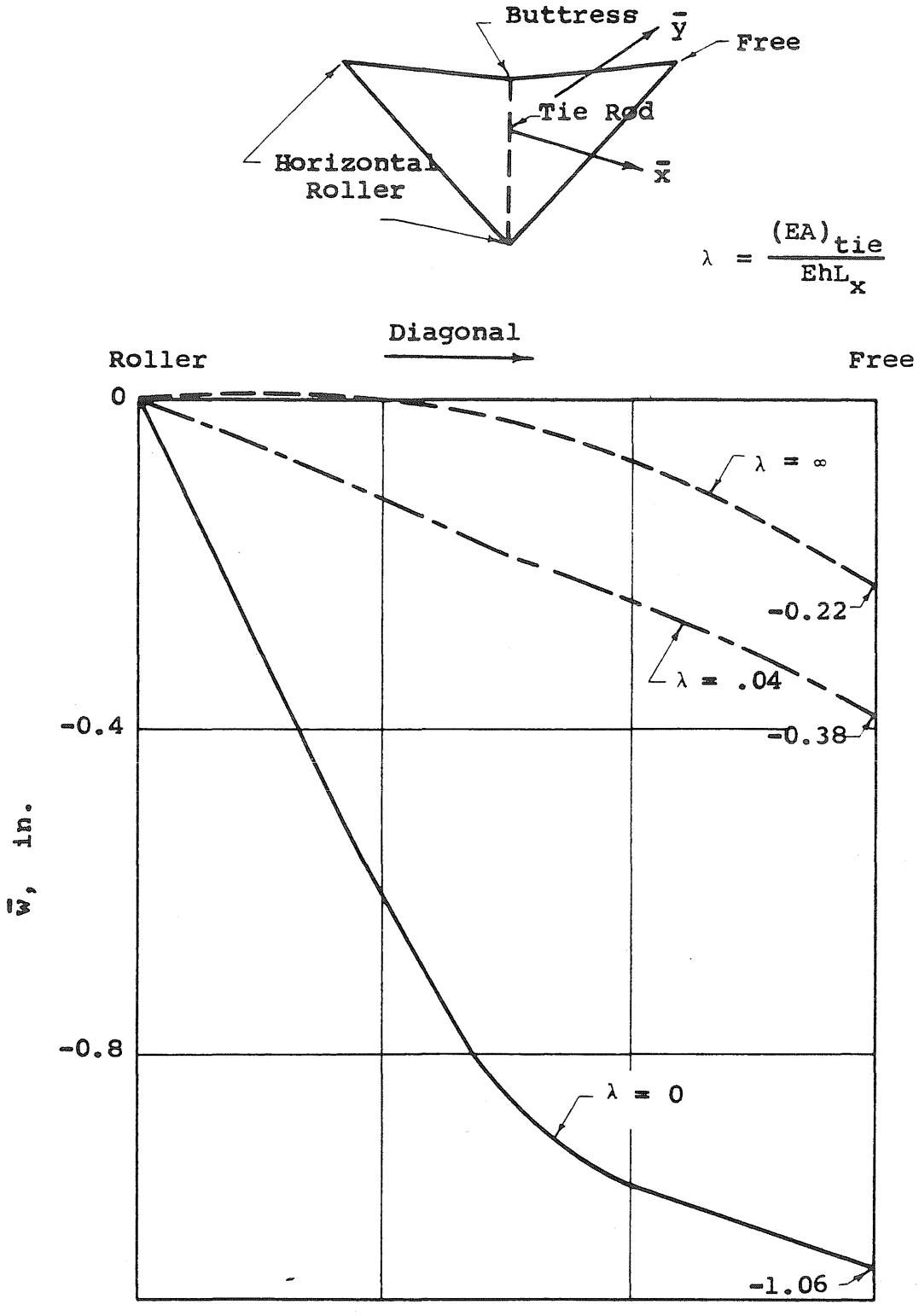

FIG. 27 DEFLECTION $\bar{w}$ ACROSS DIAGONAL OF HYPERBOLIC PARABOLOID BOUNDED BY CHARACTERISTICS, UNDER UNIFORM NORMAL LOAD, WITH LOW CORNERS CONNECTED BY TIE ROD

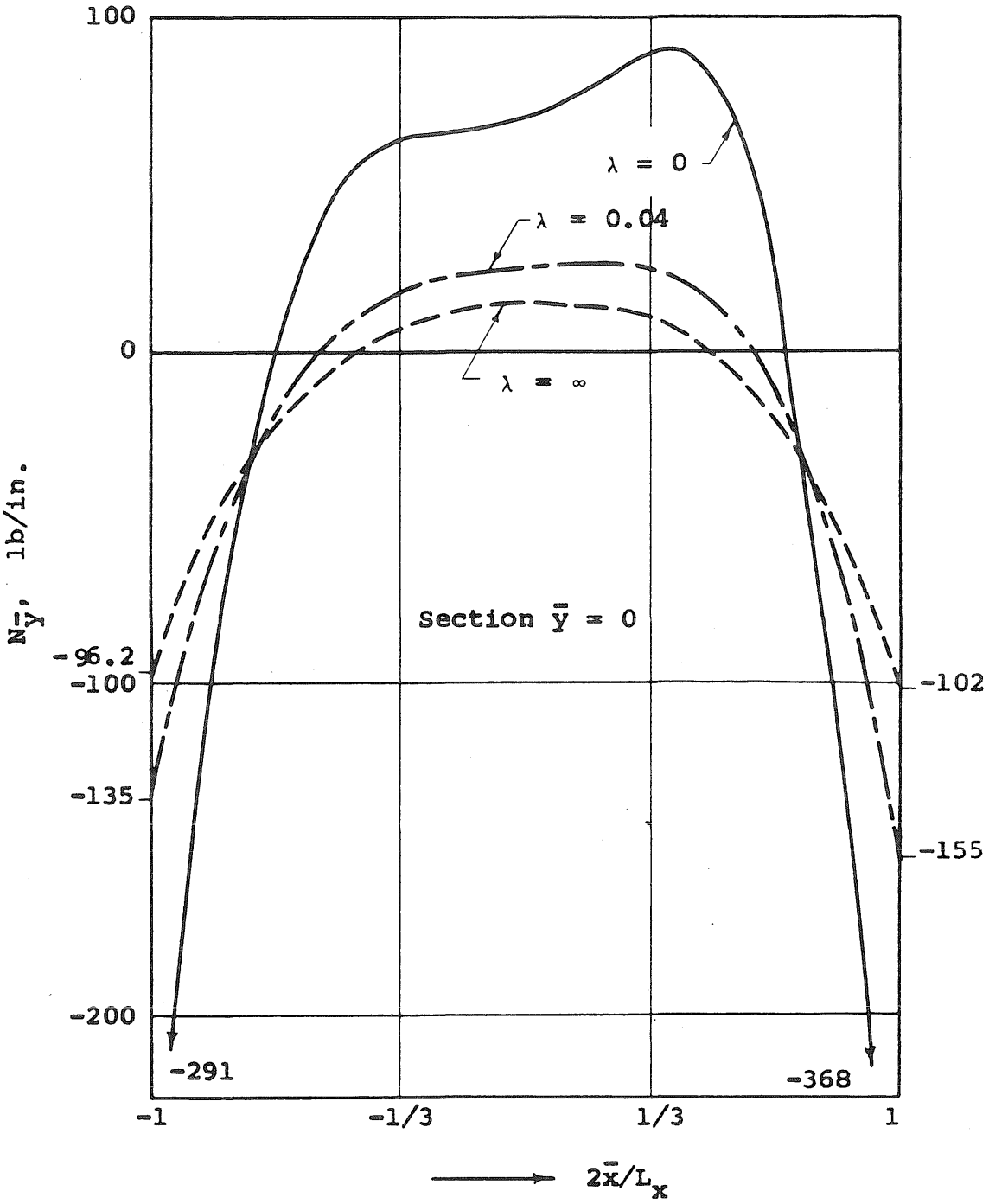

FIG. 28 FORCE $N_{\bar{y}}$ ACROSS MID-SECTION OF HYPERBOLIC PARABOLOID BOUNDED BY CHARACTERISTICS UNDER UNIFORM NORMAL LOAD, WITH LOW CORNERS CONNECTED BY TIE ROD

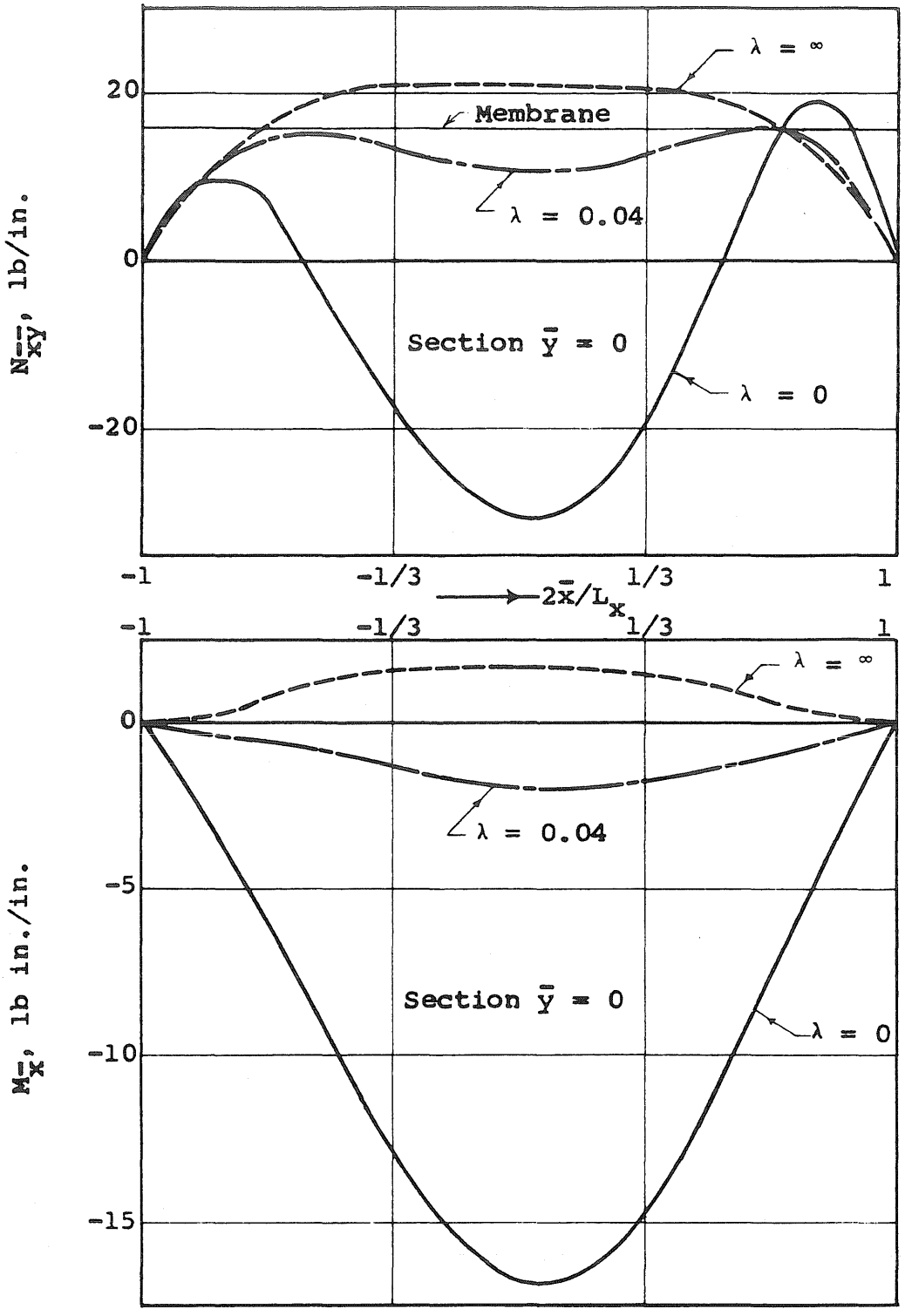

FIG. 29 FORCE $N_{\bar{x}\bar{y}}$ AND BENDING MOMENT $M_{\bar{x}}$ ACROSS MID-SECTION OF HYPERBOLIC PARABOLOID BOUNDED BY CHARACTERISTICS, UNDER UNIFORM NORMAL LOAD, WITH LOW CORNERS CONNECTED BY TIE ROD

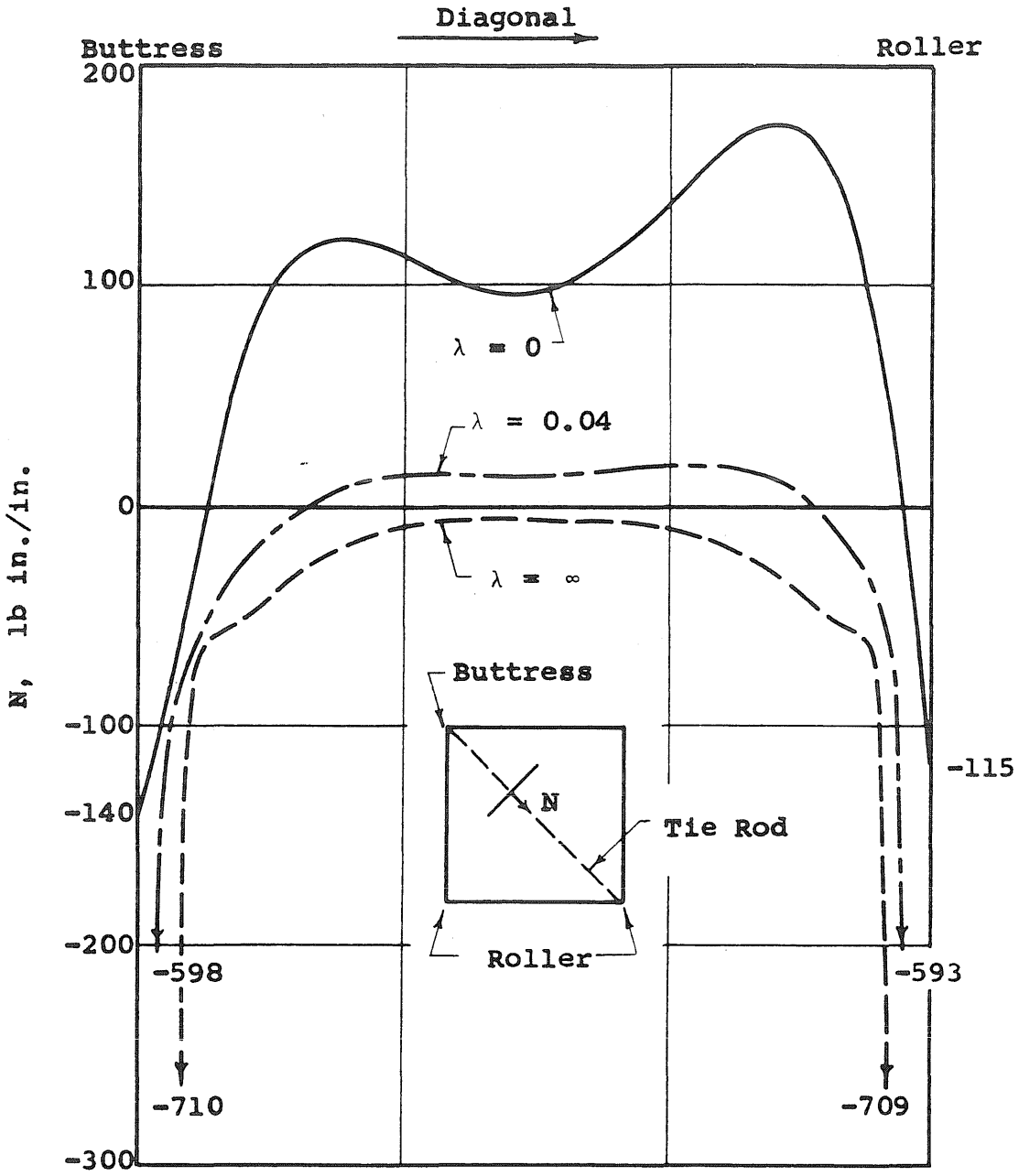

FIG. 30 ARCHING FORCE N ACROSS DIAGONAL OF HYPERBOLIC PARABOLOID BOUNDED BY CHARACTERISTICS, UNDER UNIFORM NORMAL LOAD, WITH LOW CORNERS CONNECTED BY TIE ROD

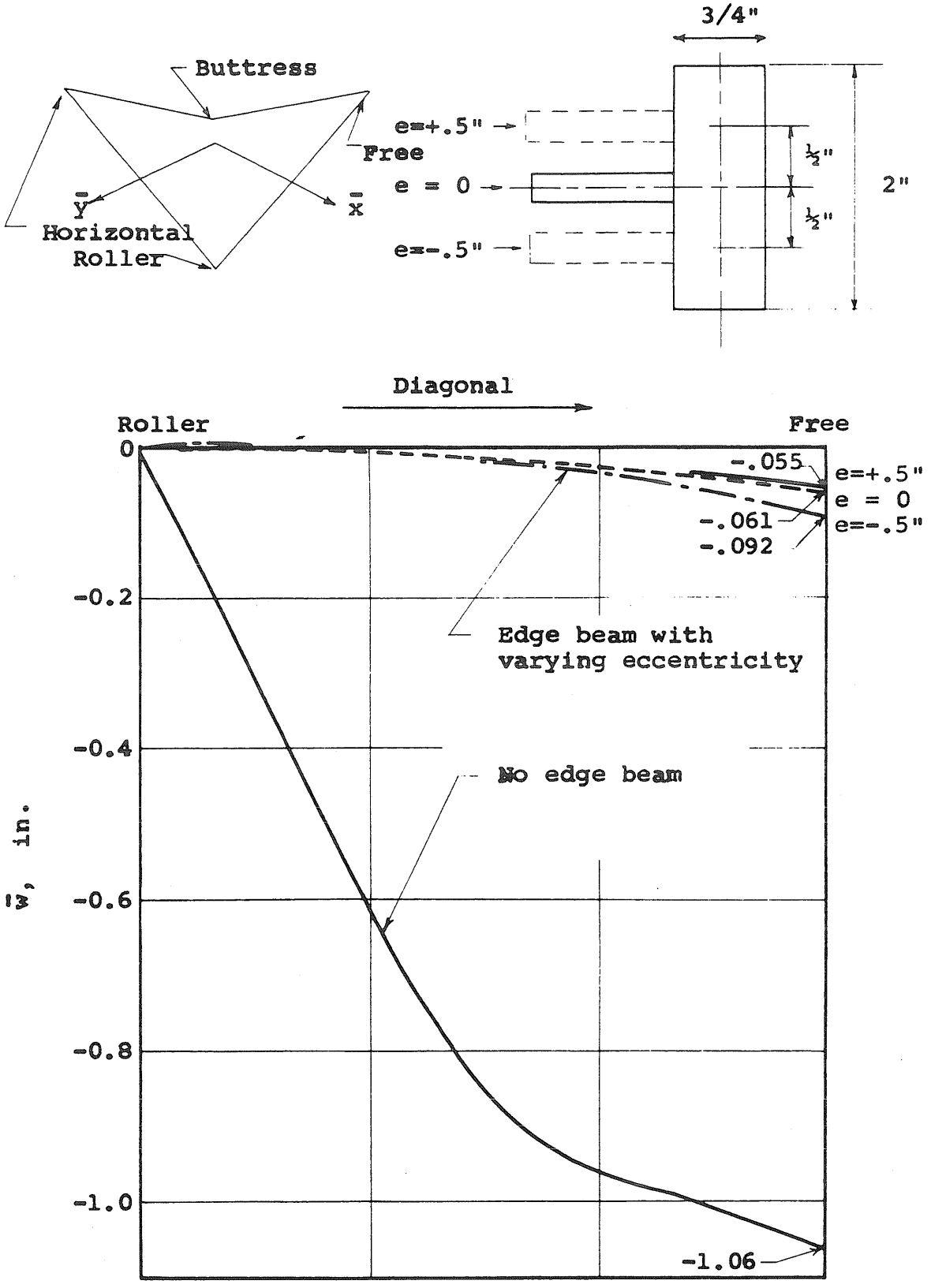

FIG. 31 DEFLECTION $\bar{w}$ ACROSS DIAGONAL OF EDGE-STIFFENED HYPERBOLIC PARABOLOID BOUNDED BY CHARACTERISTICS, UNDER UNIFORM NORMAL LOAD

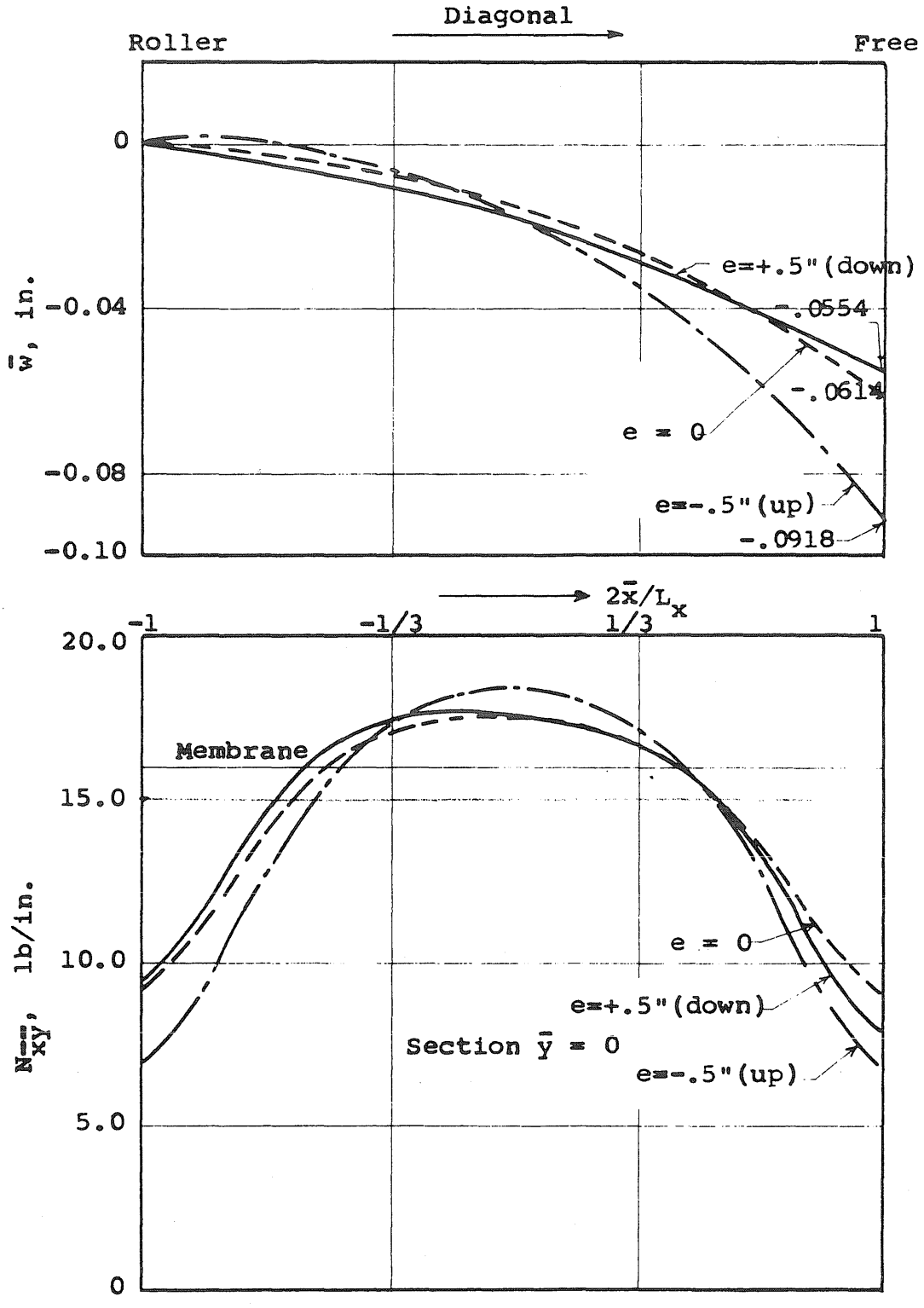

FIG. 32 DEFLECTION $\bar{w}$ AND FORCE $N_{\bar{x}\bar{y}}$ IN EDGE-STIFFENED HYPERBOLIC PARABOLOID BOUNDED BY CHARACTERISTICS, UNDER UNIFORM NORMAL LOAD

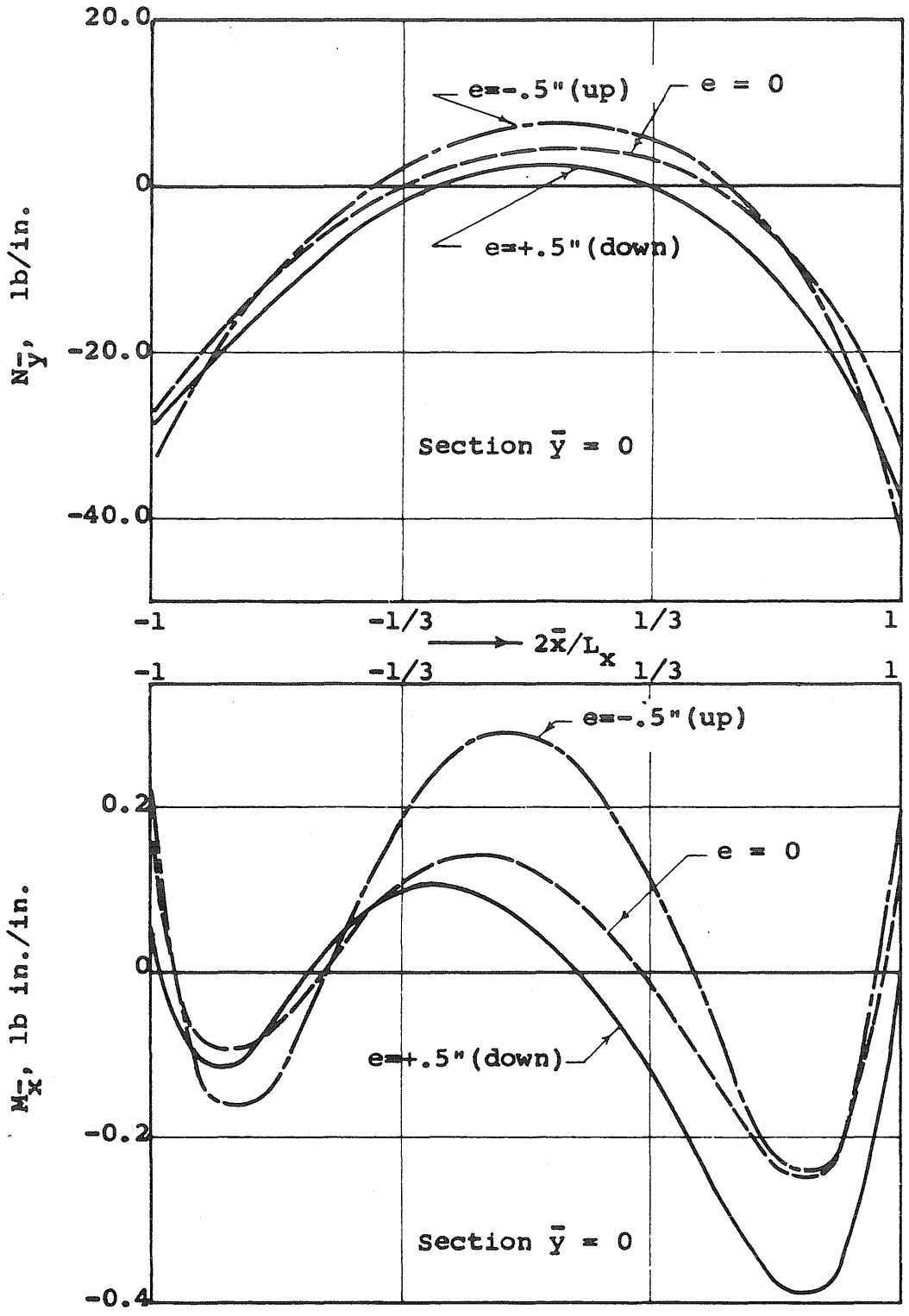

FIG. 33 FORCE $N_{\bar{y}}$ AND BENDING MOMENT $M_{\bar{x}}$ ACROSS MID-SECTION OF EDGE-STIFFENED HYPERBOLIC PARABOLOID BOUNDED BY CHARACTERISTICS, UNDER UNIFORM NORMAL LOAD

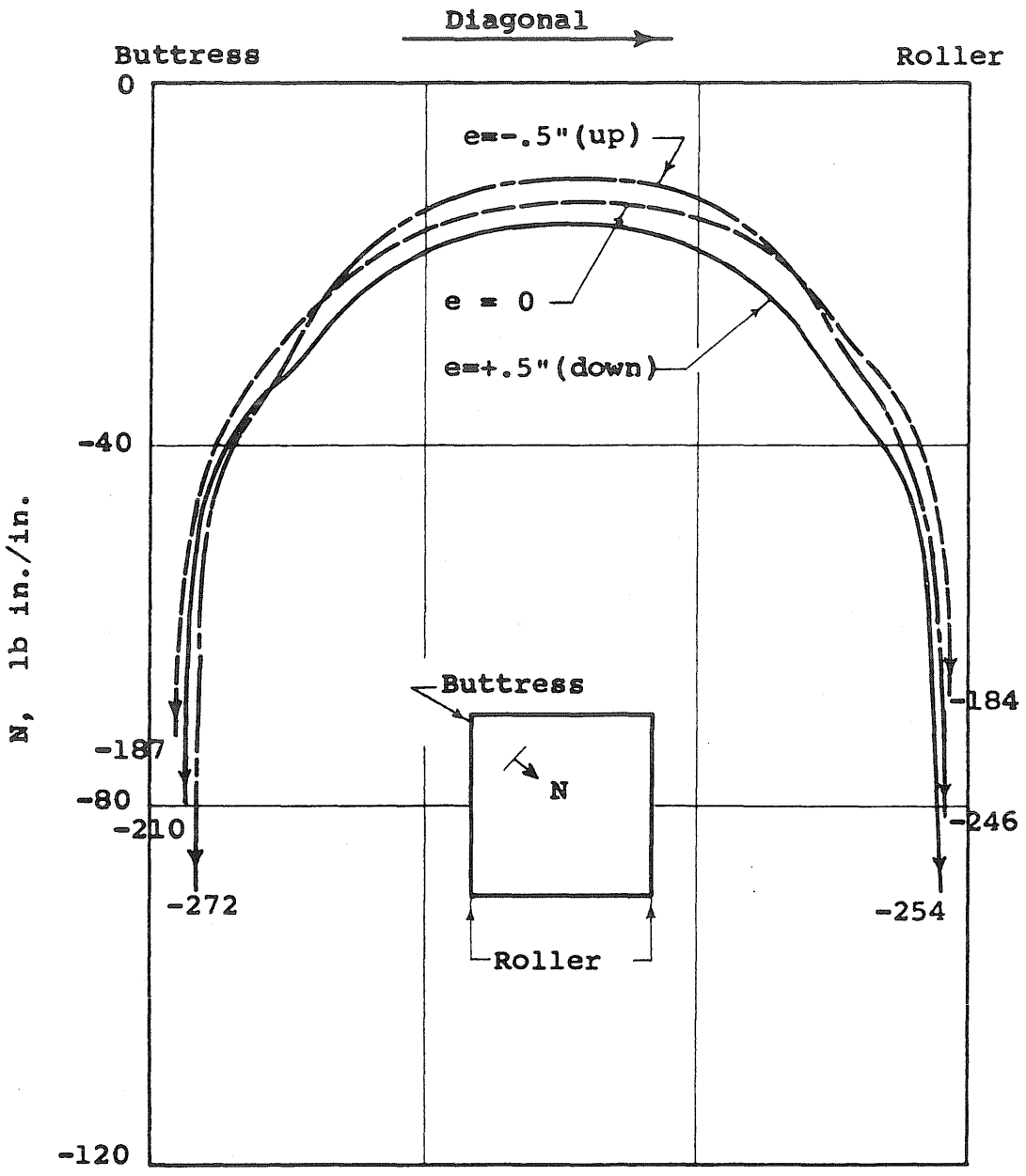

FIG. 34 ARCHING FORCE N ACROSS DIAGONAL OF EDGE-STIFFENED HYPERBOLIC PARABOLOID BOUNDED BY CHARACTERISTICS, UNDER UNIFORM NORMAL LOAD

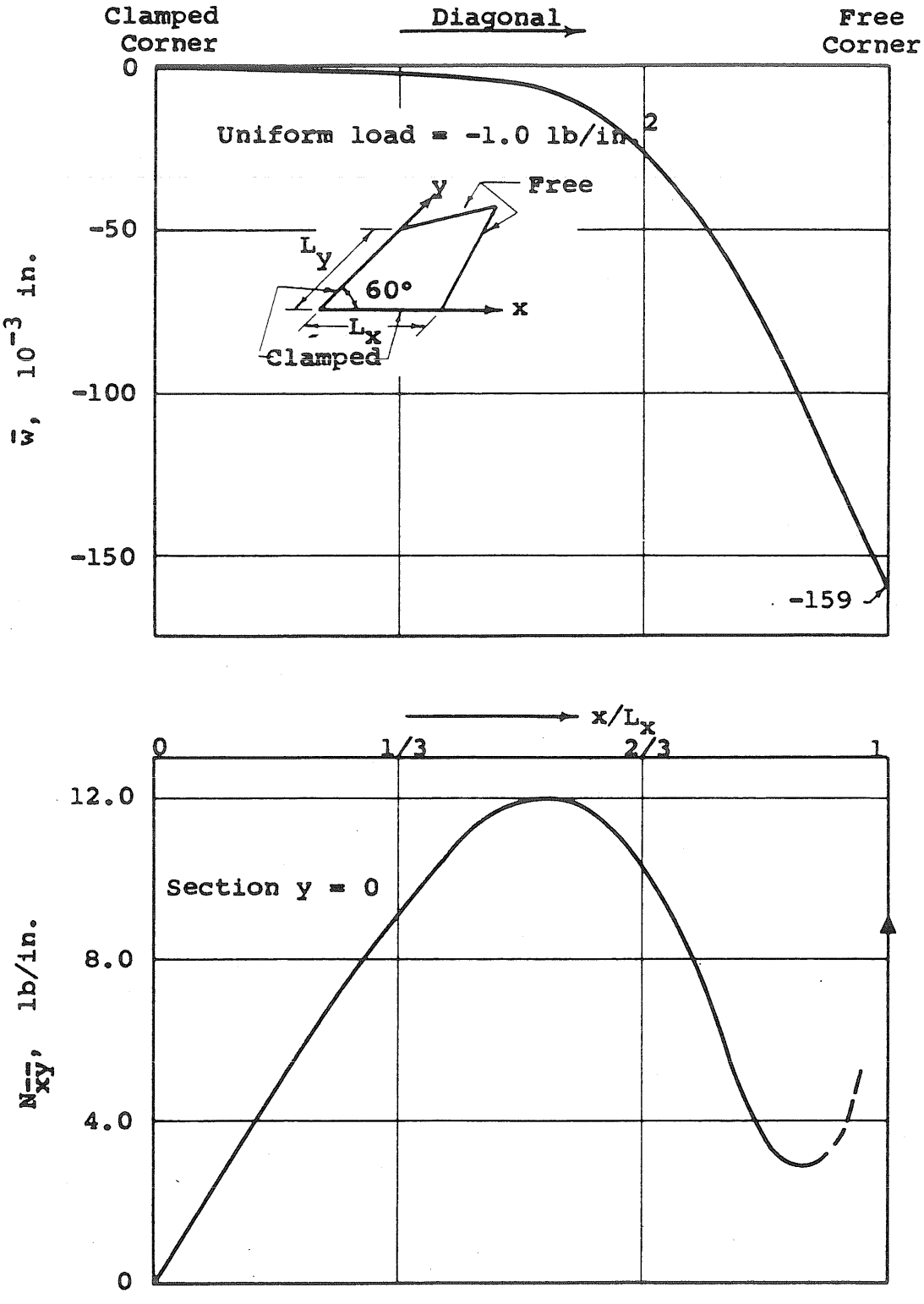

FIG. 35 DEFLECTION $\bar{w}$ AND FORCE N_{xy} IN SKEWED HYPERBOLIC PARABOLOID BOUNDED BY CHARACTERISTICS, UNDER UNIFORM NORMAL LOAD

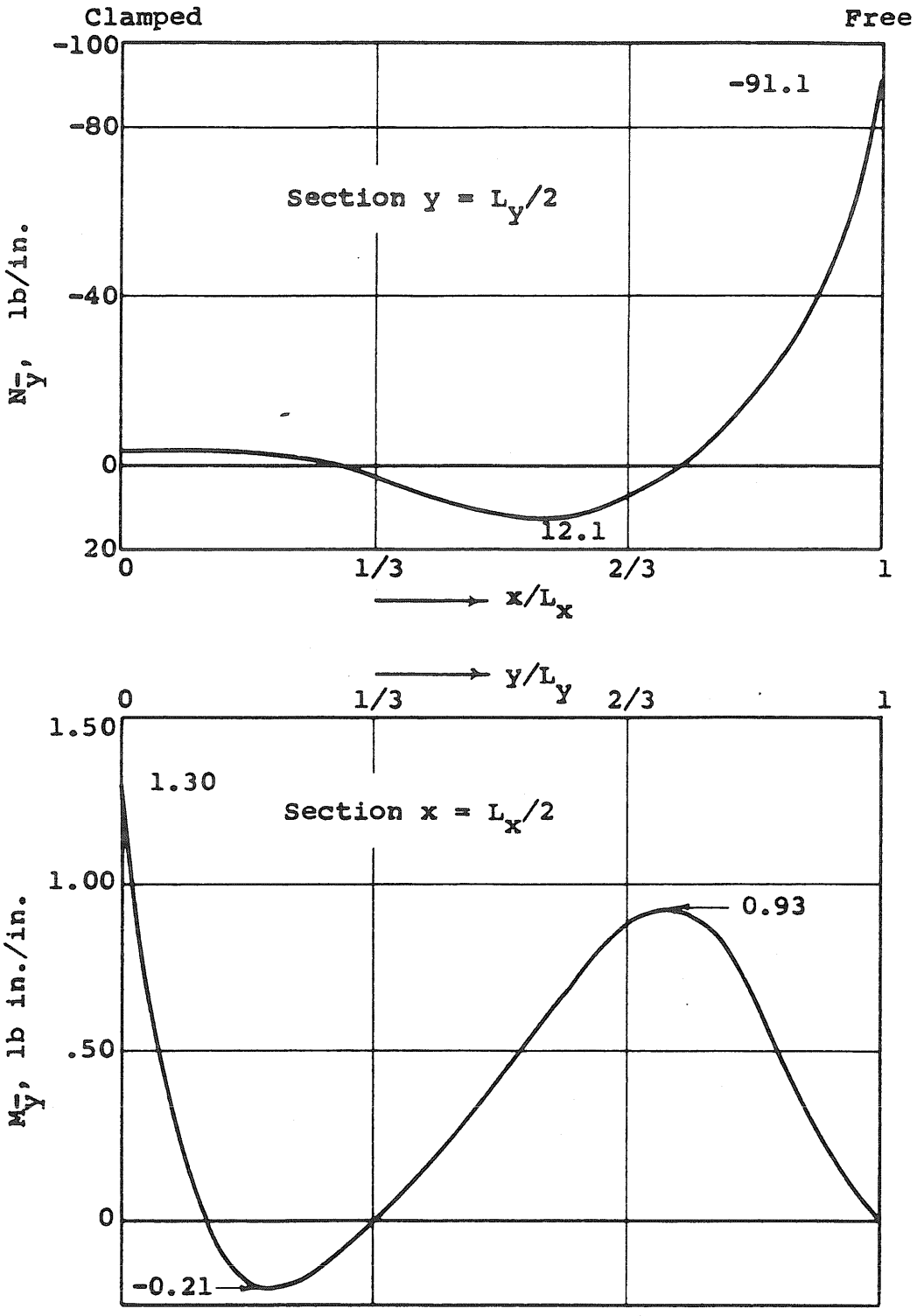

FIG. 36 FORCE N_y AND BENDING MOMENT M_y IN SKEWED HYPERBOLIC PARABOLOID BOUNDED BY CHARACTERISTICS, UNDER UNIFORM NORMAL LOAD

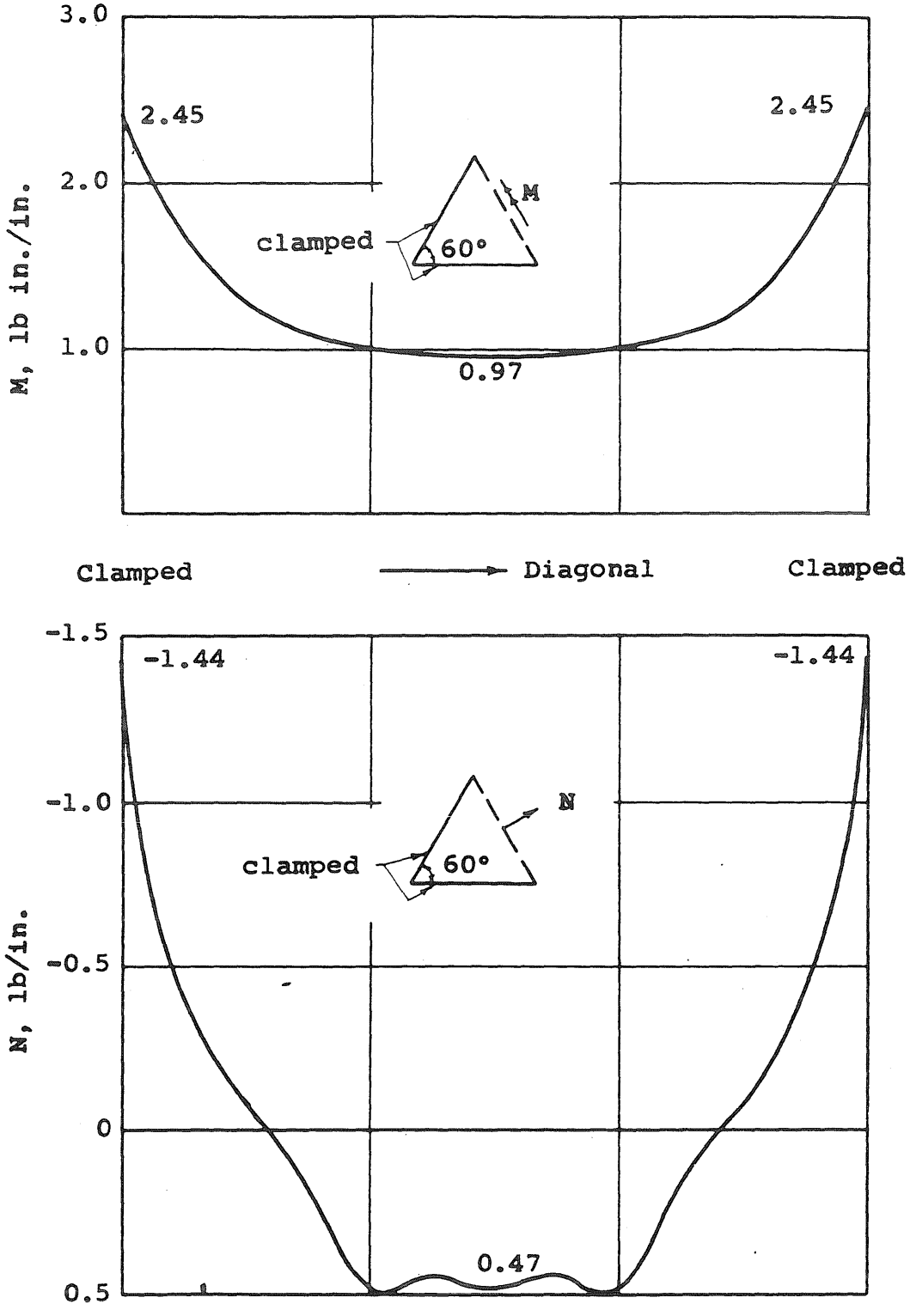

FIG. 37 BENDING MOMENT M AND FORCE N ACROSS DIAGONAL OF SKEWED HYPERBOLIC PARABOLOID BOUNDED BY CHARACTERISTICS, UNDER UNIFORM NORMAL LOAD

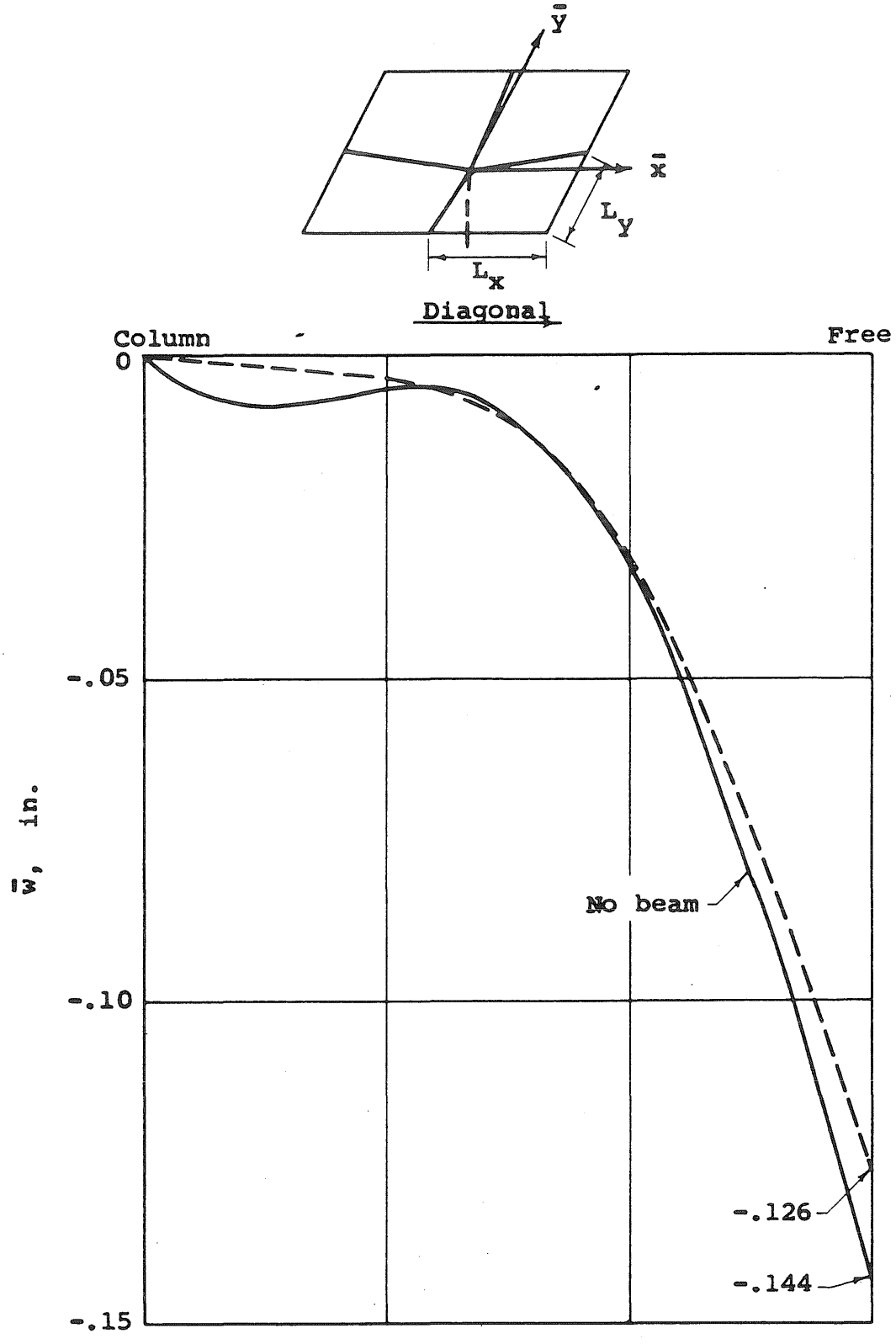

FIG. 38 DEFLECTION $\bar{w}$ ACROSS DIAGONAL OF UMBRELLA HYPERBOLIC PARABOLOID

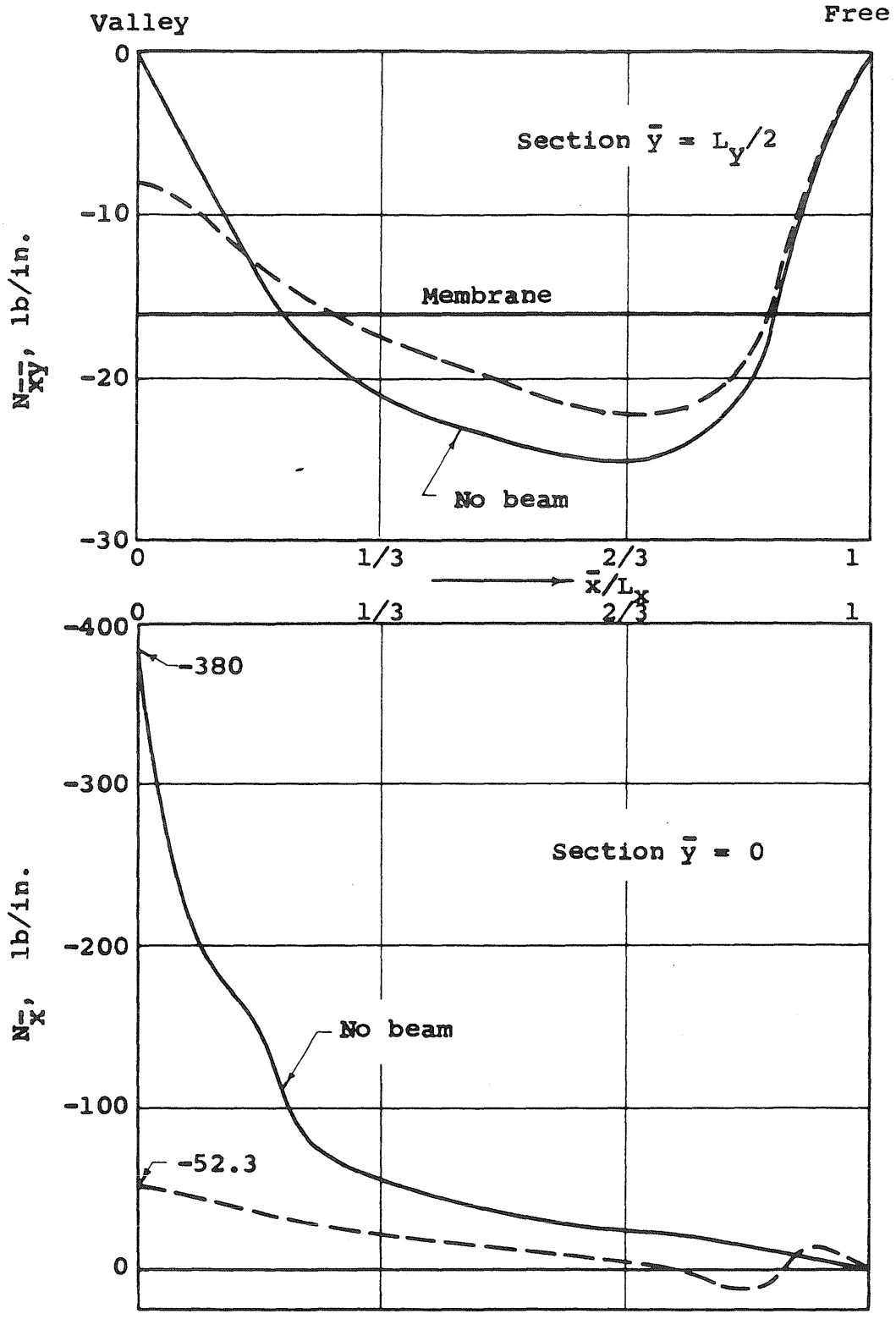

FIG. 39 FORCES $N_{\bar{x}}$ AND $N_{\bar{x}\bar{y}}$ IN UMBRELLA HYPERBOLIC PARABOLOID

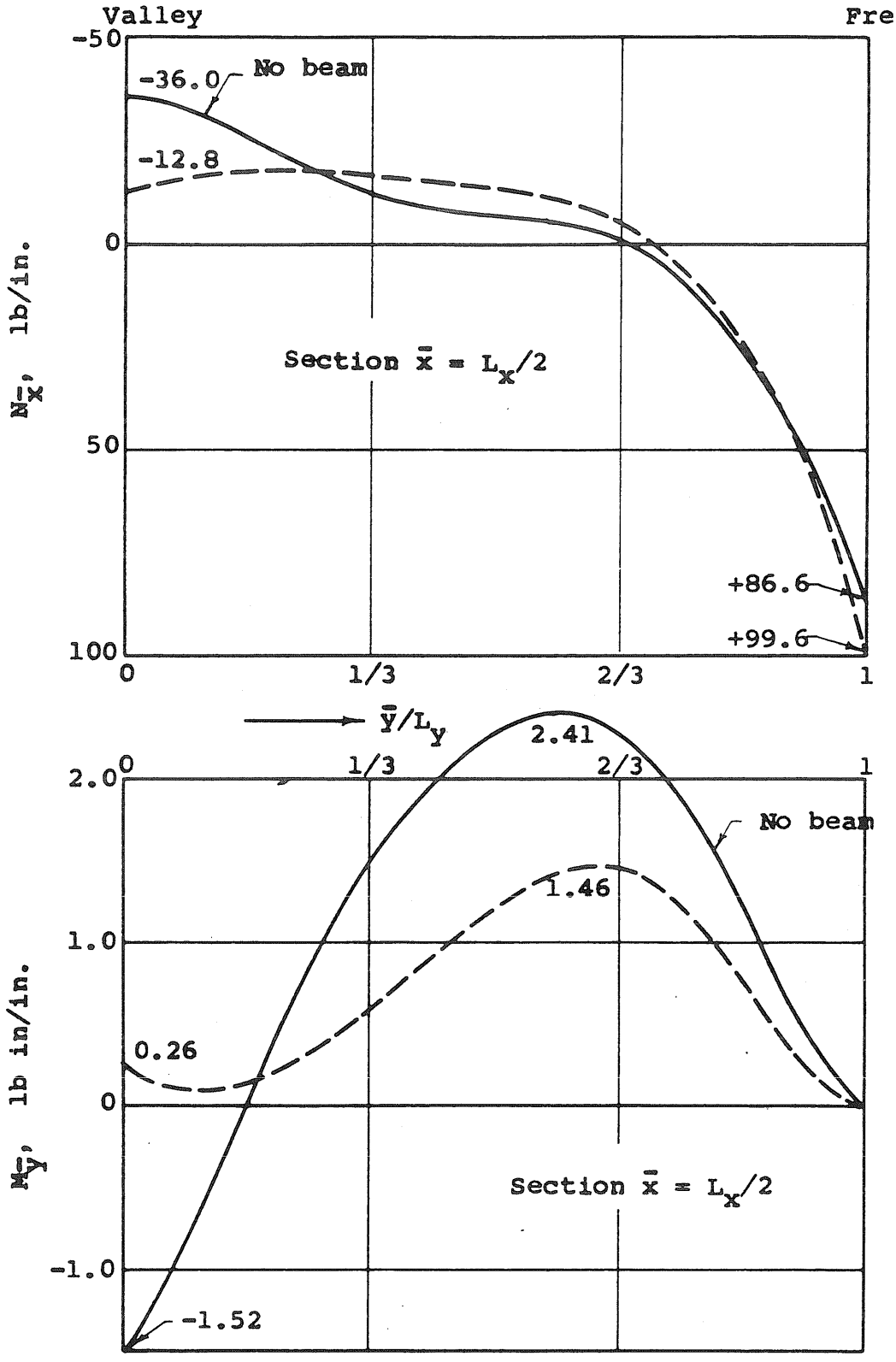

FIG. 40 FORCE $N_{\bar{x}}$ AND BENDING MOMENT $M_{\bar{y}}$ IN UMBRELLA HYPERBOLIC PARABOLOID

APPENDIX A

SHALLOW SHELL EQUILIBRIUM EQUATIONS IN OBLIQUE COORDINATES

The shallow shell equilibrium equations are given here in terms of displacement components (u,v,w) defined with respect to the oblique coordinate system introduced in Chapter II. They are then specialized for several simple cases and solutions of the Navier type are given for purposes of comparison with results of the finite element analyses.

The strain energy of the shallow shell is, according to Eqs. (2.62), (2.63) and (2.64),

$$U = \tfrac{1}{2}\int\int\{\varepsilon^{m,T}\ E^{m,T}\ \varepsilon^{m} + \varepsilon^{b,T}\ E^{b,T}\ \varepsilon^{b}\}\ \sin\chi\ dxdy \qquad (A.1)$$

which may be rewritten in terms of displacements (u,v,w) by use of the strain displacement relations Eqs. (2.54) and (2.55).

The potential of the externally distributed loading (p_u,p_v,p_w), where the components are defined by Eq. (3.13), is

$$\Omega = -\int\int(p_u u + p_v v + p_w w)\ \sin\chi\ dxdy \qquad (A.2)$$

The double integrals extend over the middle surface of the shell. For simplicity, it is assumed that no prescribed tractions act on the boundary. Then the total potential energy of the shell is

$$V = U + \Omega \tag{A.3}$$

The principle of minimum potential energy,

$$\delta V = 0 \tag{A.4}$$

yields after integration by parts, the equilibrium equations,

$$c_1 u_{,xx} + 2c_4 u_{,xy} + c_2 u_{,yy} + c_4 v_{,xx} + (c_2+c_3)\, v_{,xy} + c_4 v_{,yy} - f_1 w_{,x} - f_3 w_{,y} + \sin^2 \chi \frac{p_u}{N} = 0 \tag{A.5}$$

$$c_2 v_{,xx} + 2c_4 v_{,xy} + c_1 v_{,yy} + c_4 u_{,xx} + (c_2+c_3)\, u_{,xy} + c_4 u_{,yy} - f_3 w_{,x} - f_2 w_{,y} + \sin^2 \chi \frac{p_v}{N} = 0 \tag{A.6}$$

$$c_1 w_{,xxxx} + 4c_4 w_{,xxxy} + (2c_3 + 4c_2)\, w_{,xxyy} + 4c_4 w_{,xyyy} + c_1 w_{,yyyy} - \frac{12}{h^2} \left\{ f_1 u_{,x} + f_3 u_{,y} + f_3 v_{,x} + f_2 v_{,y} - g_1 w \right\} - \sin^2 \chi \frac{p_w}{D} = 0 \tag{A.7}$$

as coefficients of the independent variations δu, δv and δw respectively.

The notation used in Eqs. (A.5), (A.6) and (A.7) is the same as that used in the derivation of the element stiffness matrices, and is defined by Eqs. (3.37) and (3.38). For convenience, these equations are repeated here.

$$\begin{aligned} c_1 &= \csc^2 \chi \\ c_2 &= \frac{1-\nu}{2} + \cot^2 \chi \\ c_3 &= \nu + \cot^2 \chi \\ c_4 &= -\cot \chi \csc \chi \end{aligned} \tag{A.8}$$

$$f_1 = rc_1 + tc_3 + 2sc_4$$

$$f_2 = rc_3 + tc_1 + 2sc_4$$

$$f_3 = rc_4 + tc_4 + 2sc_2$$

$$g_1 = rf_1 + tf_2 + 2sf_3$$

On an edge x = constant, the vanishing of the boundary integral requires

$$(N_x \delta u + N_{xy} \delta v + R_x \delta w - M_x \delta w,_x) \Big|_{x=\text{constant}} = 0 \qquad (A.9)$$

where

$$R_x \equiv \frac{\partial M_x}{\partial x} + 2 \frac{\partial M_{xy}}{\partial y} \qquad (A.10)$$

is the effective transverse edge shear or "Kirchhoff shear", which may also be written as

$$R_x = Q_x + \frac{\partial M_{xy}}{\partial y} \qquad (A.11)$$

where Q_x is defined in Eq. (2.29), since equilibrium of moments acting on a differential element of the shell gives the relation

$$Q_x = \frac{\partial M_x}{\partial x} + \frac{\partial M_{xy}}{\partial y} \qquad (A.12)$$

(The negative sign in front of the moment M_x in eq. (A.9) results from the sign convention adopted. The positive sense of M_x is opposite to that of $w,_x$).

After insertion of the appropriate forced boundary conditions for a given problem, Eq. (A.9) yields the natural boundary conditions. If boundary tractions had been

prescribed, instead of setting N_x equal to zero as a natural boundary condition, for example, N_x would be set equal to the prescribed value N_x°.

For the case of orthogonal coordinates, Eqs. (A.5), (A.6) and (A.7) reduce to

$$\bar{u},_{\bar{x}\bar{x}} + (\tfrac{1+\nu}{2})\bar{v},_{\bar{x}\bar{y}} + (\tfrac{1-\nu}{2})\bar{u},_{\bar{y}\bar{y}} - (\bar{r}+\nu\bar{t})\bar{w},_{\bar{x}} - \bar{s}(1-\nu)\bar{w},_{\bar{y}} + \frac{p_{\bar{u}}}{N} = 0$$

$$\bar{v},_{\bar{y}\bar{y}} + (\tfrac{1+\nu}{2})\bar{u},_{\bar{x}\bar{y}} + (\tfrac{1-\nu}{2})\bar{v},_{\bar{x}\bar{x}} - (\bar{t}+\nu\bar{r})\bar{w},_{\bar{y}} - \bar{s}(1-\nu)\bar{w},_{\bar{x}} + \frac{p_{\bar{v}}}{N} = 0$$

$$\bar{w},_{\bar{x}\bar{x}\bar{x}\bar{x}} + 2\bar{w},_{\bar{x}\bar{x}\bar{y}\bar{y}} + \bar{w},_{\bar{y}\bar{y}\bar{y}\bar{y}} - \frac{12}{h^2}\Big\{(\bar{r}+\nu\bar{t})\bar{u},_{\bar{x}} + (\bar{t}+\nu\bar{r})\bar{v},_{\bar{y}} \qquad \text{(A.13)}$$

$$+\bar{s}(1-\nu)(\bar{u},_{\bar{y}}+\bar{v},_{\bar{x}}) - [(\bar{r}+\bar{t})^2 - 2(1-\nu)(\bar{r}\bar{t}-\bar{s}^2)]\bar{w}\Big\} - \frac{p_{\bar{w}}}{D} = 0$$

Equations (A.13) have been given by Apeland (4).

For purposes of comparison, some simple solutions of Eq. (A.13) of the Navier (double series) type are now given.

(1) <u>Simply Supported Shallow Shell (On Rollers) Bounded by Lines of Principal Curvature</u>

The region occupied by the shell is $0 \leq \bar{x} \leq L_x$, $0 \leq \bar{y} \leq L_y$. Since the $\bar{x},\bar{y}$ coordinates are lines of principal curvature, $\bar{s} = 0$ and Eqs. (A.13) may be satisfied by choosing for the displacement components $(\bar{u},\bar{v},\bar{w})$ and the distributed loading $(p_{\bar{u}},p_{\bar{v}},p_{\bar{w}})$ the double series expansions

$$
\begin{aligned}
\bar{u} &= \sum_{m=1}^{\infty}\sum_{n=1}^{\infty} \bar{u}_{mn} \cos \mu\bar{x} \sin \eta\bar{y} \\
\bar{v} &= \sum_{m=1}^{\infty}\sum_{n=1}^{\infty} \bar{v}_{mn} \sin \mu\bar{x} \cos \eta\bar{y} \\
\bar{w} &= \sum_{m=1}^{\infty}\sum_{n=1}^{\infty} \bar{w}_{mn} \sin \mu\bar{x} \sin \eta\bar{y} \\
p_{\bar{u}} &= \sum_{m=1}^{\infty}\sum_{n=1}^{\infty} \bar{p}^{u}_{mn} \cos \mu\bar{x} \sin \eta\bar{y} \\
p_{\bar{v}} &= \sum_{m=1}^{\infty}\sum_{n=1}^{\infty} \bar{p}^{v}_{mn} \sin \mu\bar{x} \cos \eta\bar{y} \\
p_{\bar{w}} &= \sum_{m=1}^{\infty}\sum_{n=1}^{\infty} \bar{p}^{w}_{mn} \sin \mu\bar{x} \sin \eta\bar{y}
\end{aligned}
\qquad \text{(A.14)}
$$

where $\bar{u}_{mn}, \bar{v}_{mn}$ and $\bar{w}_{mn}$ must satisfy the equations

$$
\begin{Bmatrix}
\mu^2+\left(\frac{1-\nu}{2}\right)\eta^2 & \left(\frac{1+\nu}{2}\right)\mu\eta & (\bar{r}+\nu\bar{t})\mu \\
 & \eta^2+\left(\frac{1-\nu}{2}\right)\mu^2 & (\bar{t}+\nu\bar{r})\eta \\
\text{symm.} & & \bar{r}^2+\bar{t}^2+2\nu\bar{r}\bar{t} \\
 & & +\frac{h^2}{12}\left\{(\mu^2+\eta^2)^2\right\}
\end{Bmatrix}
\begin{Bmatrix} \bar{u}_{mn} \\ \bar{v}_{mn} \\ \bar{w}_{mn} \end{Bmatrix}
= \frac{1}{N}
\begin{Bmatrix} \bar{p}^{u}_{mn} \\ \bar{p}^{v}_{mn} \\ \bar{p}^{w}_{mn} \end{Bmatrix}
\qquad \text{(A.15)}
$$

and where

$$
\begin{aligned}
\mu &\equiv \frac{m\pi}{L_x} \\
\eta &\equiv \frac{n\pi}{L_y}
\end{aligned}
\qquad \text{(A.16)}
$$

For the case of a uniform normal load p_o,

$$\begin{aligned} \bar{p}^u_{mn} &= 0 \\ \bar{p}^v_{mn} &= 0 \\ \bar{p}^w_{mn} &= \frac{16p_o}{\pi^2 mn} \left(\frac{1-\cos m\pi}{2}\right) \left(\frac{1-\cos n\pi}{2}\right) \end{aligned} \tag{A.17}$$

For the case of a concentrated central load P_o,

$$\begin{aligned} \bar{p}^u_{mn} &= 0 \\ \bar{p}^v_{mn} &= 0 \\ \bar{p}^w_{mn} &= \frac{4P_o}{L_x L_y} \sin\frac{m\pi}{2} \sin\frac{n\pi}{2} \end{aligned} \tag{A.18}$$

From Eqs. (A.17) and (A.18) it is obvious that for even values of m and n, $\bar{u}_{mn}$, $\bar{v}_{mn}$ and $\bar{w}_{mn}$ will be zero. This is also the case for all symmetric loadings.

From Eqs. (A.14) it is evident that on the edges $\bar{x} = 0$ and $\bar{x} = L_x$, the conditions

$$\begin{aligned} \bar{v} &= 0 \\ \bar{w} &= 0 \\ N_{\bar{x}} &= 0 \\ M_{\bar{x}} &= 0 \end{aligned} \tag{A.19}$$

are identically satisfied, with analogous conditions holding on the edges $\bar{y} = 0$ and $\bar{y} = L_y$. Therefore in this case, the term "simple supports" signifies "roller" supports as defined in Chapter 3.

The in-plane and bending stresses are given by the relations

$$
\begin{aligned}
N_{\bar{x}} &= -N \sum_{m=1}^{\infty} \sum_{n=1}^{\infty} [\, \mu\bar{u}_{mn} + \nu\eta\bar{v}_{mn} + (\bar{r}+\nu\bar{t})\bar{w}_{mn} \,] \sin \mu\bar{x} \sin \eta\bar{y} \\
N_{\bar{y}} &= -N \sum_{m=1}^{\infty} \sum_{n=1}^{\infty} [\, \eta\bar{v}_{mn} + \nu\mu\bar{u}_{mn} + (\bar{t}+\nu\bar{r})\bar{w}_{mn} \,] \sin \mu\bar{x} \sin \eta\bar{y} \\
N_{\bar{x}\bar{y}} &= N\left(\frac{1-\nu}{2}\right) \sum_{m=1}^{\infty} \sum_{n=1}^{\infty} (\eta\bar{u}_{mn} + \mu\bar{v}_{mn}) \cos \mu\bar{x} \cos \eta\bar{y} \\
M_{\bar{x}} &= D \sum_{m=1}^{\infty} \sum_{n=1}^{\infty} (\mu^2+\nu\eta^2)\bar{w}_{mn} \sin \mu\bar{x} \sin \eta\bar{y} \\
M_{\bar{y}} &= D \sum_{m=1}^{\infty} \sum_{n=1}^{\infty} (\eta^2+\nu\mu^2)\bar{w}_{mn} \sin \mu\bar{x} \sin \eta\bar{y} \\
M_{\bar{x}\bar{y}} &= -D(1-\nu) \sum_{m=1}^{\infty} \sum_{n=1}^{\infty} \mu\eta\bar{w}_{mn} \cos \mu\bar{x} \cos \eta\bar{y}
\end{aligned}
\tag{A.20}
$$

(2) Simply Supported Hyperbolic Paraboloid (On Knife Edges) Bounded by Characteristics

In this case, $\bar{r} = \bar{t} = 0$, and the equilibrium equations (A.13) may be satisfied by choosing

$$
\begin{aligned}
\bar{u} &= \sum_{m=1}^{\infty} \sum_{n=1}^{\infty} \bar{u}_{mn} \sin \mu\bar{x} \cos \eta\bar{y} \\
\bar{v} &= \sum_{m=1}^{\infty} \sum_{n=1}^{\infty} \bar{v}_{mn} \cos \mu\bar{x} \sin \eta\bar{y} \\
\bar{w} &= \sum_{m=1}^{\infty} \sum_{n=1}^{\infty} \bar{w}_{mn} \sin \mu\bar{x} \sin \eta\bar{y} \\
p_{\bar{u}} &= \sum_{m=1}^{\infty} \sum_{n=1}^{\infty} \bar{p}^{u}_{mn} \sin \mu\bar{x} \cos \eta\bar{y} \\
p_{\bar{v}} &= \sum_{m=1}^{\infty} \sum_{n=1}^{\infty} \bar{p}^{v}_{mn} \cos \mu\bar{x} \sin \eta\bar{y} \\
p_{\bar{w}} &= \sum_{m=1}^{\infty} \sum_{n=1}^{\infty} \bar{p}^{w}_{mn} \sin \mu\bar{x} \sin \eta\bar{y}
\end{aligned}
\tag{A.21}
$$

where $\bar{u}_{mn}$, $\bar{v}_{mn}$ and $\bar{w}_{mn}$ must satisfy

$$
\begin{Bmatrix}
\mu^2+\left(\frac{1-\nu}{2}\right)\eta^2 & \frac{1+\nu}{2}\mu\eta & \bar{s}(1-\nu)\eta \\
 & \eta^2+\left(\frac{1-\nu}{2}\right)\mu^2 & \bar{s}(1-\nu)\mu \\
 & & 2\bar{s}^2(1-\nu) \\
 & & +\frac{h^2}{12}\left(\mu^2+\eta^2\right)^2
\end{Bmatrix}
\begin{Bmatrix} \bar{u}_{mn} \\ \bar{v}_{mn} \\ \bar{w}_{mn} \end{Bmatrix}
= \frac{1}{N}
\begin{Bmatrix} \bar{p}^{u}_{mn} \\ \bar{p}^{v}_{mn} \\ \bar{p}^{w}_{mn} \end{Bmatrix}
\tag{A.22}
$$

On the edges $\bar{x} = 0$ and $\bar{x} = L_x$ Eqs. (A.21) lead to

$$\begin{aligned} \bar{u} &= 0 \\ \bar{w} &= 0 \\ N_{\bar{x}\bar{y}} &= 0 \\ M_{\bar{x}} &= 0 \end{aligned} \tag{A.23}$$

with analogous conditions holding on the edges $\bar{y} = 0$ and $\bar{y} = L_y$. These are the boundary conditions which were designated as "knife edge" supports in Chapter 3. The expressions for $\bar{p}^{w}_{mn}$ for the cases of uniform normal load and a central concentrated load are the same as for the previous case and are given by Eqs. (A.17) and (A.18).

The membrane and bending stress resultants are given by

$$\begin{aligned} N_{\bar{x}} &= N \sum_{m=1}^{\infty} \sum_{n=1}^{\infty} (\mu \bar{u}_{mn} + \nu\eta \bar{v}_{mn}) \cos \mu\bar{x} \cos \eta\bar{y} \\ N_{\bar{y}} &= N \sum_{m=1}^{\infty} \sum_{n=1}^{\infty} (\eta \bar{v}_{mn} + \nu\mu \bar{u}_{mn}) \cos \mu\bar{x} \cos \eta\bar{y} \\ N_{\bar{x}\bar{y}} &= -N\left(\frac{1-\nu}{2}\right) \sum_{m=1}^{\infty} \sum_{n=1}^{\infty} (\eta \bar{u}_{mn} + \mu \bar{v}_{mn} + 2\bar{s}\bar{w}_{mn}) \sin \mu\bar{x} \sin \eta\bar{y} \\ M_{\bar{x}} &= D \sum_{m=1}^{\infty} \sum_{n=1}^{\infty} (\mu^2 + \nu\eta^2) \bar{w}_{mn} \sin \mu\bar{x} \sin \eta\bar{y} \\ M_{\bar{y}} &= D \sum_{m=1}^{\infty} \sum_{n=1}^{\infty} (\eta^2 + \nu\mu^2) \bar{w}_{mn} \sin \mu\bar{x} \sin \eta\bar{y} \\ M_{\bar{x}\bar{y}} &= -D(1-\nu) \sum_{m=1}^{\infty} \sum_{n=1}^{\infty} \mu\eta \bar{w}_{mn} \cos \mu\bar{x} \cos \eta\bar{y} \end{aligned} \tag{A.24}$$

The double series solutions given here, while possessing the virtue of simplicity, are very poorly convergent in general. Greatly superior convergence at the cost of increased complexity may be obtained by using a single series solution, i.e. a Lèvy solution rather than a Navier solution, which reduces the partial differential equilibrium equations to ordinary differential equations. The single series method also may be applied to any shell which is simply supported on two opposite edges with virtually any boundary conditions on the remaining two edges. For the case of a concentrated load, the convergence problems are even more severe, and for practical computations the method of singularities given by Flügge and Conrad (17) is greatly superior. However in this study only a limited amount of analytical data is needed for comparison, and in the interest of simplicity the double series solutions are used, with an extremely large number of terms being computed to obtain satisfactory convergence.

APPENDIX B

STIFFNESS MATRIX FOR CURVED EDGE BEAM

In this appendix, the derivation of the stiffness matrix for a curved edge beam is briefly outlined.* In addition to the assumption of a homogeneous, isotropic elastic material, assumptions are made which are of the same order of accuracy as those made for the shell. They are:

(1) The beam axis is a portion of a circle, i.e. the radius of curvature of the axis is constant. This corresponds to the shallow shell approximation.

(2) The radius of curvature is large compared to the depth of the beam. This is the counterpart of the "thin shell" assumption.

(3) Shear deformation is neglected (The "Kirchhoff-Love Approximation").

It is also assumed that the beam cross-section possesses two axes of symmetry so that the shear centre coincides with the intersection of the principal axes.

As a result of the second assumption listed above, the strain energy of the beam may be approximated by that of a straight beam.

---

* Martin (29) has obtained the stiffness matrix for a beam of constant curvature loaded in its plane of curvature.

The beam is shown in Fig. 12. R denotes the (constant) radius of curvature, β is the total angle subtended by the beam, and ϕ locates an arbitrary point on the axis. The coordinates (X,Y,Z) in the beam cross section change directions as ϕ is varied so that X always points along the beam axis and Z is directed towards the center of curvature. The cross-sections $\phi = 0$ and $\phi = \beta$ are designated as ends 1 and 2 respectively.

A set of nodal forces and moments are applied at end 1, with the sign convention as shown in Fig. 12. The displacements and rotations corresponding to the nodal forces and moments ($P_{X_1}, P_{Y_1}, P_{Z_1}, M_{X_1}, M_{Y_1}, M_{Z_1}$) are ($\delta_{X_1}, \delta_{Y_1}, \delta_{Z_1}, \theta_{X_1}, \theta_{Y_1}, \theta_{Z_1}$) with the same positive sense.

The stress resultants acting at an arbitrary section located by the angular coordinate ϕ are determined from equilibrium considerations to be

$$
\begin{aligned}
P_X &= -P_{X_1} \cos\phi - P_{Z_1} \sin\phi \\
P_Y &= -P_{Y_1} \\
P_Z &= -P_{Z_1} \cos\phi + P_{X_1} \sin\phi \\
M_X &= -M_{X_1} \cos\phi - M_{Z_1} \sin\phi + P_{Y_1} R(1-\cos\phi) \\
M_Y &= -M_{Y_1} - P_{Z_1} R \sin\phi + P_{X_1} R(1-\cos\phi) \\
M_Z &= -M_{Z_1} \cos\phi + M_{X_1} \sin\phi + P_{Y_1} R \sin\phi
\end{aligned}
\qquad \text{(B.1)}
$$

Since the (X,Y,Z) axes are principal axes of the cross section, and in consequence of the assumptions mentioned previously, the strain energy of the beam is given approximately by

$$U = \tfrac{1}{2}\int_0^{\beta}\left[\frac{M_X^2}{GJ} + \frac{M_Y^2}{EI_Y} + \frac{M_Z^2}{EI_Z} + \frac{P_X^2}{AE}\right] R\, d\,\phi \qquad (B.2)$$

where E is Young's Modulus for the beam,

G is the shear modulus ($= \frac{E}{2(1+\nu)}$, where ν is Poisson's Ratio),

A is the cross-sectional area of the beam,

I_Y and I_Z are the moments of inertia of the cross-section about the Y and Z axes respectively,

and J is the torsional rigidity of the cross-section.

Castigliano's Theorem is now employed to relate the nodal displacements at end 1 to the nodal forces applied there, since

$$\delta_{X_1} = \frac{\partial U}{\partial P_{X_1}}, \ \cdots$$

$$\theta_{X_1} = \frac{\partial U}{\partial M_{X_1}}, \ \cdots \qquad (B.3)$$

Substitution of Eqs. (B.1) into Eq. (B.2), integration with respect to ϕ, followed by the application of Eqs. (B.3) yields

$$\delta_1 = f_{11} P_1 \qquad (B.4)$$

where

$$\delta_1 \equiv \left\{ \begin{array}{c} \delta_{X_1} \\ \delta_{Y_1} \\ \delta_{Z_1} \\ \theta_{X_1} \\ \theta_{Y_1} \\ \theta_{Z_1} \end{array} \right\}$$

and

$$P_1 \equiv \left\{ \begin{array}{c} P_{X_1} \\ P_{Y_1} \\ P_{Z_1} \\ M_{X_1} \\ M_{Y_1} \\ M_{Z_1} \end{array} \right\}$$

If the notation

$$\begin{aligned} \bar{a} &= \beta - \sin \beta \\ \bar{b} &= \cos \beta + \tfrac{1}{2} \sin^2 \beta - 1 \\ \bar{c} &= \frac{3}{2} \beta - 2 \sin \beta + \tfrac{1}{4} \sin 2\beta \\ \bar{d} &= \tfrac{1}{2} \beta - \tfrac{1}{4} \sin 2\beta \\ \bar{e} &= \cos \beta - 1 \\ \bar{f} &= \tfrac{1}{2} \beta + \tfrac{1}{4} \sin 2\beta \\ \bar{g} &= \tfrac{1}{2} \sin^2 \beta \\ \bar{h} &= \sin \beta - \tfrac{1}{2} \beta - \tfrac{1}{4} \sin 2\beta \end{aligned} \qquad \text{(B.5)}$$

is used, the (6x6) matrix f_{11} may be written as

$$f_{11} = \begin{bmatrix} \frac{R^3}{EI_Y}\bar{c}+\frac{R}{AE}\bar{f} & \cdot & \frac{R^3}{EI_Y}\bar{b}+\frac{R}{AE}\bar{g} & \cdot & -\frac{R^2}{EI_Y}\bar{a} & \cdot \\ & \frac{R^3}{GJ}\bar{c}+\frac{R^3}{EI_Z}\bar{d} & \cdot & -\frac{R^2}{GJ}\bar{h}+\frac{R^2}{EI_Z}\bar{d} & \cdot & \frac{R^2}{GJ}\bar{b}-\frac{R^2}{EI_Z}\bar{g} \\ & & (\frac{R^3}{EI_Y}+\frac{R}{AE})\bar{d} & \cdot & -\frac{R^2}{EI_Y}\bar{e} & \cdot \\ \text{Symm.} & & & \frac{R}{GJ}\bar{f}+\frac{R}{EI_Z}\bar{d} & \cdot & (\frac{R}{GJ}-\frac{R}{EI_Z})\bar{g} \\ & & & & \frac{R\beta}{EI_Y} & \cdot \\ & & & & & \frac{R}{GJ}\bar{d}+\frac{R}{EI_Z}\bar{f} \end{bmatrix} \qquad (B.6)$$

The desired (12x12) beam stiffness matrix K may be written in partitioned form as

$$K = \left[\begin{array}{c|c} K_{11} & K_{12} \\ \hline K_{21} & K_{22} \end{array}\right] \qquad (B.7)$$

where each of the submatrices in Eq. (B.7) is of order (6x6). The jth column of K_{11} represents the set of six nodal forces at end 1 due to a unit nodal displacement at end 1 in the j direction with all other displacements maintained equal to zero. Therefore,

$$K_{11} = f_{11}^{-1} \qquad (B.8)$$

The matrix K_{11} contains all the stiffness properties of the beam and the remaining submatrices of Eq. (B.7) can be obtained from it. The jth column of matrix K_{21} represents

the fixed end forces and moments at end 2 when the unit displacement or rotation is imposed in the j-direction at end 1. These are obtained directly from equilibrium considerations. Therefore

$$K_{21} = T_{21}\, K_{11} \tag{B.9}$$

where

$$T_{21} = \begin{bmatrix} -\cos\beta & \cdot & -\sin\beta & \cdot & \cdot & \cdot \\ \cdot & -1 & \cdot & \cdot & \cdot & \cdot \\ \sin\beta & \cdot & -\cos\beta & \cdot & \cdot & \cdot \\ \cdot & R(1-\cos\beta) & \cdot & -\cos\beta & \cdot & -\sin\beta \\ R(1-\cos\beta) & \cdot & -R\sin\beta & \cdot & -1 & \cdot \\ \cdot & R\sin\beta & \cdot & \sin\beta & \cdot & -\cos\beta \end{bmatrix} \tag{B.10}$$

T_{21} can be obtained by setting $\phi = \beta$ in Eqs. (B.1).

Since the beam stiffness matrix is symmetric,

$$K_{12} = K_{21}^{T} \tag{B.11}$$

The remaining submatrix, K_{22}, is obtained from K_{11} by the transformation

$$K_{22} = T_{22}\, K_{11}\, T_{22}^{T} \tag{B.12}$$

where

$$T_{22} = \begin{bmatrix} -1 & \cdot & \cdot & \cdot & \cdot & \cdot \\ \cdot & -1 & \cdot & \cdot & \cdot & \cdot \\ \cdot & \cdot & 1 & \cdot & \cdot & \cdot \\ \cdot & \cdot & \cdot & -1 & \cdot & \cdot \\ \cdot & \cdot & \cdot & \cdot & -1 & \cdot \\ \cdot & \cdot & \cdot & \cdot & \cdot & 1 \end{bmatrix} \tag{B.13}$$

That is, the diagonal elements of K_{22} are identical to those of K_{11} while some of the off-diagonal terms have their signs reversed.

In order to obtain the stiffness matrix with respect to a set of axes which are eccentric to (X,Y,Z), as shown in Fig. 12, an axis transformation of the form given in Eq. (B.12) is performed.

If K_e denotes the (12x12) beam stiffness matrix with respect to eccentric axes, and e is the eccentricity of Y_e with respect to Y as shown in Fig. 12, then

$$K_e = T_e \, K \, T_e^T \tag{B.14}$$

where

$$T_e = \begin{bmatrix} I & 0 & 0 & 0 \\ Q & I & 0 & 0 \\ 0 & 0 & I & 0 \\ 0 & 0 & Q & I \end{bmatrix}$$

and

$$I = \begin{bmatrix} 1 & \cdot & \cdot \\ \cdot & 1 & \cdot \\ \cdot & \cdot & 1 \end{bmatrix}, \qquad Q = \begin{bmatrix} \cdot & e & \cdot \\ -e & \cdot & \cdot \\ \cdot & \cdot & \cdot \end{bmatrix}$$

(The transformation (B.14) is used also to obtain the stiffness matrix given in Table 9 for the straight edge beam with respect to eccentric axes.)

It is perhaps most convenient to perform the required transformations numerically within the computer once the matrix f_{11}, given by Eq. (B.6), is known. However,

an explicit form for K_e is given in Table 10 in terms of the notation

$$\alpha = \frac{I_y}{AR^2} \qquad k_1 = \frac{EI_y}{R^3\Delta_1}$$

$$\rho = \frac{EI_z}{GJ} \qquad k_2 = \frac{EI_z}{R^3\Delta_2}$$

$$\bar{A} = \beta\bar{d}\,(1+\alpha) - \bar{e}^2$$

$$\bar{B} = \bar{a}\bar{e} - \beta\,(\bar{b} + \alpha\bar{g})$$

$$\bar{C} = R\{\,\bar{a}\bar{d}\,(1+\alpha) - \bar{e}\,(\bar{b} + \alpha\bar{g})\}$$

$$\bar{D} = \beta\,(\bar{c} + \alpha\bar{f}) - \bar{a}^2$$

$$\bar{E} = R\{\,\bar{e}\,(\bar{c} + \alpha\bar{f}) - \bar{a}\,(\bar{b} + \alpha\bar{g})\}$$

$$\bar{F} = R^2\{\,\bar{d}\,(1+\alpha)(\bar{c} + \alpha\bar{f}) - (\bar{b} + \alpha\bar{g})^2\}$$

$$\bar{G} = (\bar{d} + \rho\bar{f})\,(\bar{f} + \rho\bar{d}) - \bar{g}^2\,(\rho-1)^2$$

$$\bar{H} = -R\,\{(\bar{f} + \rho\bar{d})\,(\bar{d} - \rho\bar{h}) - \bar{g}\,(\rho-1)\,(\rho\bar{b} - \bar{g})\}$$

$$\bar{I} = R\{\,\bar{g}\,(\rho-1)\,(\bar{d} - \rho\bar{h}) - (\bar{d} + \rho\bar{f})\,(\rho\bar{b} - \bar{g})\}$$

$$\bar{J} = R^2\,\{(\bar{d} + \rho\bar{c})\,(\bar{f} + \rho\bar{d}) - (\rho\bar{b} - \bar{g})^2\}$$

$$\bar{K} = -R^2\,\{\bar{g}\,(\bar{d} + \rho\bar{c})\,(\rho-1) - (\bar{d} + \rho\bar{h})\,(\rho\bar{b} - \bar{g})\}$$

$$\bar{L} = R^2\,\{(\bar{d} - \rho\bar{c})\,(\bar{d} + \rho\bar{f}) - (\bar{d} - \rho\bar{h})^2\}$$

$$\Delta_1 = (\bar{c} + \alpha\bar{f})\,\bar{d}\,\beta\,(1+\alpha) + 2\bar{e}\bar{a}\,(\bar{b} + \alpha\bar{g}) - \bar{a}^2\bar{d}\,(1+\alpha)$$
$$- \bar{e}^2\,(\bar{c} + \alpha\bar{f}) - \beta\,(\bar{b} + \alpha\bar{g})^2$$

$$\Delta_2 = (\bar{d} + \rho\bar{c})\,(\bar{d} + \rho\bar{f})\,(\bar{f} + \rho\bar{d}) + 2(\bar{d} - \rho\bar{h})\,\bar{g}\,(\rho-1)\,(\rho\bar{b} - \bar{g})$$
$$- (\bar{d} + \rho\bar{f})\,(\rho\bar{b} - \bar{g})^2 - \bar{g}^2\,(\rho-1)^2\,(\rho\bar{c} + \bar{d})$$
$$- (\bar{d} - \rho\bar{h})^2\,(\bar{f} + \rho\bar{d})$$

It would be desirable to obtain the stiffness coefficients of the curved beam in the form

$$\gamma\ (1+k)$$

where γ is the coefficient for a straight beam and k is a curvature correction. However, it appears that such a form is not easily obtainable. It is to be noted, for example, that the approximation

$$\cos\ \beta \simeq 1$$

$$\sin\ \beta \simeq \beta$$

if applied to Eq. (B.6), is inconsistent since the various stiffnesses of the beam EI_Y, EI_Z, GJ and AE can vary widely in relative magnitudes. If dimensionless ratios of these stiffnesses are introduced, and power series approximations for sin β and cos β are used, difficulties still persist in making approximations which are accurate for a sufficiently wide range of parameters. Therefore the stiffness matrix K is obtained from f_{11} with no further approximations than were used in the derivation of f_{11}.